Application of the Recovery Curve Method to Petroleum Reservoir Material Balance Calculation

A DISSERTATION
SUBMITTED TO THE
DEPARTMENT OF PETROLEUM ENGINEERING
AND THE COMMITTEE ON GRADUATE STUDIES OF THE
UNIVERSITY OF LEOBEN, AUSTRIA,
IN PARTIAL FULLFILLMENT OF THE REQUIREMENTS FOR THE DEGREE OF
"DOKTOR DER MONTANISTISCHEN WISSENSCHAFTEN"

written by
M.Sc. Mohamed M. Gharsalla

April 2015

Advisor: O.Univ.Prof. Dipl.-Ing. Dr.mont. Dr.h.c. Zoltán E. HEINEMANN

Affidavit

I declare in lieu of oath that I did this work by myself using only literature cited at the end of this volume.

_____
Dipl.-Ing. Mohamed Mabrouk Gharsalla
Leoben, April 2015

Acknowledgments

Dedication

I dedicate this work to my parents, my father Mabrouk Gharsalla who passed away much to soon and my mother Dabshona Gharsalla who have always encouraged and supported me all my life. I am very proud and thankful to have a mother like her. May God reward her with a long and happy life.

I surely also dedicate this work to my beloved wife, Nouria Mohamed, who always believed in me and encouraged me with her endless love and support to go on.

<div dir="rtl">

إهـــــداء

الحمـــد والشـكر لله العلــي العظيـــم ,أهـــدى هـــذا العمـل إلــى مـن أضـاءا لـي شـــمعة العلـــم والحيــاة ، والـــذين كـــان لهـــم الفضـــل بعـــد الله ســبحانه وتعـــالى فـــي وصـــولي إلــى هـــذا المســتوى , والـــدتي العـــزيزة الغاليــة دبشـــونة غـــرس الله الـــتي غمرتـــني بحنانهـــا ودعـــمها وتشـــجيعها وإلـــى والـــدي العزيزالغـــالي المـــبروك غـــرس الله يرحمـــه الله الـــذى كـــان فـــي حياتـــه ســـنداً وداعـــماً لـــي وإلـــى شـــريكة حيـــاتي زوجـــتي الحـــــبيبة الغالـــــية نوريـــــة أبوالقاســـــم الـــــتي كانـــــت ســـنداًوداعماً ومشـــجعاً لـــي طـــول حيـــاتي الدراســـية وإلـــى إخوتـــي وأخواتـــي الـــذين ســـاندوني كـــذلك

</div>

Abstract

The dissertation presents the very first application of Mittermeir's material balance method to a real naturally fractured reservoir (NFR). The author of this dissertation proved and gave clear evidences about the theoretical correctness and practical viability of this new method. The work should be seen as the integration of 10 years research and development efforts conducted at the Montanuniversität Leoben and at the Sharif University of Technology, Tehran.

In 1936 Schilthuis published for the first time a material balance (MB) approach for oil and gas reservoirs. MB is still one of the basic, analytical tools for analyzing recovery mechanisms, for determining the hydrocarbons in place and the water influx. For almost 80 years no MB method fully accounting for the matrix-fracture fluid transfer was offered. From this reason, up to now, the applicability of the MB methods to NFRs remained limited. The new MB method, used in this work fully considers the physics of the matrix-fracture interaction, and thus the matrix oil recovery process. To make it generally applicable a specialized workflow was developed. Instructions were given how to use the field data, respectively, how to proceed in case if the data is incomplete and uncertain.

For NFRs, most of the oil is stored in matrix blocks acting as fluid sources/sinks to the surrounding fracture planes, in which fluid transport and production/injection takes place. The MB method is based on the recognition that the performance of water and gas displacement from matrix blocks can be depicted in the form of recovery factor versus time. These recovery curves determine the matrix-fracture oil transfer. A close relationship between the recovery curves and the observed reservoir state (pressure, position of the phase contacts, water cut, GOR, etc.), the aquifer parameters and the matrix-fracture oil transfer exists. The applied MB method matches both the reservoir pressure and the positions of the phase contacts. It also provides aquifer and matrix-fracture fluid transfer models. Applying the parameters of those models in prediction mode and assuming a future production strategy, reservoir pressure decline and phase contact movements can be forecasted.

The entire workflow and calculation scheme were presented based on the Sabah reservoir, located in the Libyan Sirte basin. It contained more than 500 MMstb original oil in place. Sabah has 35 years production history, is heavily fractured and produced through 70 wells. The aquifer inflow and the optimal analytical aquifer model was determined by matching the pressure history. Recovery curves were assessed by fine scale numerical modelling. Its plausibility was verified with the field's production profile. The phase contact history was successfully matched by tuning the beforehand determined recovery curve. The feasibility of a future water cut decrease and an increased oil production was demonstrated in forecast calculations.

For Sabah reservoir the practicability and benefits of this dual porosity MB could be clearly demonstrated.

Kurzfassung

Diese Dissertation präsentiert die allererste Anwendung von Mittermeirs Materialbilanzmethode für natürlich geklüftete Lagerstätten. Der Autor der vorliegenden Dissertation bewies und belegte die theoretische Richtigkeit und praktische Brauchbarkeit dieser neuen Methode. Die Arbeit soll als eine Integration einer zehnjährigen Forschungs- und Entwicklungsanstrengung der Montanuniversität Leoben und der Sharif Universität für Technologie, Teheran betrachtet werden.

Im Jahr 1936 publizierte Schilthuis zum ersten Mal einen Ansatz für eine Materialbilanzberechnung (MB) von Erdöl- und Erdgaslagerstätten. MB ist nach wie vor noch ein grundlegendes, analytisches Werkzeug für die Analyse von Entölungsmechanismen, für die Bestimmung der in der Lagerstätte ursprünglich vorhanden Menge an Kohlenwasserstoffen und für die Berechnung des Wasserzuflusses. Für beinahe 80 Jahre bestand keine MB Methode, welche den Matrix-Kluft Öltransfer allumfassend berücksichtigte. Daher war die Anwendbarkeit von MB Methoden für geklüftete Lagerstätten bis jetzt eingeschränkt. Die neue MB Methode, welche in dieser Arbeit verwendet wird, berücksichtigt zur Gänze die Physik der Matrix-Kluft Interaktion, und somit des Entölungsprozesses der Gesteinsmatrix. Um die Methode generell verwendbar zu machen, wurde ein spezieller Arbeitsablauf entwickelt. Anweisungen zur Verwendung vorhandener bzw. zum Vorgehen im Falle von unvollständigen bzw. unsicheren Daten wurden gegeben.

Bei geklüfteten Lagerstätten ist der Großteil des Öls in der Gesteinsmatrix eingelagert. Diese stellt die Quelle/Senke des Flusses von/zu den umliegenden Klüften dar, in welchen der Fluidtransport und die Produktion/Injektion stattfinden. Die MB Methode basiert darauf, dass sich die, durch Gas- und Wasserverdrängung induzierte Matrixentölung, bzw. deren Entölungsgrad als Funktion der Zeit darstellen lässt. Diese Entölungskurven bestimmen den Matrix-Kluft-Öltransfer. Eine enge Beziehung besteht zwischen dem beobachteten Zustand der Lagerstätte (Druck, Lage der Phasenkontakte, Verwässerung und Gas-Öl Verhältnisses), den Aquiferparametern und dem Matrix-Kluft Fluidtransfer. Die angewandte MB Methode kann sowohl die Änderungen im Lagerstättendruck als auch die Phasenkontaktbewegungen nachbilden. Ein Matrix-Kluft Transfer- als auch ein Aquifermodell werden bestimmt. Basierend darauf und der Annahme einer zukünftigen Produktionsstrategie können Vorhersagen über das Verhalten des Lagerstättendruckes und der Phasenkontakten getroffen werden.

Der gesamte Arbeitsablauf und das Berechnungsschema wurden anhand von der Sabah Lagerstätte, welche sich im libyschen Sirte Becken befindet, präsentiert. Sie enthielt mehr als 500 MMstb ursprüngliches Ölvolumen. Die Lagestätte ist stark geklüftet und wird seit über 35 Jahren mittels 70 Bohrungen ausgebeutet. Der Wasserzufluss und die optimalen analytischen Aquifermodelle wurden anhand der Nachbildung des Druckverlaufes bestimmt. Entölungskurven wurden mittels detaillierter numerischer Modellierung abgeschätzt und durch die Feldproduktion verifiziert. Die gemessenen Änderungen im Phasenkontakt konnten durch eine Anpassung der zuvor ermittelten Entölungskurve modelliert werden. Die Möglichkeit, die Wasserförderung zu reduzieren und gleichzeitig die Ölproduktion zu steigern, wurde durch Vorhersageberechnungen gezeigt.

Anhand der Sabah Lagerstätte konnte die Praktikabilität und die Vorteile der Materialbilanzrechnung für geklüftete Lagerstätten klar demonstriert werden.

Application of the Recovery Curve Method to Petroleum Reservoir Material Balance Calculation

Chapter 1

Chapter 2

Chapter 3

Chapter 4

Chapter 5

Chapter 6

Chapter 7

Chapter 8

Chapter 9

List of Figures

Chapter 1

Introduction

1.1 Motivation of Work

1.1.1 Background

Schilthuis (1936) first introduced the material balance method 79 years ago. It remains one of the basic tools for analyzing the petroleum recovery mechanism, by estimating the volume of petroleum in place in the reservoir and the water inflow to the reservoir. Unfortunately, until recently, no material balance solution has been found that is applicable to dual porosity reservoirs. The Recovery Curve Method (RCM) was introduced in numerical reservoir simulation by Heinemann (2004) and provided the first clues to possible improvement. Mittermeir (published in 2015) reformulated the material balance equations using the concept of twin barrels (instead of the usual single barrel approach), in which one barrel represents the fracture system and the second barrel represents the matrix system. The mass transfer between the two barrels is described by recovery curves.

In 2013, Prof. Zoltán Heinemann of the Montanuniversität–Leoben announced the establishment of research funding for projects on the ''Application of the Recovery Curve Method to Naturally Fractured Petroleum Reservoirs (NFR)''. Prof. Zoltán Heinemann's PHDG association offers organizational support for doctorate candidates at the Montanuniversität–Leoben (Austria), University of Miskolc (Hungary), Sharif University of Technology (Iran) or Tehran University (Iran). The present author applied for support at PHDG for scientific work related to the investigation of the applicability of Mittermeir's material balance method of mass transfer between a fracture system and a reservoir matrix to real-world reservoirs.

1.1.2 The Objectives

The primary objective of this research is to demonstrate the applicability of Mittermeir's (2015) material balance approach to a real field. Comparisons to results from numerical simulations are used to demonstrate that the results obtained by the material balance methodology are valid. The author has over 20 years of experience analyzing and modeling field production histories, including the field used in this study. Zueitina Oil Company (ZOC) is the operator of the field and has granted permission to use their data and to publish the results. Without these prerequisites the work would not have been possible.

This dissertation presents the first successful material balance application to a realistic dual porosity reservoir, thus, **the goal of this work has been achieved**. The author believes this to be a significant contribution to petroleum engineering science and practice.

1.1.3 Relevance

Fractured reservoirs are becoming significant sources of petroleum throughout the world from both old and new fields. Examples of large oil-in-place hydrocarbon reservoirs include those of the Monterey Shale play in California, West Texas carbonates, North Sea chalk reservoirs, the Asmari Limestone fields in Iran (Agha Jari, Haft Kel, and Gachsaran) and the Sabah Field in Libya. Many recently discovered oil and gas fields occur in fractured rock and their development constitutes a real challenge for the oil industry. Naturally fractured reservoirs, often-abbreviated as NFR, have been the subject of extensive studies during the past several decades.

The goals of reservoir engineering are to estimate reserves, forecast future production, to understand how fractures can be used to positively affect production and lastly, to estimate the ranges of uncertainty. For conventional reservoirs, engineers can generally provide a reasonable assessment of reservoir performance by combining information about the reservoir's geologic framework, rock and fluid properties, and results from well logs, rock mechanical tests, formation evaluation tests and most importantly, by matching the production history. Recently, reservoir-scale seismic surveys have greatly aided the reservoir characterization. However, for fractured reservoirs, obtaining the necessary data and forecasting reservoir performance is much more difficult than for conventional reservoirs. Designing an appropriate development plan requires a credible reservoir description that includes fracture sizes, orientations, connectivities and conductivities, all in the form of maps and frequency distributions. This information must be turned into a reliable fracture network characterization. Is this possible? Gilman (2006) gave the following statement: "Due to the complexity of NFR, it may appear to be rather hopeless to get a unique answer. But instead the question should be, can we estimate the range of uncertainty?"

Another difficulty to be faced is that there is no approved, generally applicable description of the dynamic processes of dual porosity systems. In the single porosity case the displacement efficiency can be estimated by the Buckley-Leverett theory, the reservoir mechanism can be

evaluated using the classical material balance approach, and numerical simulation techniques have been successfully applied for more than 50 years to several thousands of fields. For dual porosity reservoirs, methods describing oil recovery from single matrix blocks are still a matter of discussion, and no material balance calculation method now exists that considers the fracture-matrix interaction. Very few field studies have been published that demonstrate, even only qualitatively, forecasts based on simulation studies of dual porosity reservoirs.

Appropriate modeling of NFRs is much more demanding than modeling conventional reservoirs. History matching is also more difficult in the case of a dual porosity reservoir, primarily because of the difficulty of assessing fracture-matrix mass transfer. This function is influenced by several properties which in a real case cannot be measured: shape factor, matrix block height, wettability, capillary pressure, relative permeabilities and heterogeneity. In attempting to perform a history match, the reservoir engineer may modify some or all of these factors. Even if the engineer is more-or-less successful, there is no assurance that the real factors have been captured or only artifacts have been introduced. The resulting predictions, based on false premises, may easily be misleading.

To create a numerical reservoir model and perform a history match generally requires creation of about one hundred thousand to a million or more grid cells and is very time consuming. It is impossible to use such a model for the parameter studies that would be necessary to estimate uncertainties. For this purpose, the new MB technique offers compelling advantages. The combined matching of the reservoir pressure and the historical phase contacts can provide the aquifer strength and corresponding recovery factor of the matrix in addition to estimating fluids in place. The matching can be automated so that an extended parameter study takes only a few days.

1.2   The Approach

1.2.1 Working Environment

The author wishes to state that he would not have been able to conduct and complete this complex research and development work entirely by himself. Although this dissertation has been written by the author alone, it is the result of a close cooperation within Professor Heinemann's research group, which has accumulated know-how, documentation, case studies and software tools on reservoir characterization and analysis. Members of this group include theoreticians, numerical analysts, computer experts and practicing reservoir engineers. The group has a "no property right" policy on any kind of prose – in written, extended or shortened form. As a principle, all team members can use the collective knowledge of the group. Available formulations are not reformulated but used unchanged in subsequent documents, publications and in theses unless improvements in clarity and use of English can be achieved. The author of this dissertation makes use of the group's common knowledge, especially that which has not yet been published but only documented in internal reports, master's theses and PhD dissertations

of former group members. All of these are referenced in general, but not attributed in every instance.

During this research, the author had access to proprietary information. Sources of such information are not referenced unless written permission, including the right of publication, has been provided by the sourced.

In order to clearly separate collegial contributions from the individual work of the author, the author's scientific ideas, achievements and his additions to future technology are explicitly indicated at the end of this chapter.

1.2.2 Previous Related Works

Heinemann (2004) suggested in 2004 that instead of trying to estimate individual rock and fluid properties, the recovery curves should be determined and used directly in a numerical reservoir simulation model. The dimensionless recovery curves display the recovery factor as function of dimensionless time. A recovery curve could be evaluated in three ways:

- Using physical models, a piece of reservoir rock (a proxy for a matrix block) obtained from an outcrop could be saturated with oil and "recovered" under simulated reservoir conditions in an autoclave. This would be an ideal solution but is usually not practical because no reservoir-equivalent rocks are exposed at the surface .

- Calculating the recovery process numerically on a finely gridded single matrix block model surrounded by fractures. The fractures define the boundary conditions for the single porosity matrix. The recovery curves depend on the displacement mechanism and will be different for water imbibition and gravitational gas drive.

- Calculating the recovery of a matrix cell in a dual continuum model by setting the conditions for the matrix-fracture mass transfer.

The recovery curve method has been the subject of three doctoral theses. Mittermeir (2006) investigated different approaches for full-field modeling of naturally fractured reservoirs. He showed that in the view of asset owners (ie., the national oil companies), the best method was multilevel modeling instead of "top down" or "bottom up" approaches. One of the levels had to be the single matrix block investigation and the preliminary calculation of recovery curves.

Pirker (2008) presented more efficient numerical methods for calculating recovery curves for single matrix blocks. She accounted for the fact that matrix blocks are not uniform and therefore recovery curves have to be calculated for classes of blocks. Subsequently, the individual recovery curves had to be consolidated by averaging according to the frequency of each class. The averaged curve was then assigned to a simulation cell.

Amiry (2014) suggested a method based on statistical analysis of matrix blocks in outcrops of fractured formations. He showed that the recovery curve was not influenced by the actual

shapes of blocks and could be scalable with respect to the shape factor and apparent permeability. Additionally, he showed that under the same conditions, the results of the recovery curve method and those of the classical conventional method were similar and the two approaches could be combined both in space and time.

Pirker (2008) and Amiry (2014) promoted two types of applications:

1. The single matrix block recovery curves should be compared to those from dual continuum calculations. The parameters and functions used to calculate the matrix-fracture transfer term should be tuned in such a way that the two curves match. This approach should assure that the full field model based on a dual continuum does not contradict the physical reality.
2. The single matrix block recovery curves could be used directly. In the dual continuum model, the recovery factor and the state of the fractures are known at all times. By choosing the correct recovery curve it is straight forward to determine the oil expelling velocity and, thus, the transfer term of the oil component for the matrix-to-fracture interaction. The transfer term for the water and gas phases can be calculated in the conventional way.

Ghaedi (2014) investigated a third possible application of the recovery curves by determining the curves directly from historical production data. Based on the findings of the history matching fundamental rock properties such as wettability, capillary pressure and relative permeability functions are determined.

1.2.3 Utilitarianism

Utilitarianism is one of the basic principles of the PHDG. The actual research and development was conducted in close connection with real field projects. The new developments are used in parallel with standard methods, whereas new ideas can be discarded if they do not satisfy the expectations of quality and efficiency, within the time constraints of the project. This dualism provides the possibility of close control and will quickly reveal if the standard method is not the best in each step.

1.3 Software Tools

The simulation software H5 is an alternative to other commercial simulators such as ECLIPSE. It is a proprietary software system developed by Professor Zoltan Heinemann and associates and is the fifth generation of research simulators developed under the supervision of Prof. Heinemann. The first generation was written in FORTRAN-IV in 1968. The development of the fifth generation began in 2006, using FORTRAN-1995 and C++ programing languages. The various "H"-versions served as the foundations for commercial software packages including SIMULA, SURE, PRS-2012 and PRS-2015. Prior to version H4, the simulators were used as

teaching and research tools at the Montanuniversität Leoben.

PhD candidates sponsored by PHDG have access to the H5 source code so they can experiment with the existing modules and can design and implement new procedures. Student researchers cannot make unsupervised modifications to the H5 code but can develop standalone modules or simply present detailed descriptions of suggested improvements and extensions to be implemented by professional programmers. Testing and benchmarking is the responsibility of the project author. H5 can operate on ECLIPSE input without any modifications, so identical runs can be made on ECLIPSE, H5 and PRS. These runs can be started in parallel and the results must either be close to each other or the differences must be explainable.

The author has greatly benefited from the H5 software and PHDG technical support which provided the opportunity to develop and test new concepts and procedures for reservoir simulation.

1.4   Outline

Chapter 1   **Introduction**
    This is the current chapter which contains a brief introduction to the objectives and contents of this dissertation.

Chapter 2   **State of the Art of Modeling of Naturally Fractured Reservoirs**
    This chapter reviews the development history of the Material Balance method (as introduced in 1950 already), the today common understanding of the dual porosity recovery mechanism and present the relevant methods simulating naturally fractured reservoirs including the dual continuum approach, the discrete fracture methods and also those of the Single Matrix Block (SMB) applications.

Chapter 3   **Investigations Relating to Matrix Recovery Curves**
    The objectives of this chapter is to familiarize with the recovery curve method. The method of the Single Matrix Block (SMB) simulation, used in this work, is described in details. It is shown how the Matrix-Fracture-Transfer rates can be calculated from a Recovery Curve.

Chapter 4   **Material Balance for Dual Porosity Reservoirs**
    The principle of the dual porosity Material Balance calculation and its mathematical formulation are presented. The MB equations are written for the entire reservoir system and than separately for every matrix trench. The pressure match results in identification of the aquifer model and phase contact match in the recovery curves.

Chapter 5   **Practical Application of the Recovery Curve Method**
    The main part of this chapter shows how the movement of the phase contacts is calculated. The description of the workflow in modeling of naturally fractured reservoirs (NFR) should help the reader when dealing with Chapter 6.

Chapter 6   **Sabah Case Study**
> The objective of this chapter is to verify the applicability of the MB method in a study of the Sabah field. The geology of the field, the pressure and production history are presented in short. A section assesses the dynamic water-oil-contact over the entire production time. The MB method was used to determine the water influx, the parameters of the best fitting analytical aquifer and also the re-scaling factors of the recovery curve. With these parameters the future field performance was predicted.

Chapter 7   **Conclusions**

1.5   Scientific Achievements and Technical Contributions

1.5.1 Scientific Achievements

- The author presented the world's first realistic and successful Material Balance application to a naturally fractured dual porosity reservoir. The author is confident that this is an essential contribution to the petroleum engineering science and practice.

- The author stated that the recovery curve method, beyond numerical reservoir simulation, is applicable to material balance calculation too.

- The author showed that by matching the dynamic phase contacts it is possible to assess the recovery curve.

1.5.2 Technical Contributions

- Pirker (2007) and Amiry (2014) suggested to use a 9x9x37 grid resolution on a quarter single matrix block model. The author showed that a 7x7x21 resolution is satisfactory too.

- The author designed a general applicable workflow applicable to the material balance calculations.

1.6   Related Publications of the Author

Gharsalla M. M., Heinemann Z.E., Mittermeir G.M. 2014. Application of Material Balance Calculation to the Fractured Dual Porosity Sabah Field. *BKL Köolaj és Földgáz*, Budapest, Hungary, **147** (7): 1-17.

Heinemann, Z. E., Mittermeir, G.M. and **Gharsalla, M.M.** 2014. Successful Application of Material Balance Calculation to a Fractured Dual Porosity Field. Paper SPE 172325-MS presented at the Annual Caspian Technical Conference and Exhibition held in Astana, Kazakhstan, 12-14 November. http://dx.doi.org/10.2118/172325-MSP

Chapter 2

State of Art in Modeling of Naturally Fractured Dual Porosity Reservoirs

As mentioned in Chapter 1, the subject of this work, the Material Balance (MB) method, is coming from the very early time of the reservoir engineering science but the resulting solution is absolutely new. From this reason it is not possible to provide an usual literature overview, referring a greater number of closely related publications. Instead, this Chapter offers some background informations about the theory and today´s praxis of modeling naturally fractured reservoirs (NFR). All industrially-used methods for modeling NFR are based on the dual continuum modeling (DCM) approach. This approach is also the basis of the presented MB method and therefore it will be discussed in more detail. Recently, discrete fracture models (DFM) have become popular in academic research but no practical application of them is known up to now. These try to solve the difficulties in and around the NFR by involving more and more details in the investigations, contrary to the global MB approach. Results from DFM research have no importance for this work, therefore they will be mentioned in this Chapter only shortly.

2.1   The Material Balance Method
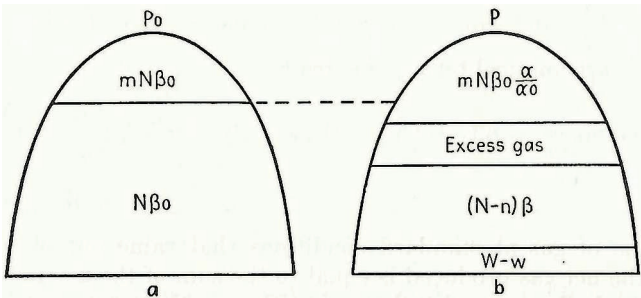
Figure 2.1: The scheme of the material balance of an oil reservoir (Pirson 1958)

The first material balance was formulated by Schilthuis (1936). The material balance equation expresses the relationship which must exist at all times in an oil and gas reservoir produced

under or near to equilibrium conditions. The left side of Figure 2.1 shows the conditions as they originally existed in the reservoir under initial pressure p_i, where NB_{oi} is the reservoir volume occupied by all the original stock-tank oil containing its complement of dissolved gas, mNB_{oi} is the reservoir volume occupied by the gas cap (in Figure 2.1 the oil formation factor is $B_{oi} = \beta_0$). After N_p of stock-tank oil have been produced (in Figure 2.1 $N_p = n$), the field pressure is reduced to p and the state of the reservoir has become as represented at the right side of Figure 2.1. The pore volume of the reservoir did not change, therefore, the sum of the expressions in sketch a and b are equal, providing a relation between original fluid in place, production, water influx and reservoir pressure. (In Figure 2.1 α_0 and α are the initial and actual gas formation factor, W the water influx and w the cumulative water production.) Simultaneously with Schilthuis'work, Katz (1936) proposed a tabulation method for the evaluation of oil in place. Pirson (1944) showed the two methods to be equivalent. Pirson (1950) listed the applicability the material balance method:

a) To perform depletion-drive calculation,
b) To determine the original oil in place and confirm volumetric estimates,
c) To verify the existence of a gas cap,
d) To determine the existence of water encroachment and its rate of influx.

The initial difficulties involved in the problem of forecasting performance was eliminated by Babson (1944) and Tarner (1944): They postulated that given the material-balance equation and the instantaneous gas-oil-ratio formula, it should be possible to find the field pressure attained for each assumed increment of stock-tank oil production. Muskat (1945) expressed the material balance equation in differential form making it advantageous to examine the influence of various factors on depletion drive performance. The Musket method has the disadvantage that it requires linear continuity in fluid properties. Pirson (1950) eliminated this by formulating the material balance in finite difference form. This step also meant the end of the development of the material balance technique for the following next 65 years. About the merit of the Material Balance Methods, the statement of Uren (1950) should be cited: "This method to calculate reserves is the most advanced and theoretically most correct of the several methods available to the engineer".

In classical Material Balance (MB) calculations the reservoir is treated analogously to a single barrel. The dual porosity nature of the reservoir could be preserved by creating two barrels, one representing the fracture the other the matrix pore volume. Assigning different pressures to both volumes (matrix and fracture) and calculating the mass transfer between the two systems is not possible for two reasons: Firstly, the pressure of the matrix cannot be measured and secondly, the mass transfer is stronger governed by capillary, gravitational and viscous forces than by the force of compression. Penuela *et al.* (2001), Sandoval *et al.* (2009) and Bashiri and Kasiri (2011) distinguished between the matrix and fracture systems but considered only the difference in the pore compressibility. Such an approach differs only slightly from a single porosity model using averaged pore compressibility and cannot be regarded as a valid extension of MB calculation to dual porosity reservoirs. Probably this is the reason why no petroleum software provider offers material balance tools especially suited for dual porosity reservoirs.

The decisive step in achieving a breakthrough in MB has been achieved by Mittermeir (2015) who used the Tarner (1944) formulation for the entire pole volume, connected the aquifer

support, i.e. the water influx into the fracture network, and used the Pirson (1950) finite difference material balance formulation for the concomitant matrix system. Gharsalla *et al.* (2014) verified the applicability and demonstrated the advantages of this approach.

2.2 Recovery Processes in Fractured Reservoirs

There are major differences between recovery performance of fractured and non-fractured reservoirs. For fractured reservoirs, the notion of "matrix block" is introduced, which at any reservoir location represents a fluid "source" term that feeds the fracture continuum.The mostly low permeable matrix contains predominantly the oil (> 95%) and the high permeable fracture provides the flow path for the fluid. A fluid exchange has to take place between the matrix and the fractures enabling to produce the oil trough the wells. The efficiency of the matrix recovery process determines the reserves and the production capacity.

The matrix recovery is induced and assisted by various mechanisms which originate from (1) rock compressibility, (2) single phase fluid expansion, (3) solution gas drive, (4) capillary imbibition, (5) gravity drainage, (6) viscous forces, (7) diffusion and (8) rock compaction. In the following, all of them can be considered but for sake of simplicity emphasis will be put on two categories of driving forces. The first group is built by the mechanisms (1) to (3), governed by the force of compression. Their impact – disregarding only the theoretically-interesting transient effects - depends solely on the change of pressure of the system. The driving force in (4) and (5) originates from the saturation of the displacing phase in the fracture around the matrix block and is purely time-dependent. The viscous (6) forces depend furthermore on the pressure gradient, which naturally changes over time, along the matrix block. The remaining mechanisms (7) and (8) are even more complex but have importance in few cases only. Diffusion acts on light components of the hydrocarbon system and can only be considered in compositional formulation. Compaction depends on both the pressure and saturation and it progresses with time.

The description of the recovery process in NFR faces two serious difficulties. The first is the description of the dual continuum: (1) how to measure the actual size of the single matrix blocks, (2) how to determine their distribution and (3) how to estimate the volume (i.e.porosity) of the fractures. The second difficulty is to capture the driving forces responsible for the matrix recovery process. Are they function of the pressure and the production rates as it was learned from single porosity reservoir processes? Or are they a function of time? Or both? This question is fundamental for the MB method, therefore it will be discussed in detail in the next section.

2.3   The Dual Continuum Concept

Lemonnier and Bourbiaux (2010) published a literature review under the title "Simulation of Naturally Fractured Reservoirs, State of the Art, Part 1, Physical Mechanisms and Simulator Formulation." The author studied all original works which were cited in this survey and realized that they made an excellent job. A recapitulation would not have sense, it is suggested to consult this work directly. Only the most relevant facts were extracted, however, the literature survey has been extended to the end of year 2014. The author refers always to the original work instead of the Lemonnier and Bourbiaux (2010) review.

Barenblatt, Zheltov and Kochina (1960), introduced the dual continuum concept and applied it to fractured reservoirs. This concept considers that the fracture continuum on the one hand, the matrix continuum on the other hand, behave like two flow continua interacting with each other. Warren and Root (1963) applied this concept to interpret well tests in the simplified framework of a fractured reservoir. A single phase is flowing in fracture continuum which locally interacts with porous parallelepiped matrix blocks, acting as a fluid source only.

$$\nabla\left[\frac{k_{rw}}{\mu_w B_w}k\nabla\Phi_w\right] + \tilde{q}_w \pm q_{wmf} = \frac{\partial}{\partial t}\left(\frac{\phi S_w}{B_w}\right) \tag{2.1}$$

$$\nabla\left[\frac{k_{ro}}{\mu_o B_o}k\nabla\Phi_o\right] + \tilde{q}_o \pm q_{omf} = \frac{\partial}{\partial t}\left(\frac{\phi S_o}{B_o}\right)$$

$$\nabla\left[\frac{k_{rg}}{\mu_g B_g}k\nabla\Phi_g + \frac{R_s k_{ro}}{\mu_o B_o}k\nabla\Phi_o\right] + \tilde{q}_g \pm q_{gmf} = \frac{\partial}{\partial t}\phi\left(\frac{S_g}{B_g} + \frac{R_s S_o}{B_o}\right)$$

Equation 2.1 gives the black oil balance equations considering three components in three phases (subscripts w, o, and g for water, oil and gas). Each continuum is a single porosity medium, therefore, the flow equations are identical for both continua. The only difference is that the transfer terms have the opposite sign: $^{+}/_{-}q_{wmf}$ for water, $^{+}/_{-}q_{omf}$ for oil and $^{+}/_{-}q_{gmf}$ for gas. k is the permeability and μ the viscosity, B is the formation volume factor and Φ the phase potential in the fracture (f) and in the matrix (m). Equivalent compositional and non-isothermal formulations are also well known. The balance equations have to be written for both continua.The last terms at the left hand side represent the rate of the mass transfer between the fracture and matrix continua.

2.3.1 Matrix Blocks and Simulation Cells
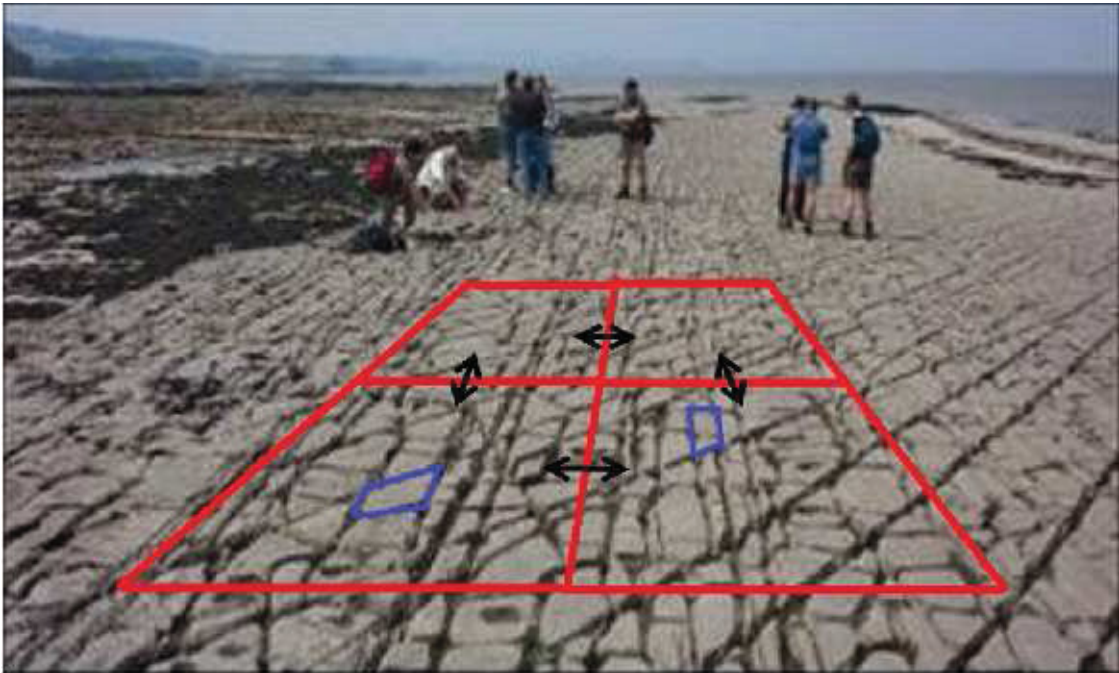
Figure 2.2: Fractured Rock, Matrix cell vs. matrix block, (by Roxar training)

In order to calculate fluid flow within the dual porosity system numerically, the Equation 2.1 has to be discretized. To avoid ambiguities one should distinguish between *matrix blocks* and *simulation cells*. The red squares in Figure 2.2 (or cubes in 3D) represent the control volumes, in other words the "*simulation cells*". The dual continuum approach considers two simulation cells at each location (i.e. at the place of each red square); one is the "*matrix cell*" and the other is the "*fracture cell*". This divides the space into two identically-shaped domains: the "*matrix domain*" and the "*fracture domain*". The fracture domain, built by the fracture cells, commonly has a much higher permeability and less porosity than the matrix domain. This means that the fracture cells can exchange fluids easily with their neighboring fracture cells (along the black arrows in Figure 2.2). Matrix cells, may or may not be able to exchange fluids with their matrix neighbors resulting in dual permeability or dual porosity models, respectively. Figure 2.2 is the two dimensional outcrop of a naturally fractured formation. This figure explains the fundamental problems that should be overcome while modeling fluid flow in such a discontinuous domain. The fractures surrounding the blue-framed "*matrix blocks*" determine their boundary conditions, imposing how the hydrocarbon will be recovered from the matrix block. On the other hand, the matrix blocks serve as the internal mass source and sink for the fracture system.

2.3.2 Time-Dependent Source/Sink Functions

Reiss *et al.* (1973) made the first attempt to apply the dual-porosity approach to calculate three-dimensional multi-phase flows in a fractured reservoir. At the beginning the fissures are filled with oil and the oil from the matrix is produced into the fissures according the fluid/rock expansion and by solution gas drive. This is a purely pressure dependent process. When the matrix block is reached by the water-oil or gas-oil interface, production is mainly due to capillary and gravity effect. The authors assumed that from this time onwards the phases are completely segregated in the fissures and the matrix block is completely surrounded by water or gas. The matrix-fracture exchange was represented by time-dependent source or sink functions, also named as recovery function or recovery curve. These functions were derived from laboratory experiments or/and from the numerical simulation of the oil recovery mechanism in a finely-gridded single-block model. Rossen (1977) used the same approach with semi-implicit handling of the source terms.

Both Reiss *et al.* and Rossen assumed that the oil recovery from a matrix block is only due to capillary and gravity effects and is only a function of the elapsed time after water (or gas) comes in contact with the matrix block via the surrounding fractures. The effects of compressibility and fracture viscous flows on matrix-fracture transfer were neglected, because it is very difficult to derive transfer functions that are only time-dependent and valid at each stage of the field exploitation. Nevertheless Reiss *et al.* believed that this simplifications are not very restrictive to usual field conditions.

Nevertheless Reiss *et al.* (1973) and Rossen (1977) did not found followers.

2.3.3 The Transfer Function and the Shape Factor

In this section the transfer function with the obligatory shape factor will be discussed followed by the single matrix block calculation.

In black-oil formulation, if the oil component is present in the oil phase only, the transfer function gets the following form:

$$q_{omf} = \sigma k_a \frac{k_{ro}}{\mu_o B_o}(\Phi_{om} - \Phi_{of}) \text{ [sm}^3\text{/s],} \tag{2.2}$$

where k_a is the apparent matrix permeability and μ_o the viscosity, B_o is the formation volume factor of the oil and Φ the phase potential in the fracture (*f*) and in the matrix (*m*). σ is called, according to the Warren-Root concept, shape factor and has to be seen as a characteristic value of the fractured dual continuum, proportional to the specific surface of the matrix block and has a dimension L^{-2}. Equation 2.2 is applicable in pseudo-steady-state conditions only.

Warren and Root (1963) gave the first definition of the shape factor σ when they introduced

their idealized sugar cube model (Figure 2.3) of fractured porous rocks for a cubic matrix block with a side length L, $\sigma = 12/L^{-2}$. The goal of later scientists was to extend the Warren-Root transfer function applicable for multi-phase displacement. The matrix-fracture fluid transfer in numerical modelling of dual porosity reservoirs has ever been and is still an area of extensive research and discussion.
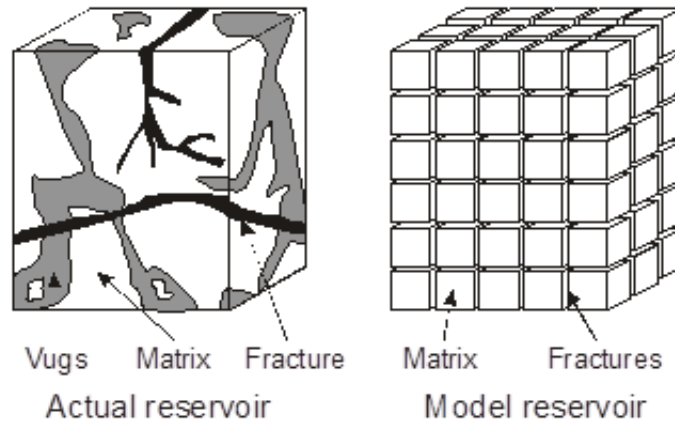
Figure 2.3: Idealization of a fractured reservoir (after Warren and Root 1963)

Kazemi *et al.* (1976) introduced a two-dimensional two-phase water-oil model in which the matrix-fracture flow rate is related to the potential difference between matrix and fracture. Gilman and Kazemi (1983) extended the two-phase Kazemi's model to three dimensions. One of the most accepted and widely implemented (e.g. in ECLIPSE) shape factor definitions used in numerical modeling was given by Kazemi *et al.*(1976,1983):

$$\sigma = 4\left(\frac{1}{L_x^2} + \frac{1}{L_y^2} + \frac{1}{L_z^2}\right), \qquad (2.3)$$

The most general definition of the shape factor was given by Heinemann and Mittermeir (2012):

$$\sigma = \frac{1}{V_{mi}} \sum_{j=1}^{N} A_{ij} \frac{\left|\bar{\bar{k}}' \vec{n}_j\right|}{\left|\vec{d}_j\right|}. \qquad (2.4)$$

V_{mk} is the volume of the *k*-th matrix block, $\bar{\bar{k}}$ is the normalized permeability tensor, $n=1,N$ is the number of surfaces A_{kn} towards the surrounding fracture network, $\vec{n}_{kn}$ is the unit normal vector, $\vec{d}_{kn}$ is the distance vector to these surfaces. It is easy to show that this expression contains all other forms of the shape factor introduced earlier.

Heinemann and Mittermeir showed that the expression Equation 2.4 is exact for the pseudo-steady-state condition, assuming linear potential and homogenous fluid distribution within the matrix block. The rigorous derivation also allows to conclude that no general and

constant shape factor can exist if one of these conditions is violated. This is one of the weakness of all methods based on the transfer function.

Gilman (2003) claims that under pseudo-steady-state conditions the shape factor is a function of fracture spacing (or intensity), and is not inherently a time-dependent parameter. Numerous other authors proposed shape factors based on numerical and/or laboratory experiments. Thomas *et al.* (1983) studied various fine-grid single-block dual-porosity models. For a three-dimensional oil-water model with near unity mobility ratio they obtain a match with a shape factor of $\sigma = 12/L^{-2}$. Coats (1988) derived the shape factor without assuming linearity for the potential gradient. His shape factor is twice the value of Kazemi *et al.*(1976). Ueda *et al.* (1989) investigated the shape factor for one and two dimensional flows. They concluded that the shape factor has to be adjusted by factor 2 for a one dimensional flow, a fact that has been verified in this work.

Lim and Aziz (1995) derived a shape factor for linear single phase transient flow. They set a constant pressure p < pi at x=0. The analytical solution of the boundary condition problem resulted in the shape factor described by the formula $\sigma = \pi^2/L^{-2}$. The Equation 2.3 modifies accordingly to:

$$\sigma = \pi^2\left(\frac{1}{L_x^2} + \frac{1}{L_y^2} + \frac{1}{L_z^2}\right).$$

(2.5)

Numerous works were published further dealing with the shape factor question, becoming a preferred university research topic. It is easy to discuss shortcomings in previous publications and to suggest alternative possibilities which seems to be applicable under specific conditions. None of those offer a general applicable solution for calculating the transfer term within the dual continuum formulation.

The present author concludes that the shape factor is a mathematical fiction, valid and applicable under the conditions defined in a mathematical model only. Nevertheless it can be regarded as a useful complex value, which characterizes the matrix blocks based on their size, form and anisotropy.

The second weakness of the transfer function given in the Equation 2.2 is the driving force, expressed by the potential difference. In single-phase case this is the pressure difference between fracture and matrix. In multi-phase case the effect of capillary pressure and the gravitational forces are vanishing in this formulation.

Gilman and Kazemi (1983) improved the formulation of gravity forces between fracture and matrix by using two different depths for the fracture and matrix nodes. Litvak (1985) and Sonier *et al.* (1986) improved this modeling approach. Their matrix-fracture exchange formula introduced a transient (time-dependent) gravity term calculated from the height of the matrix blocks and from the saturation within the matrix and surrounding fractures. Assuming a gravity-driven vertical equilibrium of fluids in both media, fracture and matrix saturations can be converted into hypothetical fluid contact levels that are used to estimate the gravity head applied on the matrix blocks of the considered cell. As a follow up of these early developments,

Balogun *et al*. (2007) suggested to use two shape factors in the transfer function: σ and σ_z, where the second one is for the gravitational term.

Thomas *et al*. (1983) modeled the effect of gravity on matrix-fracture transfers by using pseudo-relative permeability and pseudo-capillary pressure curves based on the vertical equilibrium assumption. An additional term was also added in the matrix-fracture flow terms to account for the effect of the pressure gradient across the matrix block and for diffusion of gas into the undersaturated oil of matrix blocks during non-equilibrium gas injection. Rossen and Shen (1989) used pseudo-capillary-pressure curves for both the matrix and fracture. The fracture curve can be determined directly from rock properties and matrix block dimensions, while the matrix curve can be obtained from the results of a single simulation of a fine-grid model of a single matrix block. Bourbiaux (2010) stated that the determination of effective multi- phase permeabilities or of pseudo-relative permeabilities has no general solution.

The necessity of a detailed simulation of the matrix-fracture transfers using gridded matrix blocks was emphasized by Saidi (1983), who implemented a model where the matrix-fracture transfer in each reservoir zone characterized by given rock properties are simulated using a gridded matrix block model surrounded by gridded fractures.

Pruess *et al*. (1985), proposed a subgridded two-phase and heat flow model with the Multiple Interacting Continua (MINC) approach. Chen *et al*. (1987) developed a three-dimensional compositional thermal simulator allowing the rock matrix block to be subdivided into a two-dimensional grid in order to study more precisely the effects of gravity, capillary pressure, and mass and energy transfer between fractures and matrix blocks.

Blaskovich *et al*. (1983), Hill and Thomas (1985), Quandalle and Sabathier (1989) presented the physical and numerical aspects of the dual-porosity/dual-permeability approach. This formulation is useful to take into account "block-to-block" matrix flows due to partial matrix continuity in some parts of the reservoir. Gilman and Kazemi (1988) used a dual-permeability approach in the vertical direction alone to accurately simulate the matrix flows involved in gravity-driven matrix-fracture transfers, thanks to a refined vertical discretization. Por *et al*. (1989) presented a dual-porosity/dual-permeability approach with additional connections between the matrix node of a given cell and the fracture nodes of neighboring cells for modeling the block-to-block interactions and the role of capillary contacts during gravity drainage processes.This way, the matrix oil drained into the fractures at a given cell location can re-imbibe the matrix blocks of the cell located below. The gravity driving force applied on matrix blocks is obtained via a half-block-height shift between fracture and matrix nodes.

Although dual porosity and dual permeability models have been implemented in many reservoir simulators, fracture uniformity presumed in these models does not conform with outcrop observations, which indicate that height, length, aperture, spacing and directionality of natural fractures vary substantially in the subsurface (Gillespie *et al*., 1993). Johns and Jalali-Yazdi (1991) and others extended dual continuum models to include variable matrix block sizes in order to make these models more realistic. Moinfar *et al*. (2011), however, presented examples where the dual continuum approach fails to provide accurate solutions in the presence of large scale fractures and high localized anisotropy. Thus, dual continuum models are especially appropriate for reservoirs with a large number of highly connected, small scale fractures.

Conclusion: Based on all presented work above - numerous other could be referenced too - it has been concluded that neither the Reiss *et al.* (1973) recovery curve method nor the Kazemi *et al.* (1976) concept based on transfer function offer a general applicable solution for calculating the matrix-fracture fluid exchange for simulating multi-phase fluid flow in a dual porosity naturally fractured reservoir.

2.4   Discrete Fracture Modeling (DFM)

Recently, different approaches were implemented to simulate flow directly on the discrete fractured medium generated by fracture characterization software without any prior homogenization. They used discrete element models of the fracture network alone or models of both the fracture network and the matrix blocks. Bourbiaux *et al.* (1999) applied Discrete Fracture Network modeling to the simulation at local scale of the water imbibition of a fractured medium, involving two fracture sets generated by a stochastic fracture modeling software as shown in Figure 2.4. The fractured medium horizontal dimensions are equal to 200 m (656 ft). The size of the zoom is 20 m × 16 m (65.6 ft × 52.5 ft). This example should demonstrate why the DFM approach is not relevant for our objectives. Geiger *et al.* (2009), stated that the computational cost of DFM techniques has the draw-back that their applicability to high resolution field and sector-scale reservoir simulations is reduced because it is often impractical to run DFM simulations for multiple geological realizations of NFR. Li *et al.* (2013), presented a multiple-continuum concept that considers globally connected natural fractures, locally connected micro fractures and low-permeability matrix. It is proposed to use this method to model production from shale gas reservoirs. Monifar *et al.* (2013) presented a hybrid method which includes three domains, matrix, discrete fracture and continuum-fracture domains to model complex networks of natural and hydraulic fractures. They stated that it is neither practical nor advantageous to model a large number of pre-existing natural fractures with discrete fracture model. Such an approach could be a promising solution in future developments.

Conclusion: The Discrete Fracture Modeling approach is neither practical nor advantageous for application in field and sector-scale reservoir simulations.
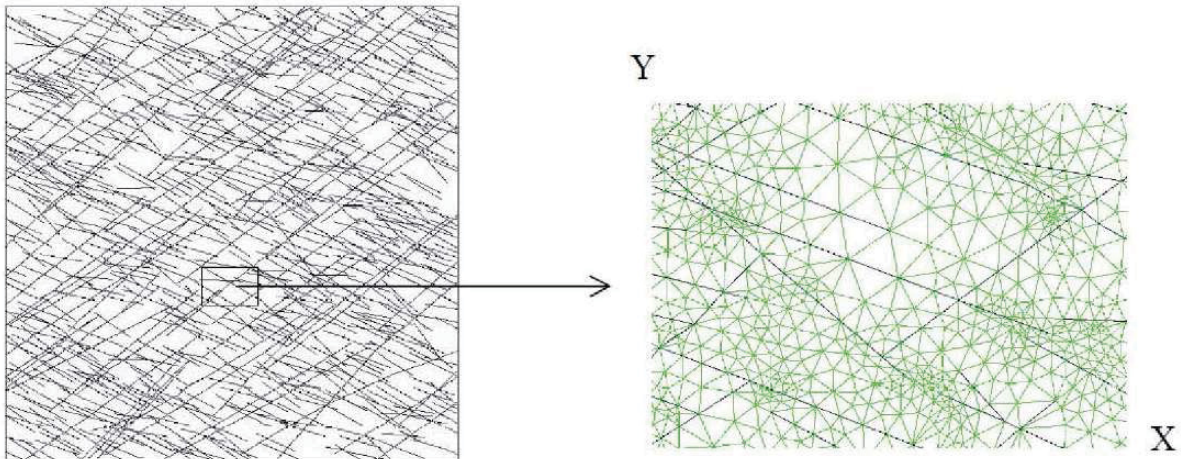
Figure 2.4: The geological image: overall view and zoom (with the matrix discretization with triangles) (after Bourbiaux *et al.*, 1999)

2.5. Single Matrix Block Simulation

The idea of using Single Matrix Block (SMB) models comes from the ambition to calculate the recovery process for every single matrix block without assuming uniform pressure and saturation in it. Probably the best way to investigate the matrix recovery process is to calculate it numerically on a finely gridded single porosity model. Such a calculation can be done for small scale laboratory measurement on cores, but also for imaginary matrix blocks situated in the reservoir. The comparison with laboratory data is necessary to increase the level of confidence for conclusions. This would be the best approach on the reservoir scale, too, but it is not applicable from many reasons, ie. it is impossible to identify all individual single matrix blocks and also it would not be possible to handle them due of the CPU and memory limits of computers. Nevertheless SMB calculations are advantageous as reference solutions and as support of conclusions derived from production data.

Different setups of single matrix block (SMB) models and conclusions can be found in the literature: Yamamoto *et al.* (1971), Kleppe and Morse (1974), Fung and Collins (1991), Kazemi, Gilman and Elsharkawy (1992),Chen et al. (1995), Gurpinar and Kossack (2000), Famy *et al.* (2005), Abushaikha and Gosselin (2008), Balogun *et al.* (2009), Ramirez *et al.* (2009) and Al-Kobaisi *et al.* (2009), Mora and Wattenbarger (2009), Wuthicharn and Zimmerman (2011), Su *et al.* (2013). These publications deal with recovery mechanism in fractured reservoirs, primarily with single and two-phase water/oil countercurrent imbibition and gas/oil drainage. A comprehensive summary of them can be found from Czerniak (2015). Without any exception they tried to evaluate a shape factor and using the matrix-fracture transfer function.

It seems that there is no chance to find definitions for shape factors which could make the transfer function Equation 2.2 applicable at least for some well defined practical cases. Nevertheless the excellent work of Su (2013) co-authored by Olivier Gosselin (Imperial

College) and Hadi Prvizi and Marie Ann Giddins (both with Schlumberger) would be sufficient to put a dot at the end of all this efforts. They made calculation on a 1x1x8 dual continuum column model and created an equivalent single porosity model with 48x48x145 = 334,080 cells (Figure 2.5). A commercial flow simulator (Eclipse) was used to calculate both models. They compared fine-grid single-porosity model with a coarse dual-porosity equivalent for gas-oil system under gravity drainage without capillary effects and derived a time dependent shape factor matching the matrix oil saturation. They suggested to use dynamic transfer function and to consider block-to-block effects. Equation 2.6 shows the error estimates for different cases of dual porosity model. How far the today situation from a general and practical solution is can be estimated from the recommendations made by Su *et al.* (2013):

1. "An in-depth study of the block-to-block effect is recommended. "A better understanding of the oil re-imbibition and the quantification of this phenomenon would increase the predictive power of the model."
2. "The effect of capillary pressure needs to be thoroughly studid."
3. "The water-oil gravity drainage study is also recommended to develop a general model for the gravity drainage recovery mechanism."

Su *et al.* concentrated on transfer function formulation existing in reservoir simulators (i.e. in Eclipse). They last recommendation - the only one with which the author agrees - is:

4. "A change of focus to the improvement of the transfer function would be a path to explore."
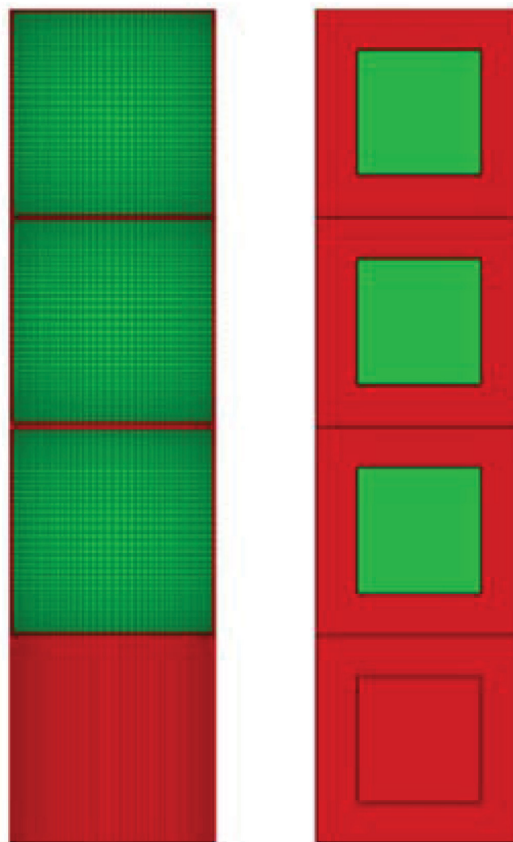
Figure 2.5: Single-porosity model vs. dual-porosity model (form Su *et al.* 2013)
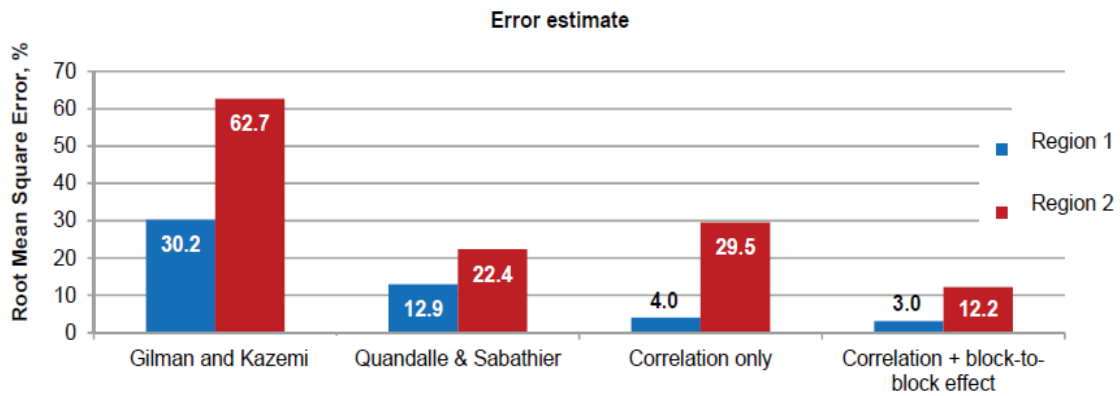
Figure 2.6: Error estimate of the single-porosity model and various cases of dual porosity model (form Su *et al.* 2013)

Su *et al.* (2013) suggest to make the transfer a time dependent function, which would mean to return to the Reiss *et al.*(1973)-Rossen (1977) concept. The reason why this approach would not be applied is that they could not merge the solely pressure dependent depletion drive and the capillary/gravitational drive in one recovery curve. Kazemi *et al.* (1979) integrated all driving forces in one expression of potential gradient (i.e.: in discretized form in an expression of potential difference). All other researcher and developer up to now followed this concept. Heinemann (2004) found the solution to use the recovery functions with contemporarily considering of the depletion drive too. The concept and its practice are explained in Chapter 3 and applied in Chapter 4 to formulate the material balance equation applicable to dual porosity reservoirs.

Chapter 3

Recovery Curve Method for Dual Porosity Reservoirs

3.1 The Recovery Curve

The result of any displacement process can be described by a single function, called recovery curve, displaying the recovery factor versus time, injected pore volume or boundary pressure. This is applied to a matrix block, too. Recovery curves for matrix blocks of NFRs can be obtained in different ways: a) By calculating the displacement process numerically on a fine-gridded single matrix block model; b) Experimentally, by putting a piece of rock in an autoclave filled with water or gas and simulating the possible pressure changes; c) Outputting it from a full field simulation run for any grid cell or a region.

From Equation 2.2:

$$E_R(t) \ = \ \frac{1}{N}\int_0^t q_{omf}(t)dt \ = \ \frac{\sigma k_a}{N}\int_0^t \left(\frac{k_r}{\mu B}\right)_o (\Phi_{of} - \Phi_{om})dt, \tag{3.1}$$

where N is the matrix's original oil in place. After some reforming,

$$E_R(t) \ = \ \frac{\sigma k_a}{N}\int_0^t \left(\frac{k_r}{\mu B}\right)_o (\Phi_{of} - \Phi_{om})dt \tag{3.2}$$

$$= \ \sqrt{\frac{\phi}{k_a}}\frac{k_a \sigma \mu_{oi}}{N s_{owi}}\int_0^t \left(\frac{k_r}{\mu B}\right)_o (\Phi_{of} - \Phi_{om})\sqrt{\frac{k_a}{\phi}}\frac{\sigma s_{owi}}{\mu_{oi}}dt$$

where s_{owi} is the initial oil-water surface tension (used to avoid conflict with the shape factor σ).

Introducing the dimensionless time:

$$t_D = \sqrt{\frac{k_a}{\phi}} \frac{\sigma s_{owi}}{\mu_{oi}} dt = \beta_D t,$$

(3.3)

gets the following form:

$$E_R(t_D) = \sqrt{\frac{\phi}{k_a}} \frac{k_a \sigma \mu_{oi}}{N s_{owi}} \int_0^{t_D} \left(\frac{k_r}{\mu B}\right)_o (\Phi_{of} - \Phi_{om}) dt_D$$

(3.4)

The dimensionless time conversion factor, β_D, is the same as defined by Mattax and Kyte (1962), the difference is that here the oil viscosity instead of those for water was applied. The index i shows that these are initial and therefore constant values.

Based on experiments Mattax and Kyte (1962) showed that in situations where water imbibition is the dominant force for displacing the oil from the matrix, the cumulative oil recovery from the matrix surrounded by water generally can be approximated by an exponential formula:

$$E_R(t_D) = E_{Rmax}(1, -e^{-\lambda t}) = E_{Rmax}\left(1, -e^{-\lambda_D t_D}\right); \quad \lambda_D = \lambda / \beta_D$$

(3.5)

Equation 3.2 shows that the recovery curves/functions are scalable regarding most of the rock and fluid properties, for instance porosity, permeability, viscosity and the dimensionless Leverett capillary curve. In spite of that, Equation 3.4 is not approved for gravitational and viscous drives. From this reason the possibility to display the recovery curve as function of a dimensionless time is restricted to cases with specific and scalable driving forces. This is the case in the Mattax and Kyte (1962) correlation, Equation 3.5, where only the capillary imbibition acts or could be the case with gas-oil gravitational drainage where no capillary pressure is active. In general cases it is more practical to remain in the time domain defining a virtual time valid for a given parameter combination and if feasible to scale up the function to other conditions.

Every recovery curve has an asymptote:

$$E_R(t)\big|_{t\to\infty} \to E_{R\,max},$$

(3.6)

which is the ultimate recovery factor. It is possible to normalize the recovery factor axis. To do so, it has to be multiplied by α being the reciprocal of the ultimate recovery factor. Figure 3.5 is the schematic of a normalized recovery curve as function of the virtual time, t_v. The actual normalized matrix recovery factor defines a virtual time, t_v, on the recovery curve time axis. Adding an arbitrary time step, which is scaled to the virtual time domain by multiplying it with a factor β, the increment in the normalized recovery factor is gained. The factor β can be smaller than, equal to or greater than 1. Conversion of this recovery increment into an oil volume, determines the amount of water or gas injected from the fracture into the matrix. Within the spectrum in which a recovery curve is considered valid, only two parameters, α and β are

necessary for scaling:

$$E_R^n = \alpha E_R; \quad t_\nu = \beta \cdot t \tag{3.7}$$

3.2. Single Matrix Block (SMB) Simulation

3.2.1 Model Building

3.2.1.1 Grid Cell Properties and Parameters

Chapter 2 listed a greater number of authors who used fine-gridded SMB models. A detailed and critical discussion about the model setups and kind of operations is given by Czerniak (2015). Heinemann (2007) suggested to make SMB calculation a standard option in commercial simulation packages, with arbitrary number of grid cells and parameters, flexible boundary settings and conditions. Such an option was also implemented in the software PRS. Pirker (2008) and Amiry (2014) contributed to the development of this tool, widely applied by the author, too. In the following the actual SMB tool will be presented. In absence of references to earlier applications the statements are related to the PRS solution. A SMB tool is indispensable for creating the recovery curves.

The fine-gridded matrix block is bordered by fracture cells with "infinite" pore volume and zero width, representing the boundary with constant or variable pressure and saturations, given by the user. Defining the flux at the boundary (von Neumann boundary condition) would not have a practical application. The boundary fracture cells inject fluids into the matrix and adsorb the fluids expelled from the matrix without altering its pressures and its saturation. The fracture cells will be re-initialized anyway at the beginning of every time step. Along these boundaries, i.e. in the fracture, no fluid is flowing, but setting the cell pressures accordingly, a pressure gradient caused by moving fluid can be emulated.

The SMB grid is a parallelepiped. The size of the matrix can be given by the extension Lx,Ly,Lz or by the shape factor. The usual properties have to be assigned to the grid model: porosity, pore compressibility, permeability values in x-, y- and z-direction: (k_x, k_y, k_z). The permeability is defined by the apparent permeability k_a and the anisotropy coefficients k'_x, k'_y, k'_z . In the isotropic case the values of the last ones are uniformly equal to 1. *The equivalent isotropic permeability* $k_a = \sqrt[3]{k_x k_y k_z}$, would give the actual directional matrix permeability values (of $k_x=k_a*k'_x$, $k_y=k_a*k'_y$ and $k_z=k_a*k'_z$) in x-, y- and z-direction in the principle Cartesian coordinate system. In the case where the vertical permeability k_z=0, the *equivalent isotropic permeability* is $k_a = \sqrt{k_x k_y}$.

In absence of viscous forces no potential gradient exists in the x- and y-directions therefore the SMB model behaves symmetrically and, thus, it is sufficient to calculate only one quarter of the model. The side length of the cube is reduced in *x*- and *y*-direction to $L_x/2$ and $L_y/2$, respectively. Acting gravity does not allow to halve the block height, therefore, the dimension in *z*-direction remains unchanged. The SMB model is used also to evaluate the quality of matrix-fracture transfer functions, therefore, it is important to make this numerical tool so precise as possible. From this reason the blocks are halved at the symmetry lines in the x and y directions and the nodes are set along these lines as it is shown on the Figure 3.1. The corner cell represents the middle of the full SMB model. Figure 3.1 shows a single matrix block model as used in the further investigations with two- and three-dimensional fracture networks.

The capillary and relative permeability functions in the matrix domain have to originate from the object under investigation. There are no restrictions regarding the PVT data, except that the PVT data for both the matrix and the fracture domains have to be the same. In our implementation both black-oil as well as compositional fluid models can be used. The SMB tool operates on a field project for which data are assigned to PVT and ROCK regions.Therefore it is satisfactory to define the serial number of the regions.

Pirker (2007) recommends the 9x9x36 grid cells for the quarter model as generally applicable. However her investigations were limited to solution gas and linear water drive without phase separation. The author (Gharsalla) performed more extended investigations. The question was not only the limit beyond that the grid resolution has no more influence on the results but also which is the overall optimum by considering the CPU time, too. The investigated x/y/z grids were 6x6x11, 7x7x21, 9x9x37 and 12x12x51. The Figure 3.2 compares the recovery curves for water drive, the Figure 3.3 for gas drive. The results show that the conclusions of Pirker where right, but also a more coarse grid could offer applicable result with considerable CPU time saving. A resolution of 7x7x21 is certainly satisfactory for most of the practical cases.
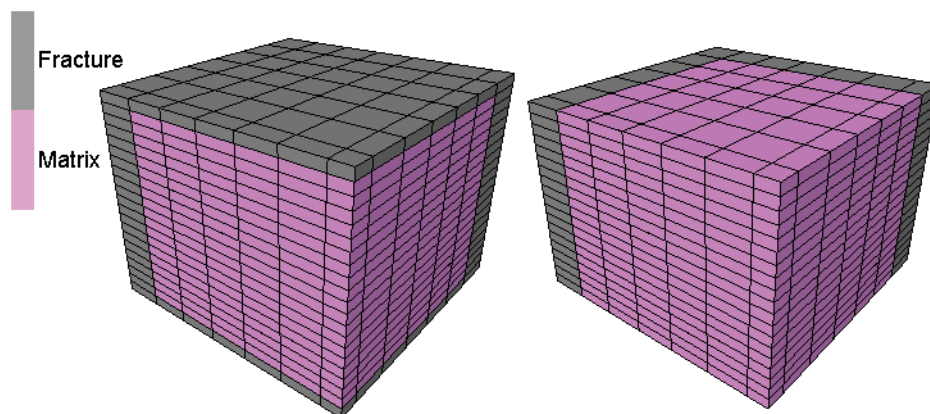
Figure 3.1: The single matrix block model.

Heinemann and Mittermeir (2011) showed that in the case of uniform boundary conditions not the shape itself but the shape factor is decisive. Consequently any arbitrarily-shaped matrix block can be mapped to any other shape as long as the shape factors remains the same. The shape factor depends on the matrix-fracture connection surfaces, its distances from the point of

gravity, the orientation of principle permeability axes (see Equation 2.4) and the surface to volume ratio. The boundary conditions are uniform when the pressure and the saturations are identical at every open side of the of the matrix block and the driving forces are limited to compression and capillary forces. Mora and Wattenbarger (2009a) conducted numerical experiences with irregularly shaped single matrix block using fine-grid simulation with constant pressure boundary conditions. For all the cases analyzed the numerically derived shape factors were within a limit of +/-10% difference.

In cases where also gravitational and/or viscose forces are considered the boundary conditions cannot be uniform and therefore, the equivalency is given only if the matrix block lengths in the direction of the potential gradient are also the same. However, Amiry (2014) showed that not the shape of the matrix itself but the shape factor given by Equation 2.4 and in the case of gravitational and viscous drive the lengths of the block in direction of the potential gradient are decisive. Amiry (2014) concluded that any arbitrarily-shaped matrix block can be mapped to any other arbitrary shape as long as the surface-to-volume ratio and the matrix block length measured along the displacement direction are identical. By accounting only for the gravitational force, this direction is vertical, and the condition reduces to claiming the same matrix block heights. By acting for viscous force the resulting direction of the potential gradient has to be considered. Regarding the viscous force the potential gradient in the flow direction is decisive.

Nevertheless, it is impossible to elicit the individual shapes of all native matrix blocks, therefore, the question addressing second order differences has no practical importance. Amiry (2014) suggested to accept two matrix blocks as being similar (in point of view of the fluid transfer) if their shape factor and height are identical.

The matrix block model is discretized into grid cells. The simple geometrical shapes of the cubic single matrix block models do not require any special gridding technique, therefore simple Cartesian grids are used to discretize the matrix block and the surrounding fracture planes. These fracture planes can be set up in different combinations.They can surround the entire matrix block or only the (vertical) sides. Fracture planes are added to the sides of the matrix block.

The matrix domain is considered to be homogeneous. It should be seen that all parameters in the single matrix examination are highly hypothetical. Note that none of the principal permeability directions is necessarily vertical. Nevertheless for simplicity it is advisable to align the model vertically and assume that the permeability coordinate axes are identical with the geometrical ones. The fracture cells represents a boundary therefore their properties do not effect the matrix displacement process. A fracture cell communicates with a single matrix cell but not with the neighboring fracture cells. That means that no flow takes place within the fracture plans. From technical reason parameters are defaulted in the fracture cells: E.g.: extension in direction of the matrix neighbor is 0.0001 m and pore volume is 10000-times of a matrix cell. In this case the matrix-fracture transmissibility is determined by the matrix side only and fluid expelling from the matrix does not change the saturation in the fracture cell. The fracture cells will be re-initialized anyway at the beginning of every time step.
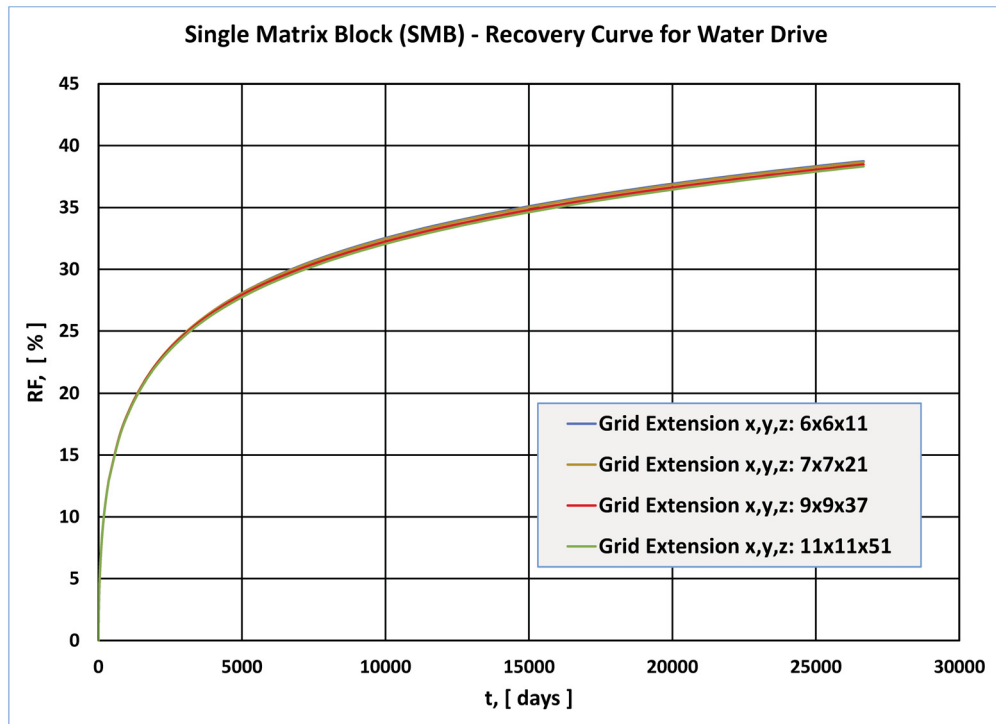
Figure 3.2: Sensitivity analysis on grid cell number, water drive.
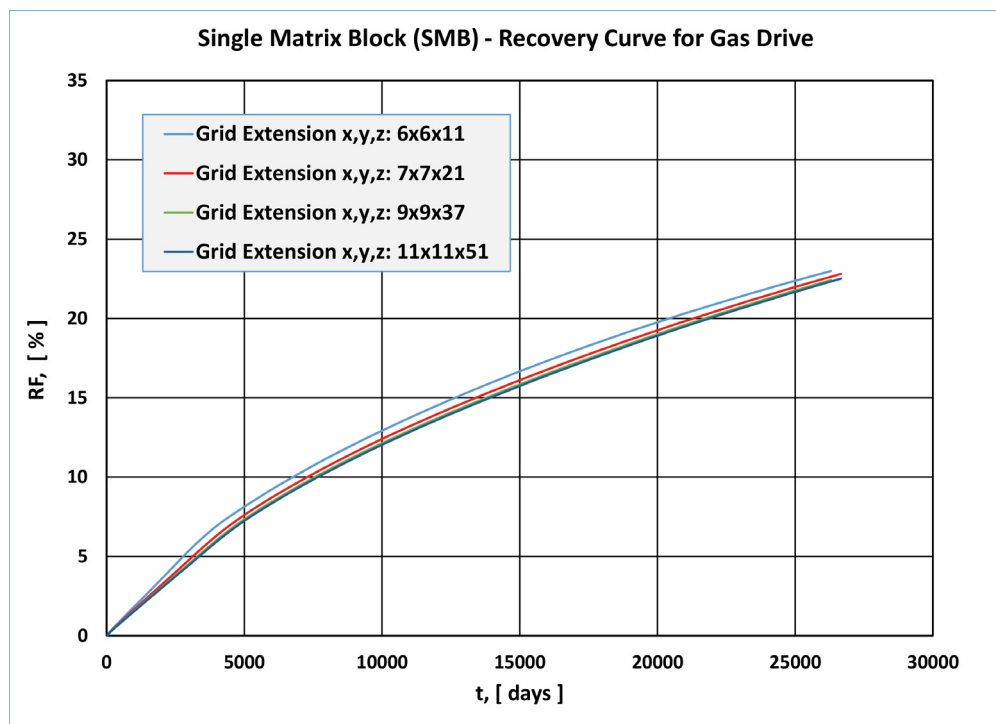
Figure 3.3: Sensitivity analysis on grid cell number, gas drive.

3.2.2 Operating of Single Matrix Block Models

The fracture, depending on the desired scenario, is either fully saturated with oil, water or gas. The fracture cell pressure provides the desired boundary conditions e.g. hydrostatic pressure distribution, any pressure gradient along the grid block side or fluid movement in a given direction. The fluid content can be changed from one phase to the other and then back and the pressure can be decreased or increased gradually. Note that in this context the fracture domain is not intended to be a medium of fluid flow, but just a boundary to the matrix cells. The fracture volume has no effect in the process as its content is not counted in the calculations. However, it has to be large enough, so that the saturation of the fracture cells does not effectively change while oil and gas flows out from the matrix until it is removed from the fracture at the end of each time step. No capillary pressure or relative permeability is needed for the single phase fracture cells. The capillary pressures in the fracture are considered being zero. This is a direct consequence of assuming a single phase in the fracture but also an implication of some practical considerations.

Expansion and solution gas drive can be modeled by filling and re-filling the fracture with oil having slightly higher bubble-point pressure than the matrix oil. In this case neither gravitational nor capillary forces become effective. The pressure will be lowered step by step in the fracture simulating a depletion drive. The recovery factor is given by the actual amount of oil in the matrix and can be displayed as a function of the average pressure. The same process can be calculated by handling the matrix block as barrel using finite difference material balance (see Pirson 1958, 508, his Eq. 10-45) which provides the average matrix gas saturation directly.

For modeling a water drive the fracture has to be filled with water. The result of the SMB calculation provides the oil recovery rate but also the average water saturation of the matrix as a function of time. Likewise, for a gas drive the fracture is filled with gas and the average matrix gas saturation is recorded.

Figure 3.4 shows water and gas drive recovery curves calculated on a single matrix block model at constant pressure. In this case the driving force results from the capillary pressure and the gravitational forces. In both cases the results with vertical and with all-side fracture arrangements are displayed.
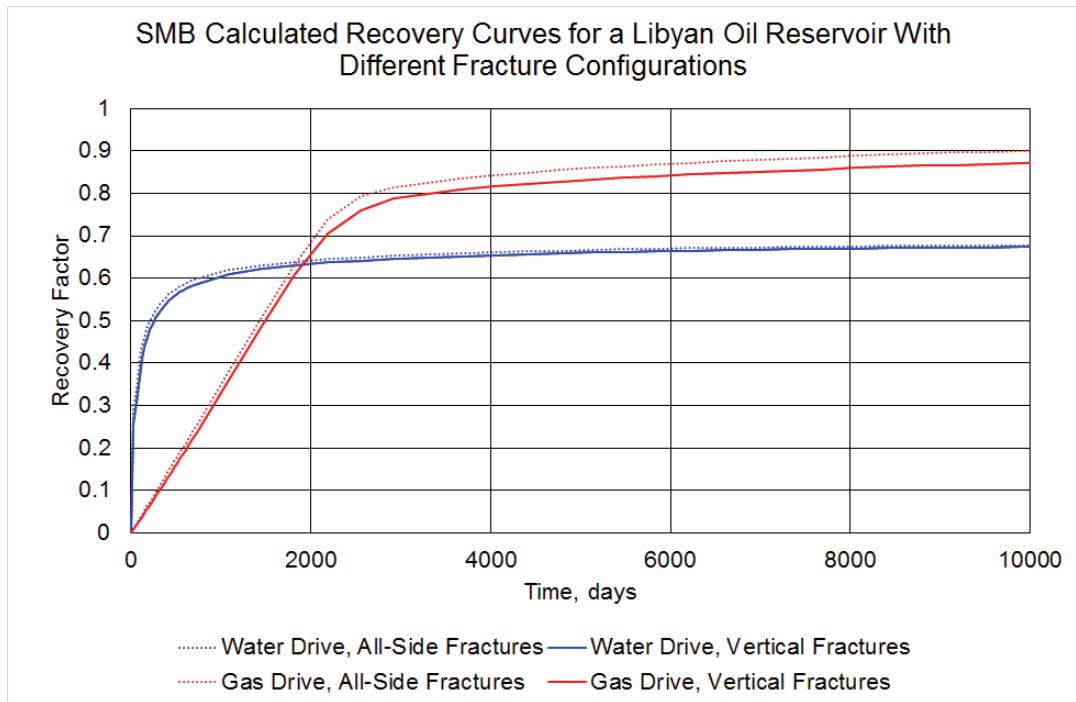
Figure 3.4: SMB water and gas displacement recovery curves with different fracture configurations

Figure 3.5 shows the schematic of a normalized recovery curve $E^n(t)$. The recovery process is governed by two parameters, the asymptotic value $(1/\alpha)$ of the recovery function and the time scaling factor, β. The virtual time t_v is determined by the normalized recovery factor $E^n_j = \alpha E_j$ where α is the reciprocal of the ultimate (maximum) recovery factor for the given displacement mechanism. The recovery increment $\Delta_{j+1}E = (E^n_{j+1} - E^n_j)/\alpha$ during the next time step $\Delta_{j+1}t$ can be read at the virtual time $t_{vj+1} = t_{vj} + \beta\Delta_{j+1}t$.
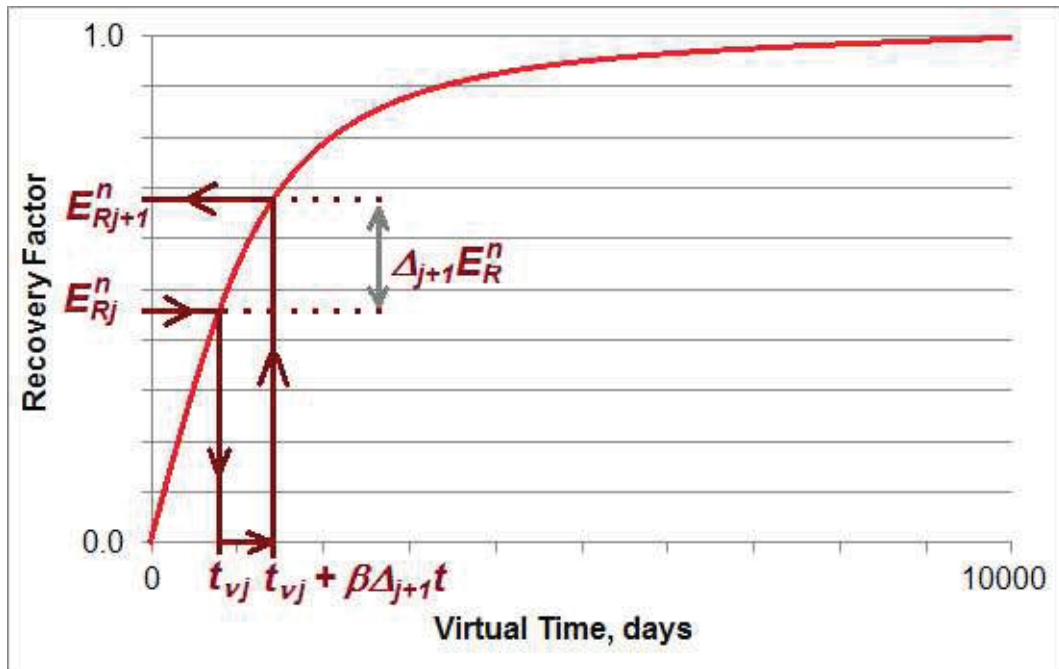
Figure 3.5: Schematic of a normalized recovery curve; determination of recovery increment based on virtual time

3.3 Matrix-Fracture Fluid Transfer Based on Recovery Curves

Heinemann (2004) separated the time dependent capillary imbibition and gravitational drives from the time independent expansion drive. For the first ones he applied the concept of Reiss *et al.* (1973) and Rossen (1977) and used the recovery curves and for the second the Kazemi *et al.* (1976) transfer function. At the beginning the fractures are filled with oil and the oil from the matrix is produced into the fractures according the fluid/rock expansion and by solution gas drive. This is a purely pressure depending process.

After the matrix block is reached by the water or/and gas the fracture injects water or/and gas into the matrix. Figure 3.6 shows a theoretical case in which both the water and gas tables (dynamic phase contacts) cut the matrix block. Practically, this will not happen because the oil zone between the two contacts has to be a multiple of the simulation cell thicknesses. Considering full phase segregation the fracture cell saturations S_{wf} and S_{gf} give the proportion of the matrix cell in which the fracture injects water and gas into the matrix cell. In most of the cases the recovery curves will be obtained from single matrix block simulation considering a single displacing phase in the fracture.
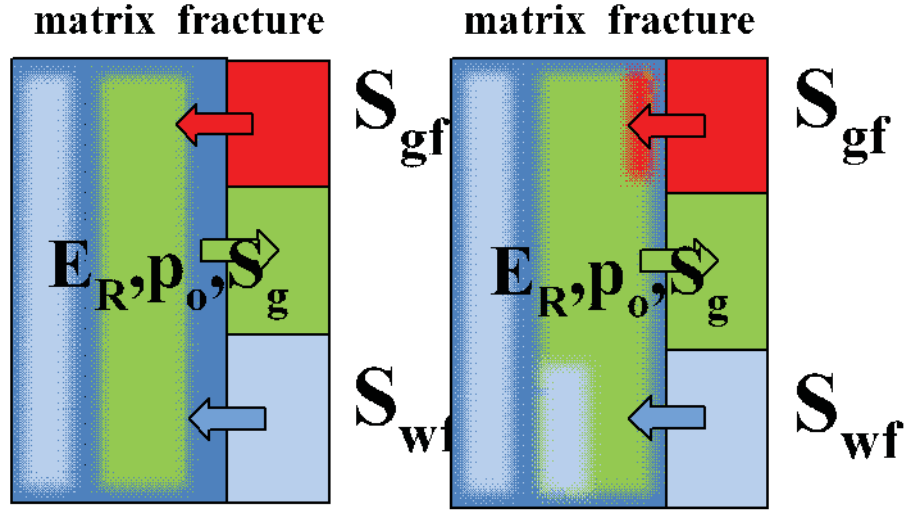
Figure 3.6: Explanation to matrix-fracture fluid transfer using recovery curves with homogenous (a) and segregated (b) fluid distribution in the matrix

The situation when using these curves is equivalent to the assumption that the recovery factor resulting from both the water and gas drive curves remains valid independently from the recovery history. Figure 3.5 shows a schematic of a normalized recovery curve which will be given separately for water and gas drives. Let E_R be the cell recovery factor at time t_j. The normalized recovery factor values of $\alpha^w E_R$ and $\alpha^g E_R$ correspond to the virtual times t_v^w and t_v^g on the normalized water and gas recovery curves respectively. Adding now an arbitrary time step $\Delta_{j+1}t$ and reading the normalized recovery factors at the new virtual time on the recovery curves

$$t_{vj+1}^w = t_{vj}^w + \beta^w \Delta_{j+1}t; \tag{3.8}$$

$$t_{vj+1}^g = t_{vj}^g + \beta^g \Delta_{j+1}t \tag{3.9}$$

results in the recovery factor increments:

$$\Delta_{j+1}E_k^w = (E_k^{nw}(t_{vj+1}^w) - E_k^{nw}(t_{vj}^w))/\alpha^w; \tag{3.10}$$

$$\Delta_{j+1}E_k^g = (E_k^{ng}(t_{vj+1}^g) - E_k^{ng}(t_{vj}^g))/\alpha^g \tag{3.11}$$

It is assumed that the amount of the injected water can be estimated from the water drive recovery curve which was elaborated for a two phase water displacement. Let be $\Delta_{j+1}E_k^w$ the oil recovery increment from the water drive for the time step interval $\Delta_{j+1} = t_{j+1} - t_j$. In an undersaturated case the specific water inflow during the same time period is:

$$q_{wmf} = N_k \Delta_{j+1} E_k^w \cdot (S_{wf} B_o / B_w)_{j+1} , \qquad (3.12)$$

$$q_{gmf} = N_k \Delta_{j+1} E_k^g \cdot (S_{gf} B_o / B_g)_{j+1} . \qquad (3.13)$$

In the saturated case (below the initial bubble-point pressure) free gas saturation exists in the matrix already. The water injected by the fracture to the matrix tranche will also displace free gas, flowing from the matrix to the fracture, and therefore:

$$q_{wmf} = N_k \Delta_{j+1} E_k^w \cdot S_{wfj+1} \cdot [B_{oj+1} + B_{gj+1}(\overline{R_{pk}} - R_{sj+1})] / B_{wj+1} \qquad (3.14)$$

The injecting agent would comprise the fluids exiting the matrix cell but due to their concurrent expansion fluids expel from the matrix cell. The amount of fluids transferred into the fracture can be calculated by the transfer function:

$$q_{omf} = \sigma k_a \frac{k_{ro}}{\mu_o B_o} (p_{om} - p_{of}) \text{ [sm}^3/\text{s]}, \qquad (3.15)$$

The same equation is applied to the water and free gas phase, by replacing the subscript "o" by "w" and "g".

The water and gas drive recovery curves will be determined at constant pressure, favorably at the bubble point pressure. Heinemann and Mittermeir (2015) showed that if the relative permeability endpoints do not change, they remain valid at different pressures. The efficiency of the displacement depends on the oil mobility only, therefore, the recovery increment will be:

$$\Delta E_R^w(p) = \left(\left(\frac{k_{ro}(S_{gc})}{\mu B} \right)_o \Big/ \left(\frac{1}{\mu B} \right)_{ob} \right) \Delta E_R^w(p_b) \qquad (3.16)$$

$$\Delta E_R^g(p) = \frac{\mu(p)B(p)}{\mu(p_b)B(p_b)} \Delta E_R^g(p_b) \qquad (3.17)$$

Chapter 4

Material Balance for Naturally Fractured Dual Porosity Reservoirs

In the following at first the elements of the applied dual porosity material balance technique will be presented. Afterwards the workflow will be introduced.

4.1 The Twin Barrels

As mentioned already, the starting point of any dynamic reservoir calculation is the geocellular model, initialized in black oil mode. Setting horizontal tranches of unit thickness (arbitrary thicknesses are also possible) starting at the initial Oil Water Contact (OWC) through the grid model and summating the fluid amounts along the tranches results in two columns. One column represents the matrix and the second the fracture continuum. This is illustrated in Figure 4.1.
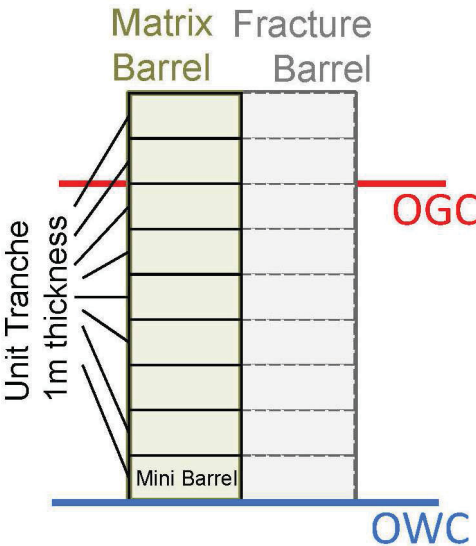
Figure 4.1: Dual porosity MB at initial conditions

As a consequence, the vertical distribution of the fluids and the position of the initial Oil-Water-Contact (OWC) and Oil Gas Contact (OGC) are known. The tranches are numbered (k=1, 2, .., M) starting from the initial OWC upwards. M corresponds to the top of the reservoir. The vertical distributions of the oil in place and other properties and variables (e.g.: pore volume, initial water saturation, etc.) are reserved similarly. The extensive values (e.g.: OOIP, pore volume) are the sum over the horizontal tranches through the reservoir, the intensive values (e.g. S_{wi}, which is the initial water saturation) are averaged over that.

In the following different indices will be used:

- o, g, w denote the phases oil, gas and water,
- i is the initial value,
- m and f denote the matrix and fracture respectively,
- k is the serial number of the unit tranches, measured from the original OWC upwards,
- j is the time step counter, t_j is the production time.

In the grid model every cell has its own pressure. In the MB model only one average pressure is considered. Besides the fluids in place also the pore volume can be summed up for the tranches but this has to be corrected corresponding to the reservoir volume of the fluids at the average pressure. The fluid in a tranche k has to be flashed at the average pressure giving the pore volume (V_k):

$$V_k = N_k B_o(p_i, R_{si}) + G_k B_g(p_i) + W_k B_w(p_i) \tag{4.1}$$

where N_k, G_k, W_k are original amounts of oil, free gas and water in the tranche k, the B_o, B_g, B_w, are the formation volume factors for the three phases oil, gas and water, p_i is the average initial pressure and R_{si} the average solution gas/oil ratio (GOR). Index i denotes the initial state. Please note that the initial pressure p_i corresponds to the entire MB model and not only to one tranche.

Equation 4.1 has to be applied to both the matrix (index m) and to the fracture (index f) continuum. The fracture column defines the boundary condition for the matrix column.

The Material Balance (MB) given in Equation 4.2 is valid for saturated and undersaturated oil reservoirs, for gas reservoirs with and without water influx from an aquifer, considering the compressibility of the rock and the connate water and possible water and gas injections.

$$N\left[B_o - B_{oi} + B_g(R_{si} - R_s) + \frac{B_{oi}(c_\phi + S_{wi}c_w)(p_i - p)}{1 - S_{wi}}\right] + G(B_g - B_{gi}) + W_e B_w \tag{4.2}$$

$$= N_p[B_o + B_g(R_p - R_s)] + W_p B_w - (W_I B_w + G_I B_g)$$

Usually the constant term for the rock and water compressibility is replaced by an apparent pore volume compressibility factor $c_{\phi a}$ given by:

$$c_{\phi a} = \frac{c_\phi + S_{wi}c_w}{1 - S_{wi}} = \frac{c_\phi + S_{wi}c_w + c_w - c_w}{1 - S_{wi}} = \frac{c_\phi + c_w}{1 - S_{wi}} - c_w \tag{4.3}$$

The initial free gas volume G can be also expressed by the gas cap factor m, the original oil in place N and the formation volume factors of oil (B_{oi}) and gas (B_{gi}).

$$G = \frac{mNB_{oi}}{B_{gi}} \tag{4.4}$$

Inserting the relations Equation 4.3 of and Equation 4.4 in Equation 4.2:

$$N[B_o - B_{oi} + B_g(R_{si} - R_s)] + NB_{oi}c_{\phi a}(p_i - p) + mNB_{oi}\left(\frac{B_g}{B_{gi}} - 1\right) + W_e B_w \tag{4.5}$$

$$= N_p[B_o + B_g(R_p - R_s)] + W_p B_w - (W_I B_w + G_I B_g)$$

Dividing Equation 4.5 now by the gas formation volume factor B_g gives:

$$N\left[\frac{B_o}{B_g} - \frac{B_{oi}}{B_g} + (R_{si} - R_s)\right] + \frac{NB_{oi}}{B_g}c_{\phi a}(p_i - p) + mNB_{oi}\left(\frac{1}{B_{gi}} - \frac{1}{B_g}\right) + \frac{W_e B_w}{B_g} \tag{4.6}$$

$$= N_p\left[\frac{B_o}{B_g} - R_s\right] + N_p R_p + \frac{W_p B_w}{B_g} - \left(\frac{W_I B_w}{B_g} + G_I\right)$$

Equation 4.6 can now be written for time points j and $j+1$. Writing Equation 4.6 for time point j will lead to:

$$N\left[\frac{B_{oj}}{B_{gj}} - \frac{B_{oi}}{B_{gi}} + (R_{si} - R_{sj})\right] + \frac{NB_{oi}}{B_{gj}}c_{\phi a}(p_i - p_j) + mNB_{oi}\left(\frac{1}{B_{gi}} - \frac{1}{B_{gj}}\right) + \frac{W_{ej} B_{wj}}{B_{gj}} \tag{4.7}$$

$$= N_{pj}\left[\frac{B_{oj}}{B_{gj}} - R_{sj}\right] + N_{pj} R_{pj} + \frac{W_{pj} B_{wj}}{B_{gj}} - \left(\frac{W_{Ij} B_{wj}}{B_{gj}} + G_{Ij}\right)$$

For writing Equation 4.6 at time point $j+1$ the index j of Equation 4.7 simply has to be replaced by $j+1$. Please note that for variables of cumulative production/injection (N_p for produced oil, W_I for injected water, etc.) the increment Δ_{j+1} of the production/injection for the time step will be written.

$$N\left[\frac{B_{oj+1}}{B_{gj+1}} - \frac{B_{oi}}{B_{gj+1}} + (R_{si} - R_{sj+1})\right] + \frac{NB_{oi}}{B_{gj+1}}c_{\phi a}(p_i - p_{j+1}) \tag{4.8}$$

$$+ mNB_{oi}\left(\frac{1}{B_{gi}} - \frac{1}{B_{gj+1}}\right) + \frac{(W_{ej} + \Delta_{j+1}W_e)B_{wj+1}}{B_{gj+1}}$$

$$= (N_{pj} + \Delta_{j+1}N_p)\left[\frac{B_{oj+1}}{B_{gj+1}} - R_{sj+1}\right] + N_{pj}R_{pj} + \Delta_{j+1}N_p\overline{R_p}$$

$$+ \frac{(W_{pj} + \Delta_{j+1}W_p)B_{wj+1}}{B_{gj+1}} - \left(\frac{(W_{Ij} + \Delta_{j+1}W_I)B_{wj+1}}{B_{gj+1}} + (G_{Ij} + \Delta_{j+1}G_I)\right)$$

It should be noted that for time point j the cumulative gas production G_{pj} could be expressed by the cumulative oil production N_{pj} and the overall production gas/oil ratio R_{pj}. This means:

$$G_{pj} = N_{pj}R_{pj} \tag{4.9}$$

Therefore at time point $j+1$ the cumulative gas production G_p is equal to:

$$G_{pj+1} = G_{pj} + \Delta_{j+1}G_p = G_{pj} + \Delta_{j+1}N_p\overline{R_p} \tag{4.10}$$

where $\overline{R_p}$ is the average production gas/oil ratio for the time period t_j, t_{j+1}. Subtracting Equation 4.7 from Equation 4.8 results in the differential form of the material balance:

$$N\Delta_{j+1}\left(\frac{B_o}{B_g} - R_s\right) - NB_{oi}\Delta_{j+1}\left(\frac{1}{B_g}\right) + NB_{oi}p_ic_{\phi a}\Delta_{j+1}\left(\frac{1}{B_g}\right) - NB_{oi}c_{\phi a}\Delta_{j+1}\left(\frac{p}{B_g}\right) \tag{4.11}$$

$$+ mNB_{oi}\Delta_{j+1}\left(\frac{1}{B_g}\right) + W_{ej}\Delta_{j+1}\left(\frac{B_w}{B_g}\right) + \Delta_{j+1}W_e\left(\frac{B_w}{B_g}\right)_{j+1}$$

$$= N_p\Delta_{j+1}\left(\frac{B_o}{B_g} - R_s\right) + \Delta_{j+1}N_p\left[\left(\frac{B_o}{B_g} - R_s\right)_{j+1} + \overline{R_p}\right]$$

$$+ W_{pj}\Delta_{j+1}\left(\frac{B_w}{B_g}\right) + \Delta_{j+1}W_p\left(\frac{B_w}{B_g}\right)_{j+1} - W_{Ij}\Delta_{j+1}\left(\frac{B_w}{B_g}\right) - \Delta_{j+1}W_I\left(\frac{B_w}{B_g}\right)_{j+1} - \Delta_{j+1}G_I$$

From Equation 4.11 the increment in oil production ΔN_p for the time period t_j, t_{j+1} is expressed as:

$$\Delta_{j+1}N_p = \frac{(N-N_p)\Delta_{j+1}\left(\dfrac{B_o}{B_g} - R_s\right)}{\left[\left(\dfrac{B_o}{B_g} - R_s\right)_{j+1} + \overline{R_p}\right]} \tag{4.12}$$

$$+ \frac{NB_{oi}\Delta_{j+1}\left(\dfrac{1}{B_g}\right)(p_i c_{\phi a} - 1) - NB_{oi}c_{\phi a}\Delta_{j+1}\left(\dfrac{p}{B_g}\right) + mNB_{oi}\Delta_{j+1}\left(\dfrac{1}{B_g}\right)}{\left[\left(\dfrac{B_o}{B_g} - R_s\right)_{j+1} + \overline{R_p}\right]}$$

$$+ \frac{W_{ej}\Delta_{j+1}\left(\dfrac{B_w}{B_g}\right) - W_{pj}\Delta_{j+1}\left(\dfrac{B_w}{B_g}\right) + \Delta_{j+1}W_e\left(\dfrac{B_w}{B_g}\right)_{j+1} - \Delta_{j+1}W_p\left(\dfrac{B_w}{B_g}\right)_{j+1}}{\left[\left(\dfrac{B_o}{B_g} - R_s\right)_{j+1} + \overline{R_p}\right]}$$

$$+ \frac{W_{Ij}\Delta_{j+1}\left(\dfrac{B_w}{B_g}\right) + \Delta_{j+1}W_I\left(\dfrac{B_w}{B_g}\right)_{j+1} + \Delta_{j+1}G_I}{\left[\left(\dfrac{B_o}{B_g} - R_s\right)_{j+1} + \overline{R_p}\right]}$$

For sake of easier explanation in the main part of this work Equation 4.12 will be written for a unit initial oil volume. In this case the cumulative oil production N_p becomes the recovery factor E itself. The terms for the produced water (W_p), the water encroachment (W_e) and the injected cumulative amounts of water (W_I) and gas (G_I) have to be scaled to unit oil in place. In the applied notation those scaled amounts will be expressed by lower case symbols w for water and g for gas. Finally the increase in recovery factor $\Delta_{j+1}E = E_{j+1} - E_j$ during a single time step $\Delta t = t_{j+1} - t_j$ is given by Equation 4.13. For reasons of simplicity, especially not to overload the herein presented equations with a lot of subscripts, the symbol E instead of the standardized symbol E_R will be used throughout this work for the overall recovery factor.

$$\Delta_{j+1}E = \frac{(1-E)\Delta_{j+1}\left(\frac{B_o}{B_g}-R_s\right)}{\left[\left(\frac{B_o}{B_g}-R_s\right)_{j+1}+\overline{R_p}\right]} \tag{4.13}$$

$$+ \frac{B_{oi}\Delta_{j+1}\left(\frac{1}{B_g}\right)(p_i c_{\phi a}-1)-B_{oi}c_{\phi a}\Delta_{j+1}\left(\frac{p}{B_g}\right)+mB_{oi}\Delta_{j+1}\left(\frac{1}{B_g}\right)}{\left[\left(\frac{B_o}{B_g}-R_s\right)_{j+1}+\overline{R_p}\right]}$$

$$+ \frac{w_{ej}\Delta_{j+1}\left(\frac{B_w}{B_g}\right)-w_{pj}\Delta_{j+1}\left(\frac{B_w}{B_g}\right)+\Delta_{j+1}w_e\left(\frac{B_w}{B_g}\right)_{j+1}-\Delta_{j+1}w_p\left(\frac{B_w}{B_g}\right)_{j+1}}{\left[\left(\frac{B_o}{B_g}-R_s\right)_{j+1}+\overline{R_p}\right]}$$

$$+ \frac{w_{Ij}\Delta_{j+1}\left(\frac{B_w}{B_g}\right)+\Delta_{j+1}w_I\left(\frac{B_w}{B_g}\right)_{j+1}+\Delta_{j+1}g_I}{\left[\left(\frac{B_o}{B_g}-R_s\right)_{j+1}+\overline{R_p}\right]}$$

4.2 Pressure Match and Water Encroachment

The pressure behavior of the two barrels does not differ from the single porosity case. Production and injection take place within the fractures and water encroaches from the aquifer through the fractures. It can be assumed that the matrix pressure will be instantaneously equalized. It is difficult to imagine that a matrix-fracture pressure difference could exist over longer time. From this reason the water inflow and the aquifer model can be assessed in a manner similar to a single porosity case.

The overall material balance (as it was already presented by Tarner (1944)) has to consider both domains in one common barrel. From Equation 4.5 the water influx can be expressed as a function of time (see Equation 4.14), calculated for every time step by inserting the cumulative production/injection for oil, gas and water and by calculating the PVT values at the actual average reservoir pressure p_j.

$$W_e(t_j) \;=\; -\frac{1}{B_{wj}}\{N[B_{oj} - B_{oi} + B_{gj}(R_{si} - R_{sj})] + NB_{oi}c_{\phi a}(p_i - p_j) + mNB_{oi}(B_{gj}/B_{gi} - 1) \quad (4.14)$$

$$- N_{pj}[B_{oj} + B_{gj}(R_{pj} - R_{sj})] - W_{pj}B_{wj} + (W_{Ij}B_{wj} + G_{Ij}B_{gj})\}$$

It has to be emphasized that N is here the overall OOIP of the fracture and the matrix. Based on the function $W_e(t_j)$ one of the well-known analytical aquifer models such as Fetkovich (1971), Van Everdingen and Hurst (1949) or Carter and Tracy (1960) can be identified as the best fitting one and their parameters can be determined. The Fetkovich model has two governing parameters, the other two three.

Such models can be used to predict the future water inflow and pressure development. It is clear that the water enters in the fracture system and from that invades parts of the matrix. Equation 4.14 does not provide any information about the fluid transfer between the two continua or distinguishes between its actual fluid contents.

4.3   Oil Recovery from the Matrix

The matrix tranches can be regarded as mini-barrels, isolated from each other, but communicating with the fractures. The fracture pressure and the fluid(s) at the tranche face provide the boundary conditions for the matrix recovery process. Three basic situations exist. Firstly, the pressure drops at the fracture face and invokes fluid expansion and solution gas drive in the matrix. The fluids move, as soon as they become mobile, from the matrix to the fracture. This is the classic case of a depletion drive. The production term is given by the amount of fluids expelled from the matrix. Secondly, the water table arrives at a given matrix tranche and the fracture system injects water into the matrix. The efficiency of gas displacement evoked by an expanding initial or secondary gas cap can be evaluated in a similar manner.

The incremental recovery factor for a matrix tranche can be calculated from the finite difference material balance given by Pirson (1958, 508, his Eq. 10-45). The derivation of the incremental recovery factor can be found in Section 4.1. The matrix tranche has no gas cap (m=0), no water influx ($w_e = 0$) and no water production ($w_p = 0$) takes place from it. For one time step $\Delta_{j+1}t \;=\; t_{j+1} - t_j$ the pressure change is $\Delta_{j+1}p \;=\; p_{j+1} - p_j$. Applying those assumptions to Equation 4.13 the recovery factor increment for one matrix tranche k is given by:

$$\Delta_{j+1}E_k = \frac{(1-E_k)\Delta_{j+1}\left(\frac{B_o}{B_g}-R_s\right)+B_{oi}\Delta_{j+1}\left(\frac{1}{B_g}\right)(p_i c_{\phi a}-1)-B_{oi}c_{\phi a}\Delta_{j+1}\left(\frac{p}{B_g}\right)}{\left[\left(\frac{B_o}{B_g}-R_s\right)_{j+1}+\overline{R_p}\right]}$$

$$+\frac{w_{Ikj}\Delta_{j+1}\left(\frac{B_w}{B_g}\right)+\Delta_{j+1}w_{Ik}\left(\frac{B_w}{B_g}\right)_{j+1}+\Delta_{j+1}g_{Ik}}{\left[\left(\frac{B_o}{B_g}-R_s\right)_{j+1}+\overline{R_p}\right]}$$ (4.15)

where Δ_{j+1} denotes the change of the following entity during the time interval $\Delta_{j+1}t = t_{j+1}-t_j$.

In an undersaturated case ($p_j > p_b$) R_s will be constant ($R_{sj} = R_{sj+1} = R_{si}$) and no free gas will be flowing between the matrix and the fracture, therefore, the average production gas/oil ratio will be equal to the initial solution gas/oil ratio ($\overline{R_p} = R_{si}$). In saturated case ($p_j < p_{bi}$) the GOR for the matrix to fracture oil transfer $\overline{R_{pk}}$ is given by Equation 5.7.

The oil will be recovered form the tight matrix by a combination of different driving mechanisms. They are listed in Section 2.2 already: (1) rock compressibility, (2) single phase fluid expansion, (3) solution gas drive, (4) capillary imbibition, (5) gravity drainage, (6) viscous forces and (7) diffusion. The first group is built by the mechanisms (1) to (3), governed by the force of compression and are incorporated in the *first term* of Equation 4.15. Their impact – disregarding only the theoretically interesting transient effects – depends just on the pressure change of the system. The driving force in (4) originates from the saturation of the displacing phase in the fracture around the matrix block and is purely time-dependent. The gravitational (5) and viscous (6) forces depend furthermore on the pressure gradient, which naturally changes over time, along the matrix block. The mechanism (4) to (6) are the fracture to matrix injection, represented by *second term* of Equation 4.15. There $\Delta_{j+1}w_{Ik}$ and $\Delta_{j+1}g_{Ik}$ are the amounts of water and gas injected from the fracture to matrix. Those terms will be defined in more detail later on in Equation 5.4 and Equation 5.5 for water and Equation 5.10 for gas respectively. Compaction cannot have influence on the rigid matrix blocks and diffusion could be considered solely in compositional formulation.

The positions of the phase contacts and the volume of the oil column are determined by the amount of the oil transferred from the matrix to the fracture system; therefore, a close relationship must exist between the position of the phase contacts and the recovery curves. This means that it is possible to evaluate the aquifer by matching the pressure and to determine the recovery curves by matching the phase contacts over the entire production history.

The recovery curve valid for a matrix block is influenced by rock properties such as shape factor, porosity, permeability, and relative permeability, and also by wettability, capillary

pressure, gravitational and viscous forces. A recovery curve based on field data (i.e., on production history) makes it possible to verify some of those properties. In reservoirs where only two mobile phases exist, the parameter identification seems to be straight forward. In more complicated situations, such as three mobile phases, the combination of different displacement mechanisms and processes requires greater explanation and assessment of their limitations.

Note that material balance calculation is a proxy method offering fast results and does not replace numerical simulation models.

Chapter 5

Application of the Recovery Curves in Material Balance Calculation

The Matrix-Fracture Transfer Rates evoked by water or gas displacement is determined by the recovery curves which will be considered in the Equation 4.15 as a water and a gas injection term. The MB equation provides, therefore, the recovery factor increment containing the contribution from the depletion drive, too. How the recovery curve were calculated and how they are used in a discrete numerical model was already explained in Chapter 3. Their implementations in the numerical simulation and in the MB models are slightly different, therefore some aspects will be repeated here.

The recovery curve method is tightly connected to the classical matrix-fracture transfer calculation. Both are based on the same physical description. A reservoir engineer dealing with a NFR has to evaluate/estimate the shape factors, the permeability, the porosity and the height of the matrix blocks, the relative permeability and capillary pressure functions. If all these properties do not explain the observations then a fitting is cumbersome. The aggregated effects of all mentioned properties are on the recovery curves the maximum recovery factor (asymptote of the curve) and the time scale. A sound engineering judgment helps assessing and fitting such a curve in most of the cases.

After production startup the average pressure of the reservoir will drop. Water encroachment at the bottom and expansion of a (primary or secondary) gas cap will cause a movement of the phase contacts (OWC and OGC). The pressure and saturation changes in the fracture alter the boundary conditions at any elementary matrix tranche. Depending on the governing recovery mechanism the recovery increment is either determined by the pressure change (depletion – single phase expansion and solution gas drive) or the elapsed time (water imbibition and gas drainage – water and gas drive).

5.1 Assumptions

The herein introduced dual porosity material balance method is based on the following assumptions:

1. The model is based on the dual porosity – single permeability approach; the fluid distribution will be balanced vertically in the fracture but not in the matrix column.
2. Full phase segregation is considered in the fracture column.
3. The matrix permeability is large enough that the fracture-matrix pressures equalize. In practical cases this means that the matrix permeability is greater than 0.01 mD and pressure differences are less than 1 bar (14.7 psi).
4. The initial matrix water saturation, resulting from the geocellular model, will not be uniform. These water saturations are considered as irreducible.
5. No water flow from the matrix into the fracture will be considered. This means the increase of the matrix water saturation is irreversible.
6. Three recovery mechanism will be considered for the matrix:
   6.1 Depletion (single phase expansion, solution gas drive). This drive mechanism is active in the entire model. Those parts of the model, where this is the sole drive mechanism are referred to as Zone 1 in the following.
   6.2 Water displacement. Water drive is active only for those portions of the matrix where the belonging fracture is water filled. This water zone – later also referred to as Zone 3 – is below the dynamic OWC.
   6.3 Gas displacement. Analogously to the water drive, this drive mechanism is active only for those matrix cells where the belonging fracture contains free gas only. This gas zone is above the dynamic OGC and will be referred to as Zone 2.
7. Production occurs from the fracture domain and the rates are defined for oil, gas and water independently. No outside production constraints (maximum water cut, maximum GOR, minimum pressure, etc.) will be applied.
8. The phase conditions inside the fracture must fit to the imposed target production, leading to inherent production constraints. Considering the production GOR two cases must be considered. First it cannot be less than the solution GOR and second it cannot be greater than the solution GOR in absence of free gas in the fracture. The water cut (WC) has to be zero as long as no water exists in the fracture.

A saturated reservoir with an initial gas cap should be considered. Figure 5.1 sketches this reservoir at two states. At initial state where $t_j = 0$ and at a state with elapsed production time $t_j > 0$. For $t_j > 0$ the average pressure has dropped from p_i to p_j. One can distinguish between three zones determined by the phase contacts in the fracture system. The corresponding dual porosity MB model is sketched in Figure 5.2.

At the time point j the actual state of any tranche k is defined by the uniform pressure p_j, the recovery factor E_{kj} and for the water invaded zone eventually by the gas saturation S_{gkj} also. The recovery factor itself determines the oil saturation for all tranches $k = 1, M$:

$$S_{okj} = (1 - S_{wki}) \cdot (1 - E_{kj}) B_{oj} / B_{oi} \tag{5.1}$$

where S_{wik} is the initial water saturation, considered also as irreducible. Note that the initial water saturation resulting from the geocellular model will not be uniform.
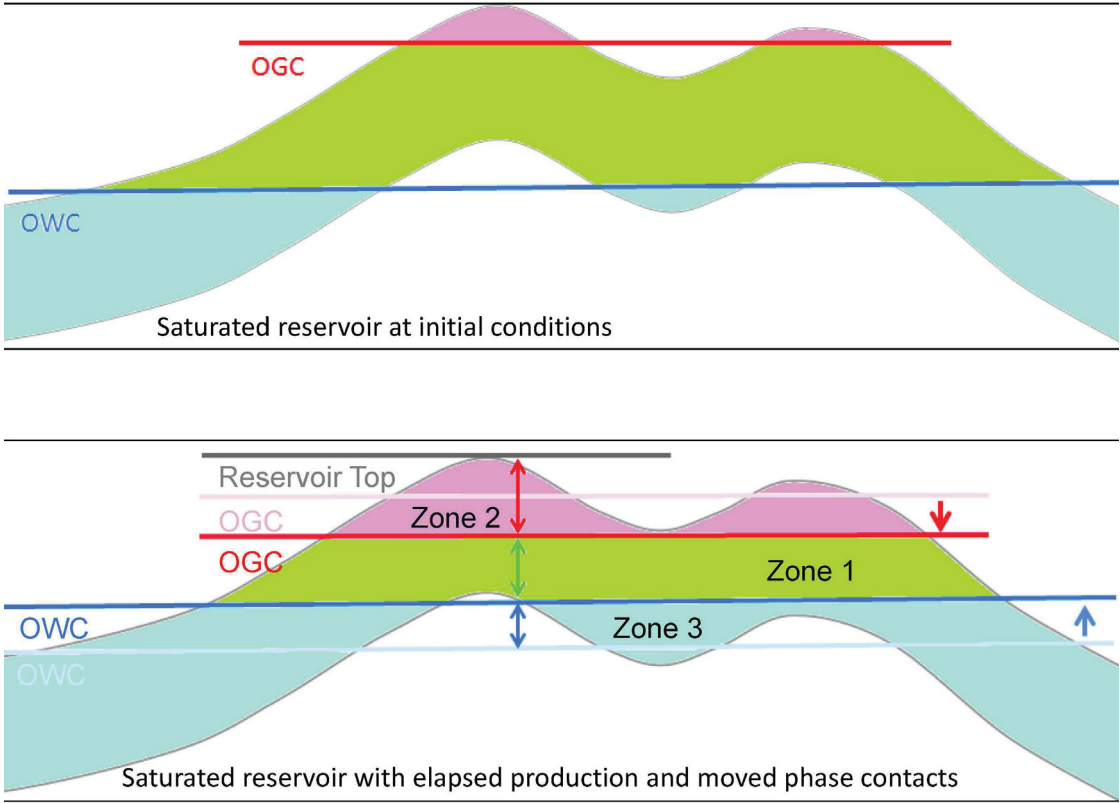
Figure 5.1: Schematics of an initially saturated reservoir and how the phase contacts will move due to production
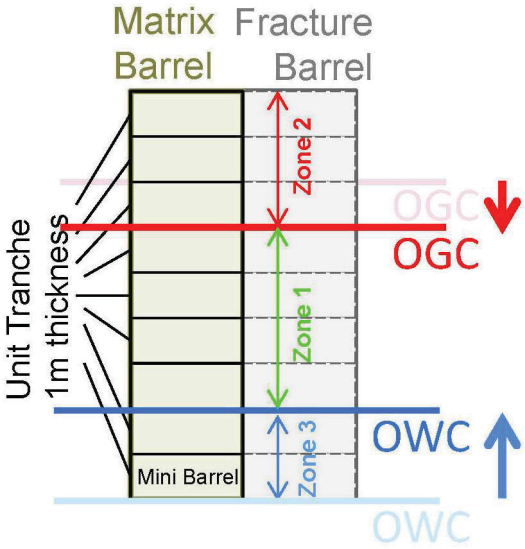
Figure 5.2: Dual porosity MB model with moving phase contacts

In most of the cases the recovery curves are created by single matrix block simulation considering a single displacing phase in the fracture. The situation using these curves is equivalent with the assumption that the recovery factor resulting from both the water and gas drive curves remains valid independently from the recovery history.

Figure 3.5 shows the schematic of a normalized recovery curve $E^n(t)$. The recovery process is governed by two parameters, the asymptotic value $(1/\alpha)$ of the recovery function and the time scaling factor, β. The virtual time t_v is determined by the normalized recovery factor $E^n_j = \alpha E_j$ where α is the reciprocal of the ultimate (maximum) recovery factor for the given displacement mechanism. The recovery increment $\Delta_{j+1}E = (E^n_{j+1} - E^n_j)/\alpha$ during the next time step $\Delta_{j+1}t$ can be read at the virtual time $t_{vj+1}=t_{vj}+\beta\Delta_{j+1}t$.

Figure 3.5 shows a schematic normalized recovery curve which will be given separately for water and gas drives.

Let E_R be the tranche recovery factor at time t_j. The normalized recovery factor values of $\alpha^w E_k$ and $\alpha^g E_k$ correspond to the virtual times t_v^w and t_v^g on the normalized water and gas recovery curves respectively. Adding now an arbitrary time step $\Delta_{j+1}t$ and reading the normalized recovery factors at the new virtual time on the recovery curves:

$$t^w_{vj+1} = t^w_{vj} + \beta^w \Delta_{j+1}t; \qquad t^g_{vj+1} = t^g_{vj} + \beta^g \Delta_{j+1}t \qquad (5.2)$$

results in the recovery factor increments:

$$\Delta_{j+1}E^w_k = (E^{nw}_k(t^w_{vj+1}) - E^{nw}_k(t^w_{vj}))/\alpha^w; \qquad \Delta_{j+1}E^g_k = (E^{ng}_k(t^g_{vj+1}) - E^{ng}_k(t^g_{vj}))/\alpha^g \qquad (5.3)$$

It is assumed that the amount of the injected water can be estimated from the water drive recovery curve which was elaborated for a two phase water displacement. Let be $\Delta_{j+1}E^w_k$ the oil recovery increment from the water drive for the time step interval $\Delta_{j+1} = t_{j+1} - t_j$. In an undersaturated case the specific water inflow during the same time period is:

$$\Delta_{j+1}w_k = \Delta_{j+1}E^w_k \cdot (B_o/B_w)_{j+1} \qquad (5.4)$$

In the saturated case (below the initial bubble-point pressure) free gas saturation exists in the matrix already. The water injected by the fracture to the matrix tranche will also displace free gas, flowing from the matrix to the fracture, and therefore:

$$\Delta_{j+1}w_k = \Delta_{j+1}E^w_k \cdot [B_{oj+1} + B_{gj+1}(\overline{R_{pk}} - R_{sj+1})]/B_{wj+1} \qquad (5.5)$$

The matrix to fracture gas transfer is governed by the production GOR, R_{pk}, which is determined by the relative permeability:

$$R_{pkj} = R_{sj} + \left(\frac{B_o \mu_o k_{rg}}{B_g \mu_g k_{ro}}\right)_{kj} \tag{5.6}$$

The average outflow gas-oil-ratio $\overline{R_{pk}}$ for the time interval $\Delta_{j+1}t$ is:

$$\overline{R_{pk}} = (R_{pkj+1} + R_{pkj})/2 \tag{5.7}$$

For the relative permeability the gas saturation in the matrix has to be estimated based on the known oil saturation and the cumulative intruded water:

$$
\begin{aligned}
S_{gkj} &= 1, - S_{okj} - S_{wkj} \\
&= 1, - S_{wki} - (1, - S_{wki})(E_{kj}B_{oj}/B_{oi} + w_{kj}) \\
&= (1, - S_{wki})(1 - E_{kj}B_{oj}/B_{oi} - w_{kj})
\end{aligned} \tag{5.8}
$$

The cumulative intruded water is the sum of all increments:

$$w_{kj} = \sum_{n=1,j} \Delta_n w_k \tag{5.9}$$

The scenario explained above, where water has invaded the fracture, and therefore is "injecting" water into the matrix displacing oil – and for the saturated case the water will also displace free gas from the matrix to the fracture – is valid for Zone 3 (see also Figure 5.1 and Figure 5.2). For Zone 2, where the fracture is gas saturated, the amount of gas "injected" from the fracture to the matrix is determined by the gas recovery curve and is given by:

$$\Delta_{j+1}g_k = \Delta_{j+1}E_k^g \cdot (B_o/B_g)_{j+1} \tag{5.10}$$

Equation 5.1 to Equation 5.10 refer to a matrix tranche with serial number k. The $\Delta_{j+1}E_k$ is valid for the time step and therefore an explicit value.

5.2   Monitoring of Phase Contacts

Having the recovery factor E_{kj} the cumulative transferred oil from the matrix into the fracture can be easily calculated:

$$Q_{mf}(t_j) = \sum_{k=1}^{M} OOIP_k \cdot E_{kj} \tag{5.11}$$

The actual amount of the oil in the fracture is:

$$N_{fj}(t_t) = N_{fi} + Q_{mf}(t_t) - Q_o(t_f) \tag{5.12}$$

where Q_o is the cumulative oil production and N_{fi} is the original amount of oil in the fracture situated between the initial water and gas oil contacts (OWC and OGC).

In the fracture system complete phase segregation is assumed. If the vertical distribution of the fracture volume V_{fk} with $k = 1, M$ is known then also the positions of the phase contacts can be determined. The volume of the oil column between the actual phase contacts is given by the following relation:

$$\sum_{k=K_{owc}}^{K_{ogc}} V_{fk} \approx [N_{fi} + Q_{mf}(t_j) - Q_o(t_j)]B_{oj} \tag{5.13}$$

The $LeftTerm \approx RightTerm$ sign expresses that due to the vertical resolution applied for the actual approach the phase contacts will be placed in the vertical tranches with ±1m tolerance. The fracture oil column is situated in the interval K_{owc} and K_{ogc}. Above the level K_{ogc} the fracture column is filled with free gas. Below K_{owc} the fracture column contains only water. For reasons of simplicity it is assumed that the connate and residual saturations of the fracture equal zero. The same is true for the OGC determination in absence of water inflow. If both free gas and water inflow exist then the position will be more uncertain and will need supplementary considerations.

In an undersaturated case no free gas exists in the fracture so the position of the actual OWC is determined by the following relation:

$$\sum_{k=K_{owc}}^{M} V_{fk} \geq [N_{fi} + Q_{mf}(t_j) - Q_o(t_j)]B_{oj} > \sum_{k=K_{owc}+1}^{M} V_{fk} \tag{5.14}$$

The actual OWC is then situated between the depth K_{owc} and $K_{owc}+1$ measured upwards from the original OWC. $k=0$ corresponds to the depth of the original OWC. Please note that M corresponds to the top depth of the reservoir.

The determination of the OGC position in absence of water influx is similarly simple:

$$\sum_{k=1}^{K_{ogc}} V_{fk} \geq [N_{fi} + Q_{mf}(t_j) - Q_o(t_j)]B_{oj} > \sum_{k=1}^{k=K_{ogc}-1} V_{fk} \tag{5.15}$$

The actual OGC is then situated between the depths K_{ogc} and $K_{ogc}-1$ measured upwards from the original OWC.

For the three phase case – gas on top of the fracture column (Zone 2), oil in the middle (Zone1)

and water at the bottom (Zone3) – placement of the phase contacts (OWC and OGC) is no longer trivial. For setting the OWC it is necessary to consider Equation 5.5 – which is burdened by the uncertainty of estimating the gas saturation – for calculating the water amount intruded into the matrix. Summing up Equation 5.5 for the interval between the first tranche above the initial OWC and the actual OWC (k_{OWC}) the cumulative water intrusion in the matrix system is given by:

$$W_{mj} = \sum_{k=1}^{M} w_{kj} \tag{5.16}$$

The cumulative water influx (W_{ej}) to the entire reservoir (matrix and fracture) is calculated from Equation 4.14 as usually according to the pressure history. The aquifer, being the source of the water encroachment W_e is connected to the fracture system only. Therefore, the amount of water residing within the fracture pore volume at the time j is:

$$W_{ej} - W_{mj} - Q_w(t_j) \tag{5.17}$$

The following relation has to be satisfied:

$$\sum_{k=1}^{K_{owc}} V_{fk} \leq [W_{ej} - W_{mj} - Q_w(t_j)]B_{wj} < \sum_{k=1}^{k=K_{owc}+1} V_{fk} \tag{5.18}$$

The actual OWC is then situated between the depths K_{owc} and $K_{owc}+1$ measured upwards from the original OWC.

The amount of gas in the matrix is the sum of the free and dissolved gas:

$$G_{mj} = \sum_{k=1}^{M} V_{mk}\left(\frac{S_{gk}}{B_g} + \frac{S_{ok}}{B_o}R_s\right)_j \tag{5.19}$$

Let G_i be the original gas amount in the entire model then the actual amount of the free gas in the fracture is:

$$G_{fj} = G_i - G_{mj} - N_{fj}R_{sj} - Q_g(t_j) \tag{5.20}$$

$$\sum_{k=K_{ogc}}^{M} V_{fk} \leq G_{fj}B_{gj} < \sum_{k=K_{ogc}-1}^{M} V_{fk} \tag{5.21}$$

By definition, the fracture volume residing between the estimated OWC and OGC must be equal to the volume of the oil column given by Equation 5.21. Satisfying this requirement is a difficult matter and it needs a careful and critical estimation of the relative permeability functions.

5.3 Determining Phase Contacts in the Field

Defining the depths of the fluid contacts, including the gas/oil contact (GOC) and the oil/water contact (OWC), or the gas/water contact (GWC), is essential for volumetric calculations and important for detailed petrophysical interpretations. For example, accurate porosity calculations require subdividing the reservoir's vertical extent by fluid type to account for differences in the average fluid saturations and the resulting differences in fluid densities and sonic travel times in the gas cap, oil column, and aquifer. For water saturation (Sw) calculations, the depth to the OWC or GWC, or more generally the free water level (FWL), is required to estimate Sw from capillary pressure (P_c) data. These depths, to the extent that they occur, must be determined in every wellbore.

5.3.1 Methods for Phase Contacts Determination at the Wellbore

5.3.1.1 Mud logs

Mud logs record quantities and compositions of mud gases and include descriptions and analyses of drill cuttings. These provide information about the fluid content and lithology of the rock as it is drilled. Mud log gas analysis data are plotted against drilled depth; the plot is a semi-quantitative record of the gas content over the reservoir interval. The mud log can be used to determine the GWC or OWC because the background gas content per unit volume of aquifer brine is extremely low compared with that of free gas or gas dissolved in oil. The methane-concentration log is most useful for defining the top of the reservoir and the GWC of a gas reservoir. Detailed gas analyses can also identify a GOC from the increase in the ratio of heavier hydrocarbons compared to methane with greater depth. Drill cuttings characteristics of fluid content can assist in identifying oil and gas reservoirs, including the top of the reservoir, the GOC and OWC, and, possibly, the base of the reservoir.

5.3.1.2 Water-based mud cores

Cores from wells drilled using water-based mud can provide direct evidence of the OWC and the GOC. Because of differences in the color of oil stains, the depths to gas, oil, tar, and relict-oil intervals may be determined visually from the cores.

5.3.1.3 Wireline log methods

Resistivity logs can be used to determine the OWC and GWC depths in a wellbore. Usually, the hydrocarbon-bearing portion of the reservoir exhibits high resistivity readings and the formation water–bearing portion gives low resistivity readings because of the presence of salts in the formation water. The resistivity logs are used to calculate S_w, and where there is a significant and relatively abrupt decrease in S_w values (decreasing from near 100% PV upward through the reservoir interval), that depth is defined as the water contact depth. If the reservoir is not too shaly, the neutron log can be key to identifying gas-bearing intervals. A GOC, or a GWC, can be defined at the depth at which the neutron porosity significantly decreases and the density and sonic porosities slightly increase as one moves up through the reservoir interval. Figure 5.3 shows an example of the OWC and GOC determination from well log measurements.
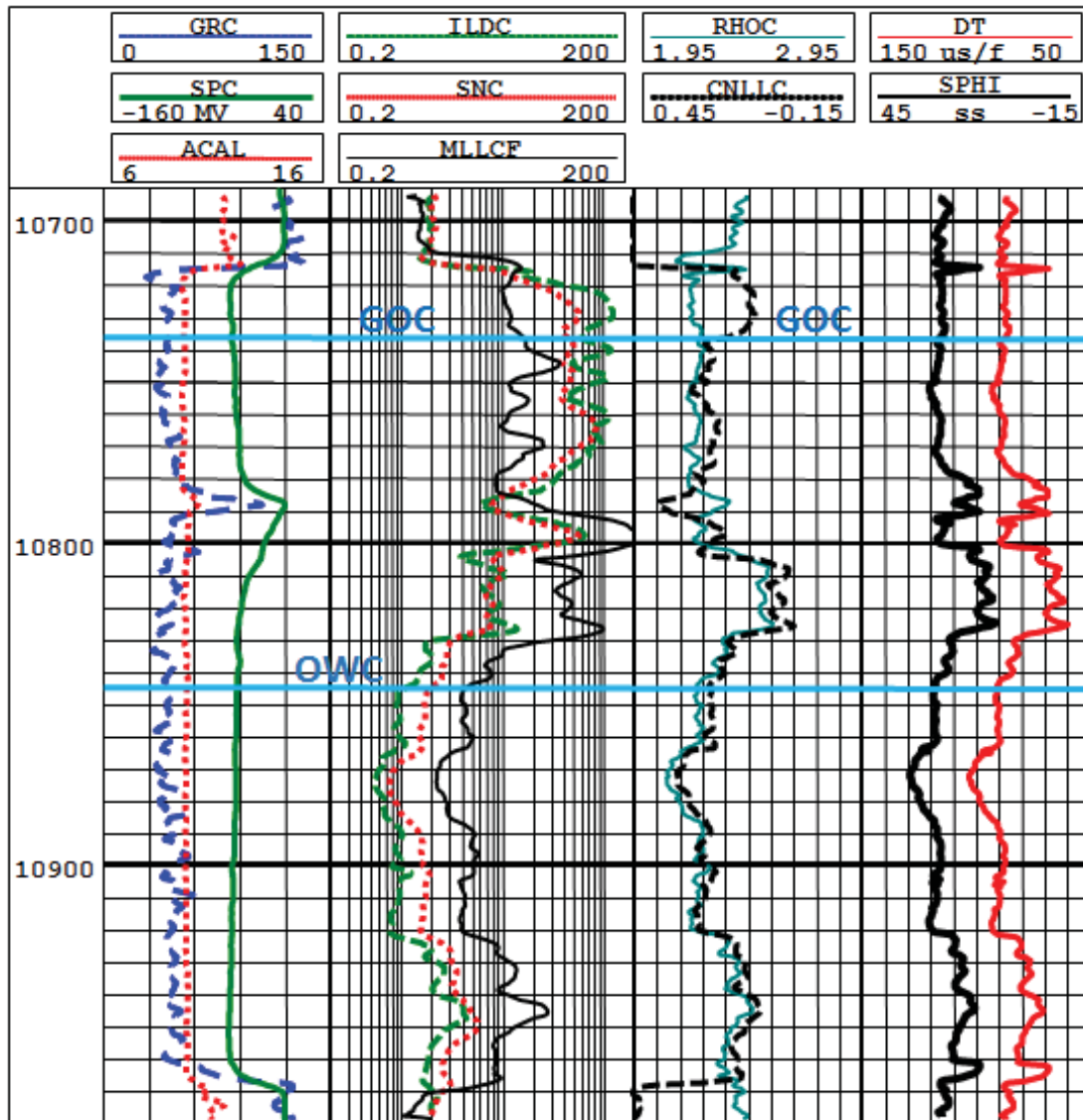
Figure 5.3: Example of the OWC and GOC determination from well log measurements (from NExT PERF Short Course Notes, 1999)

5.3.1.4 Formation pressure surveys

The best data to determine fluid contacts are given by the formation-pressure testing tools such as the repeat formation tester (RFT), the formation multi-tester, the modular dynamics tester (MDT), and the reservoir cauterization tool (RCI) that perform pressure surveys over intervals of the reservoir. As the measurement tool moves vertically downward from the gas cap into the oil column, or from the hydrocarbon column into the aquifer, there will be breaks in the formation pressure versus depth trends. Gas, oil and water have different fluid pressure gradients moving from a very low gas pressure gradient (0.10 psi/ft or less) to a higher oil pressure gradient (typically 0.25 to 0.35 psi/ft) and then to the pressure gradient characteristic of water (0.40 to 0.55 psi/ft). If adequate data can be collected, the fluid contacts can be determined very accurately by identifying the depths at which the characteristic pressure gradients change. Figure 5.4 shows an example of fluid contacts determination by plotting pressure measurements from the reservoir versus depth. The intersections of different pressure gradient lines identifies the gas-oil and oil-water contacts.
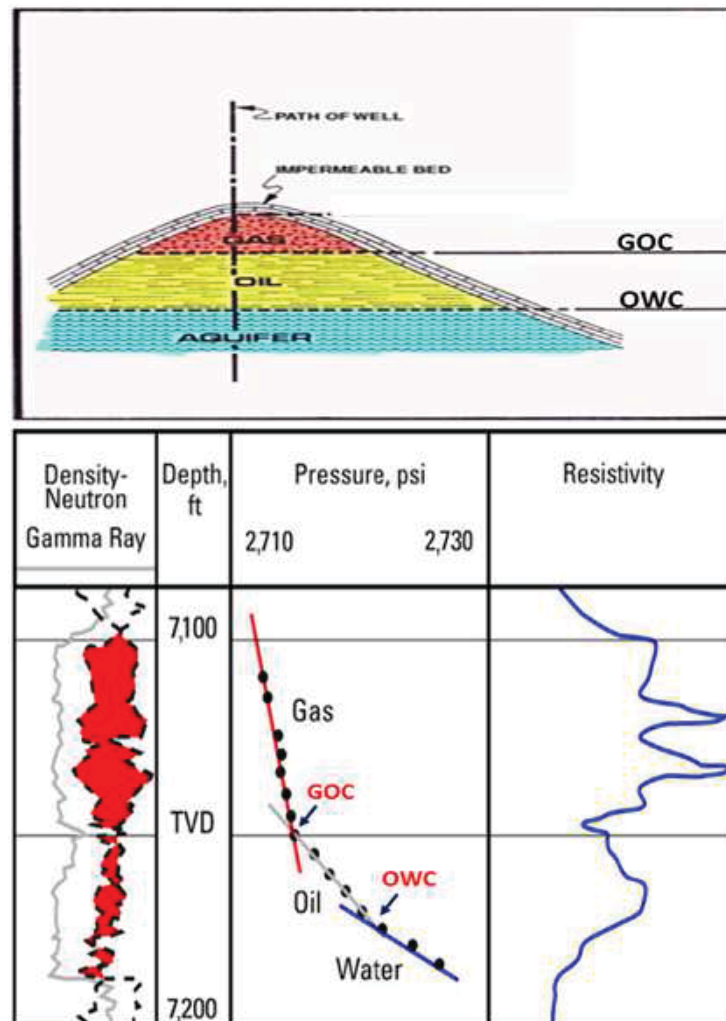
Figure 5.4: Example of fluid contacts determinations from pressure gradients (PetroWiki)

5.3.1.5   Seismic surveys

With the introduction of 3D seismic surveys, acoustic-impedance contrasts between gas, oil and water-bearing formations are increasingly used for reservoir charactrization and evaluation of reservoir behaviour. The impedance is dependent on the density and acoustic velocity of each fluid. Many reservoirs exhibit a significant change in acoustic impedance at the fluid contacts, allowing the contacts defined at the wells to be propagated into undrilled areas of the reservoir. These same impedance changes may also be seen in vertical seismic sections and assist in identifying the top of the reservoir, GOC, GWC, and OWC.

5.3.1.6   Oil Rim Tools

Production logging and pressure measurement tools record reservoir fluids continuously in real time from naturally producing wells. Interpreting these records may be straight forward, but because approximately 95% of the world's oil wells are unable to produce naturally and require the use of a pump, this can create problems for instrument systems. The producing zone is usually below the pump, where few analysis tools can be used while the pump is running. True oil rim measurement systems that operate continuously in real time below the pump were introduced recently (Shanks, 2013). These provide information in the form of dynamic estimates of OWC and GOC depths, and reservoir pressure and temperature measurements. This provides accurate observations of reservoir levels, depletion, and fluid behavior and steam flood applications for reservoir monitoring purposes.

5.3.2 Definition of Terms for Phase Contact Description

Many definitions of Oil-Water Contact (OWC) and Water-Oil Contact (WOC) can be found in the literature. The following version is from the Society of Petroleum Engineers (SPE):

"Oil-Water Contact: Local boundary between the oil and the bottom water. OW Contact may vary in the field depending on individual drawdowns and local variations in vertical permeability."

In order to develop a concept for determining the oil-water contact (OWC) in a field, several terms must be defined. The following three zones must be distinguished, plus two additional definitions are required:

Free-Water Level (FWL): The FWL is the vertical position at which the capillary pressure (primary drainage) is zero. The level of zero capillarity or FWL that determines the theoretical saturation profile usually is somewhat subjective if it is interpreted from wireline logs. However, it must be understood that in a heterogeneous reservoir the FWL is not a uniform surface, but varies with rock quality and wettability. The FWL is not a flat surface except in a completely homogeneous medium.
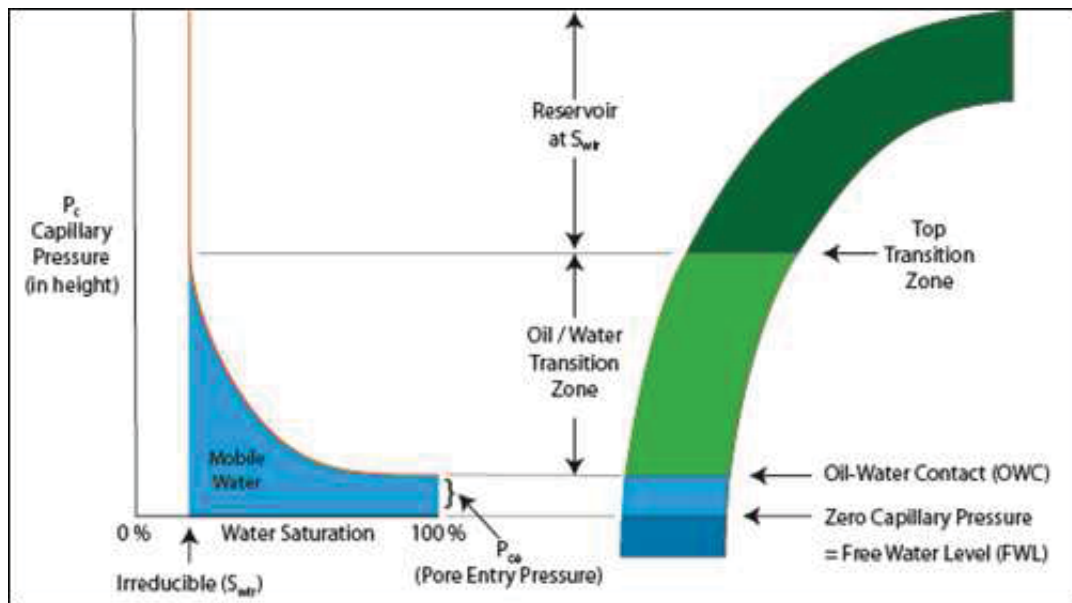
Figure 5.5: Saturation height function (capillary pressure) and contacts in a typical oil reservoir under water-wet conditions, from Holmes (2002)

Oil-Water Contact (OWC): The OWC is the vertical position at which the capillary pressure is equal to the pore entry pressure. As shown schematically in Figure 5.5, close to the OWC the oil/water pressure differential (i.e., the capillary pressure) is small. Therefore, only the largest pores can be filled with oil. However, the larger pores may form much of the volume of the pore space, so the capillary pressure curve is usually flat at higher water saturations.

Transition Zone (TZ): The reservoir interval from the oil/water contact (OWC) to a level at which water saturation reaches an irreducible limit is referred to as the capillary transition zone. Figure 5.5 illustrates a typical capillary transition zone in a homogeneous reservoir interval within which both the oil and water phases are mobile. The balance of capillary and buoyancy forces controls this capillary transition zone during the primary drainage phase of oil migration into an initially water-filled reservoir trap. Most reservoirs are originally water-wet, so a certain threshold pressure must be reached before the capillary pressure in the largest pores can be overcome and oil can begin to enter the pores. Hence, the largest pore throat determines the minimum capillary rise above the free-water level (FWL). As the distance above the OWC increases, an increasing proportion of smaller pores are entered by oil because of the increasing capillary pressure with height above the FWL. The height of the transition zone and its saturation distribution is determined by the range and distribution of pore sizes within the rock, as well as the interfacial force and density difference between the two immiscible fluids.

Oil-Down-To (ODT): ODT usually refers to the depth to which oil stains have been seen in drill cuttings or cores. ODT is also defined as the depth of the deepest tested zone that has produced crude oil during a well test such as a drill stem test (DST). An ODT level is not a physically defined property, but only an empirical observation. If the total depth of the well does not reach a zone that is 100% water bearing, or wire line logs have not been run down to the bottom of the oil leg, the ODT is useful for verifying petrophysical interpretations. The ODT level may be interpreted as the bottom of the transition zone.

Water-Up-To (WUT): WUT is the complement of the ODT. The WUT level may be interpreted as the top of the transition zone.

The situation in oil-wet and mixed-wet reservoirs is more complicated. Even though an initially water filled rock may be water-wet, this may change during fluid migration. At the microscopic scale, the surfaces of solid particles, including the inner surfaces of pores, are very rough. If the oil "wets" the rough surface, oil molecules attach to the rough solid surface by adhesion and the entire pore becomes oil-wet. The wetness is controlled by cohesion forces between oil molecules when this occurs. The interfacial force between two fluids is the result of the difference of cohesive forces of the fluid molecules of the two fluids. These microscopic effects cannot be reproduced by standard laboratory measurements. However, this is the reason for the phenomenon of hysteresis, which can be observed in the laboratory if repeated drainage-imbibition cycles are simulated. Because of rock quality variation, the OWC will usually differ between wells, especially in carbonate mixed-wet and oil-wet reservoirs.

An oil-wet system yields the relationships shown schematically in Figure 5.6. The obvious difference with the water-wet system shown in Figure 5.5 is that the oil saturation may be greater than zero below the OWC and below the FWL. Oil saturated rock may be even located below the zero capillarity level in an oil-wet reservoir. This is a result of partially negative capillary pressure. In a strongly oil-wet system movable oil may exist below the FWL and would be within the transition zone. Note that the schematics in Figure 5.6 and Figure 5.7 show two theoretical in situ conditions of a mixed-wet system; these are not results from capillary drainage measurements, which cannot produce negative capillary pressure effects.
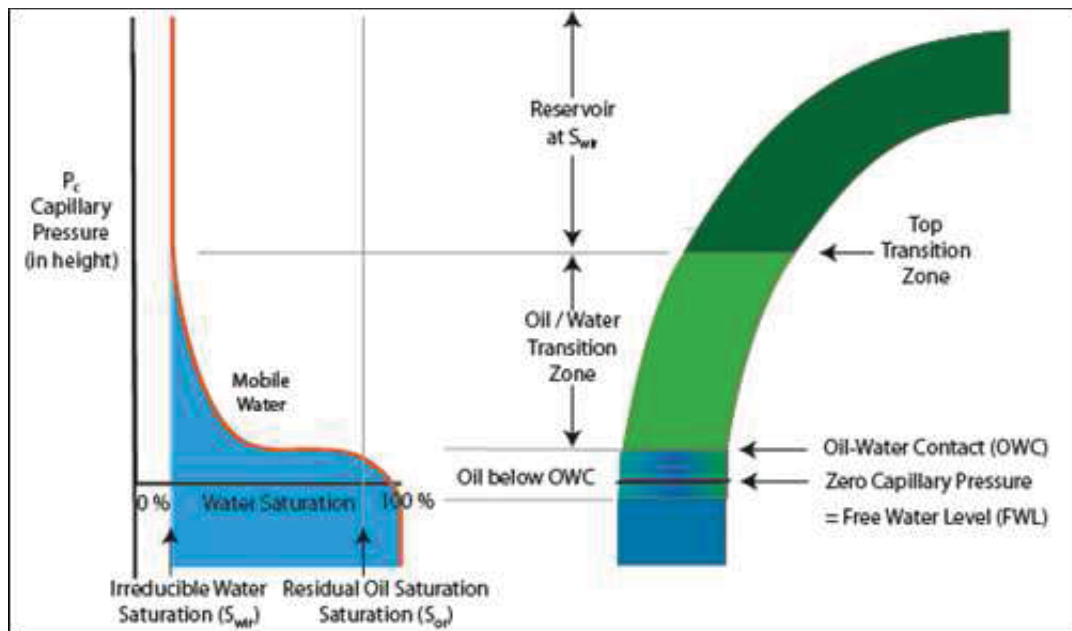
Figure 5.6: Saturation height function (capillary pressure) and contacts in an oil reservoir under slightly mixed-wet conditions, modified from Holmes (2002).
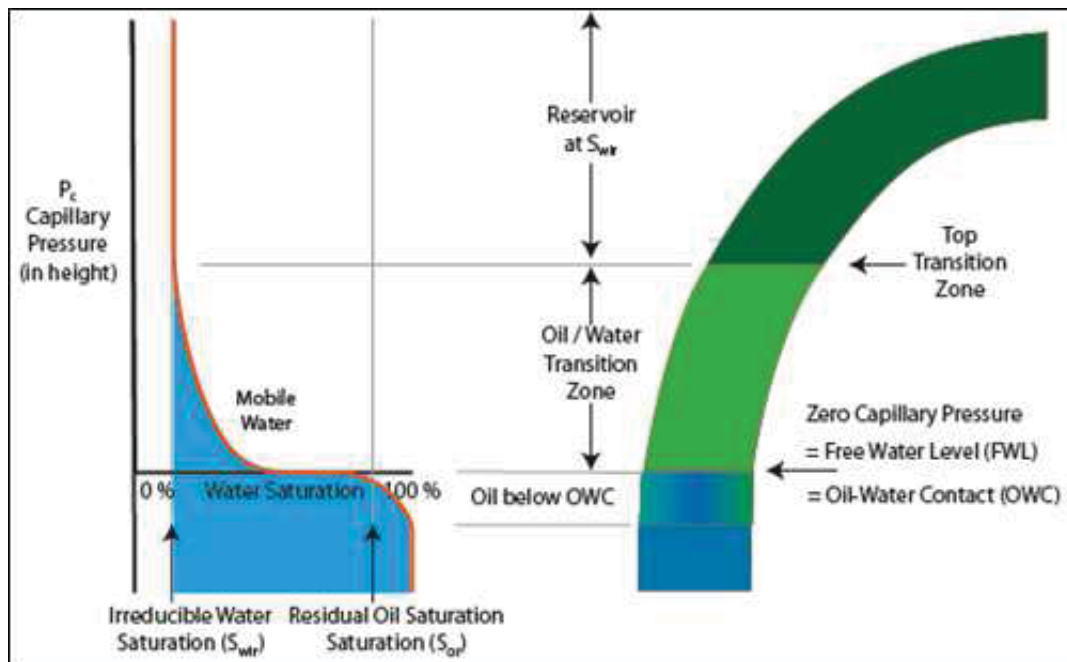
Figure 5.7: Saturation height function (capillary pressure) and contacts in an oil reservoir under mixed-wet (or neutral-wet) conditions, modified from Holmes (2002).

5.4   Workflow for Modeling of Natural Fractured Reservoirs

During the past decade, a great number of publications have dealt with the workflow of reservoir characterization, uncertainty assessment and reservoir simulation for both conventional and fractured reservoirs. The work of Breit and Dozzo (2004) and Wynn and Tiefenthal (2006) should be mentioned here vicariously.

Oil fields have a long life, especially naturally fractured dual porosity ones. Some dual porosity reservoirs such as the Naftshahr Field in Iran operate over 80 years already and for newly discovered ones production for over 100 years are forecasted (Azadegan Field in Iran). Their modeling is not a one time sequential job but a cyclic multi-level process. In every cycle models describing the geology and the historical and future dynamic behaviors of the reservoir and the field have to created newly or the existing ones have to be revised. The results are models at different levels. Note that after the most thorough investigations, the reservoir parameters will still not be known, only the model was parametrized (based on estimation).
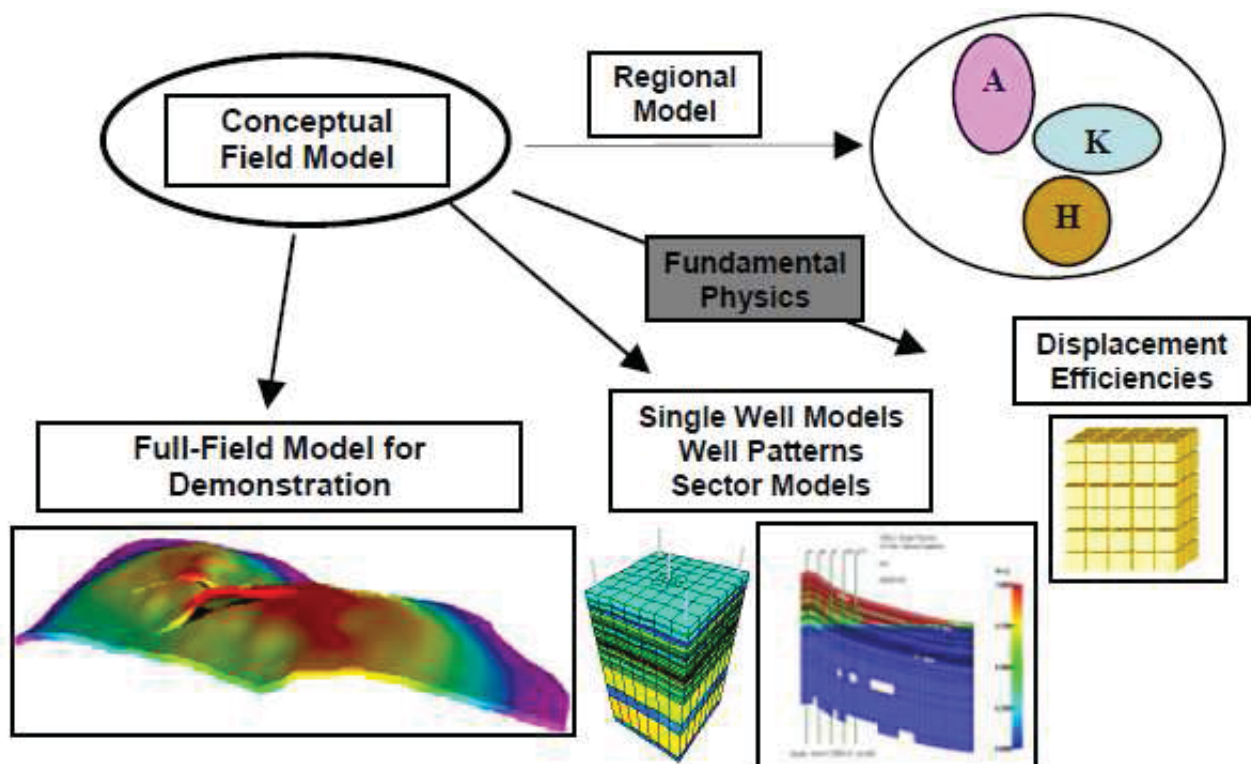
Figure 5.8:   Levels of dynamic reservoir modeling (from Heinemann G.F. *et al.* 2007)

The investigations have to be performed at all levels starting at the petrographic thin sections to regional impacts. Figure 5.8 visualize this statement (restricted to dynamic modeling). Always all, or most of the modeling steps have to be performed. The question is the sequence

and the priority of them. In this respect three approaches are possible a) bottom up, b) top down and c) multilevel reservoir modeling, abbreviated MLRM. Figure 5.9 from Gabor F. Heinemann *et al.* (2007) explains the differences between the three modeling concepts. Nevertheless, none of the approaches can satisfy all requirements depending on the reservoir size, production time, reservoir properties but also on the interest of the asset owner, concessionaire and operator.
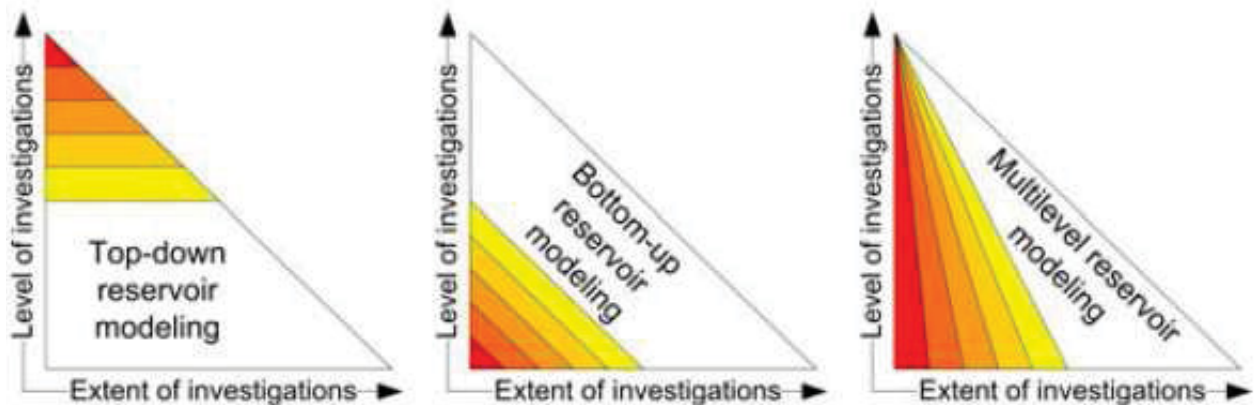
Figure 5.9: Reservoir modeling approaches (from Heinemann G.F. et al. (2007))

Most of the recently discovered giant oil reservoirs are naturally fractured which necessitate dealing with a high level of complexity during development. Consequently, negotiations between field owners (government, National Oil Company (NOC)) and the potential International Operating Companies (IOC) are time consuming and may lead to an unnecessary loss of business opportunities. The IOCs' objective is to maximize the profit using their capital and know-how anywhere in the world within time frames of 10 to 20 years, whereas the NOCs' goal is to generate as much value as possible from their assets over their life cycle. The different key objectives lead compulsorily to different reservoir evaluation workflows.

To meet the IOCs' needs BP's Top-Down Reservoir Modeling (TDRM) approach may be most suitable, in which the simplest appropriate models are used. Details and complexity will be only added, if the previous investigations show favorable economics; i.e. in the TDRM approach unprofitable projects - in IOCs' point of view – are not analyzed in detail.

TDRM is not optimal for NOCs offering oil fields in bidding processes, requiring deepest possible understanding of the reservoirs' geology, physics, production potential and ultimate recovery as a basis for their negotiations. The multilevel workflow presented by Heinemann G.F. *et al.* (2007) aims to achieve the owner's (NOC) objectives in the most efficient way; i.e. asses and minimize uncertainty, reduce project turnaround time and finally end up with a reliable and consistent full field model. The approach is neither "top-down" nor "bottom-up" but it is rather a "MultiLevel Reservoir Modeling" (MLRM), performing investigations in parallel on different scales in an iterative loop. The spiral in Figure 5.10 explains two aspects: (1) every working step induces a supplementary one on the next level, (2) the next spiral starts before the previous terminated. The modeling work is performed in parallel on every level.
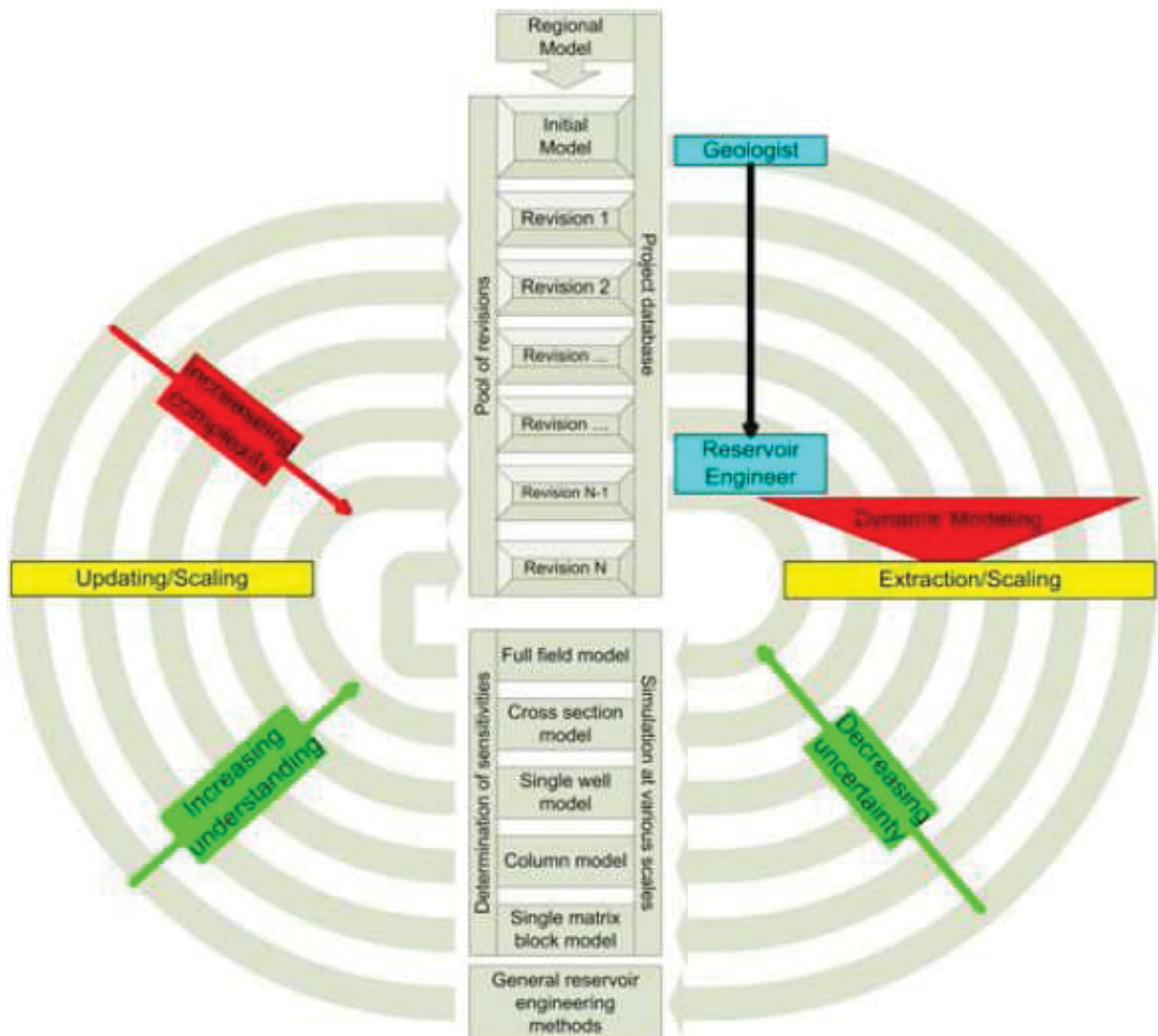
Figure 5.10: Multilevel reservoir modeling workflow (from Heinemann G.F. *et al.* 2007)

Regarding Figure 5.8 it must be recognized that no material balance calculation - obligatory for all single porosity reservoirs - is mentioned, from the simple reason that up to now no such method existed for dual porosity cases. In the future MB calculations will be certainly obligatory applied. Their importance will be different, depending on the used modeling approach.

In the TDRM approach a MB investigation can screen out projects with minor potential quickly, saving oneself time on consuming numerical modeling (history matching, prediction) work.

The MLRM approach can not discard a numerical modeling step. It performs investigations in parallel on different scales in an iterative loop. MLRM requires consistent highly sophisticated simulation tools with special options for gridding, upscaling/downscaling and well management.

Dealing with naturally fractured reservoirs means to deal with uncertainty. According to Gilman (2006) modeling of naturally fractured reservoirs (NFR) requires that a number of complex issues comes together in a consistent manner. Despite these difficulties, the principles of modeling a single porosity and a dual porosity/dual permeability reservoir are the same:

1. A geocellular model of the reservoir, containing the matrix properties is created.
2. Fracture properties are added to the model. Former non-reservoir areas (impermeable zones), which act as sealing barriers in non-fractured reservoirs may become productive.
3. For simulating fractured reservoirs using the dual continuum approach it is of special importance to select an appropriate matrix-fracture interaction model (e.g.: gravity drainage model).
4. The geocellular model is transformed to a dynamic reservoir model by vertical and horizontal upscaling techniques. A comprehensive summary about current upscaling technology can be found in the reference - Durlofsky (2005).
5. Finalize the dynamic model by introducing wells to the grid model and by adding SCAL, PVT and if available historical production data. Finally, operation conditions and constraints for the wells are chosen to run the numerical model.
6. Analyze the results and draw conclusions.

Even though the overall workflow for modeling naturally fractured reservoirs looks familiar, for fractured reservoirs it is much more difficult to obtain the required data and forecast the reservoir performance than for conventional reservoirs.

Chapter 6

Sabah Case Study

6.1 Introduction

In this chapter the method proposed by Mittermeir (2015) is verified in a case study, performed on the Sabah field. The recovery curves method was used for calculating the material balances for naturally fractured reservoirs. In this way the matrix-fracture fluid exchange could be fully considered. To give persuasive evidence it is necessary to present the geology and the production history of the field. All those investigations were done over a period of 50 years by many professionals which can not be referenced in this work. Some parts of this chapter were extracted from proprietary documents of Zueitina Oil Company, Libya. The author does not claim intellectual property rights on these parts of the chapter.

6.2 Geology of the Field

The Sabah Field is located in concessions NC74F and NC131 in the southwestern part of Sirte Basin, Libya, on a local high within the NW–SE trending Zella graben (Figure 6.1). Most of the field lies in concession NC74F, with the field's northern flank extending into concession NC131. The reservoir is within an anticlinal structure cut by a complex series of right-lateral strike-slip faults. Sabah Field was discovered by Alwerath Oil Company in 1964 when well G01 encountered oil in the Paleocene Beda Formation. Seventy wells (including sidetracks) have been drilled in the field by the operator, Zueitina Oil Company (ZOC). Sabah field is a highly fractured carbonate reservoir that has produced for more than 35 years.
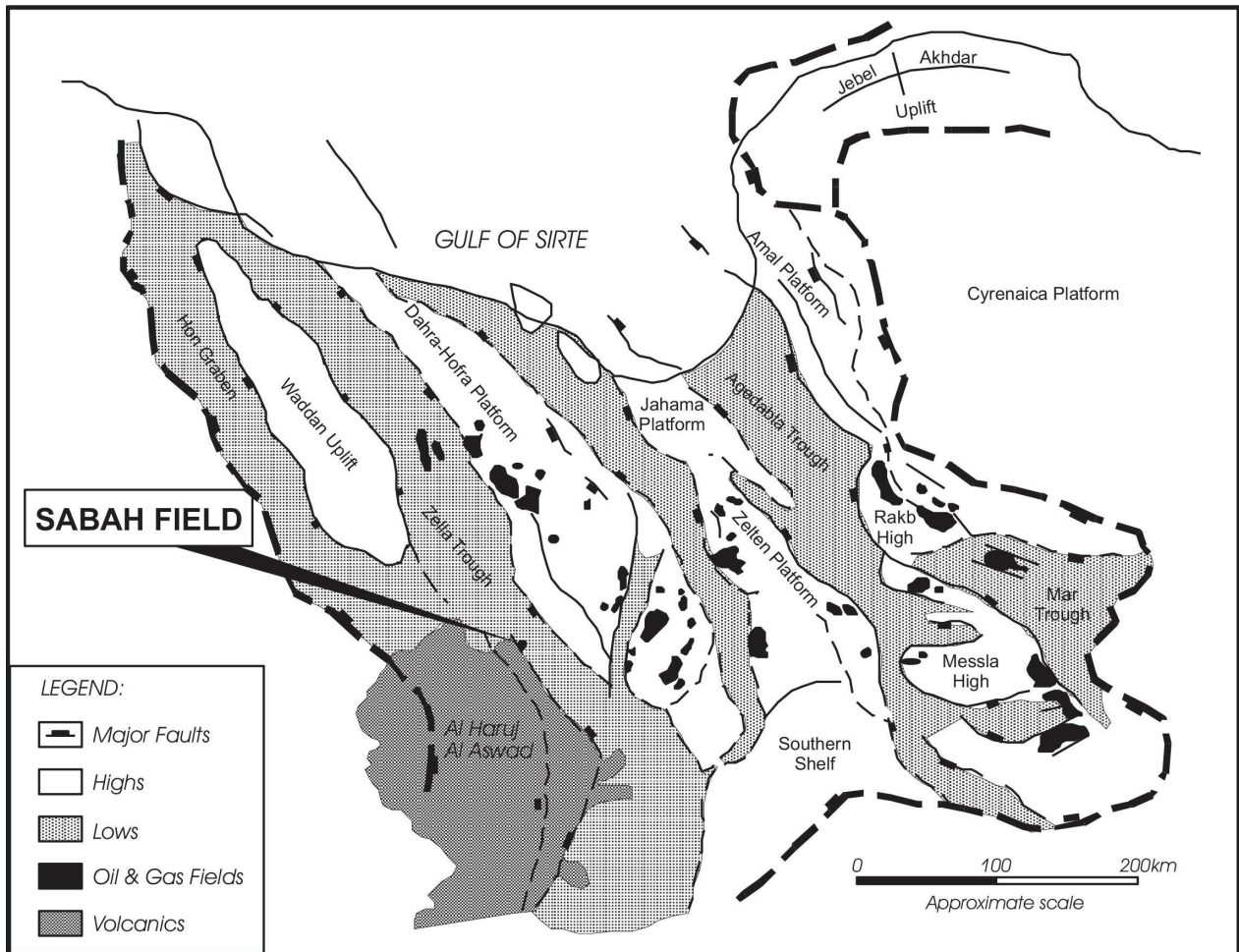
Figure 6.1: Schematic structural map of the Sirte Basin with Location of Sabah Field (with courtesy of Mansur (1987)

6.2.1 Regional Geology of Sirte Basin

The relevant phases in the structural evolution of the Sirte Basin began in the Early Cretaceous with the creation of a system of rifts that developed along pre-existing zones of weakness in the basement complex of North Africa. According to Van der Meer and Cloetingh (1993) these structures are mostly oriented NNW. Rifting was followed during the mid–Cretaceous by a tectonically quiet period. In the Late Cretaceous (Santonian), a compressional episode resulted from the collision of the African-Arabian and Eurasian plates, causing folding and inversion of many basins along the Afro-Arabian Tethyan margin. Subsequent relaxation of compressional forces created a tensional environment expressed by the resumption of rifting that lasted through the end of the Cretaceous, creating the Sirt-Kalash, Marada, Tagrifet-Zellah and Hon troughs of northern Libya. The Cretaceous-Cenozoic boundary is marked by a regional unconformity.

The stratigraphic succession in the NC74 area of the western Sirte Basin (Figure 6.2) can be grouped into five intervals: the Pre-Cretaceous (I), the lowermost Upper Cretaceous to the top of the Upper Cretaceous (II), the uppermost Upper Cretaceous to the middle of the Lower Eocene (III), the mid-Lower Eocene to the upper Middle Eocene (IV) and the upper Middle Eocene to the Present (V). Stratigraphic interval I includes the metamorphic and igneous basement plus the overlying poorly sorted granite wash and orthoquartzite of the Gargaf Group. Stratigraphic interval II documents the evolution of the Sirte Basin from a purely intracratonic basin containing only continental style deposits, to a continental margin, failed-rift basin. Stratigraphic interval III represents regionally uniform rates of subsidence and marine transgression, leading to deposition of carbonates and shale. The marine sequence was interrupted by at least two periods of emergence or near-emergence when restricted sabkha environments developed and evaporites were deposited.

Stratigraphic interval IV consists of interbedded evaporite and restricted shallow marine carbonates, succeeded by carbonate and clastic sediments deposited in open marine shelf to deeper marine environments, overlain in turn by limestone and anhydrite. Most rocks of stratigraphic interval V have either been eroded or were never deposited in the NC74F area. In the Sabah field, volcanic basalts of Miocene to Pliocene age cap the sedimentary succession.
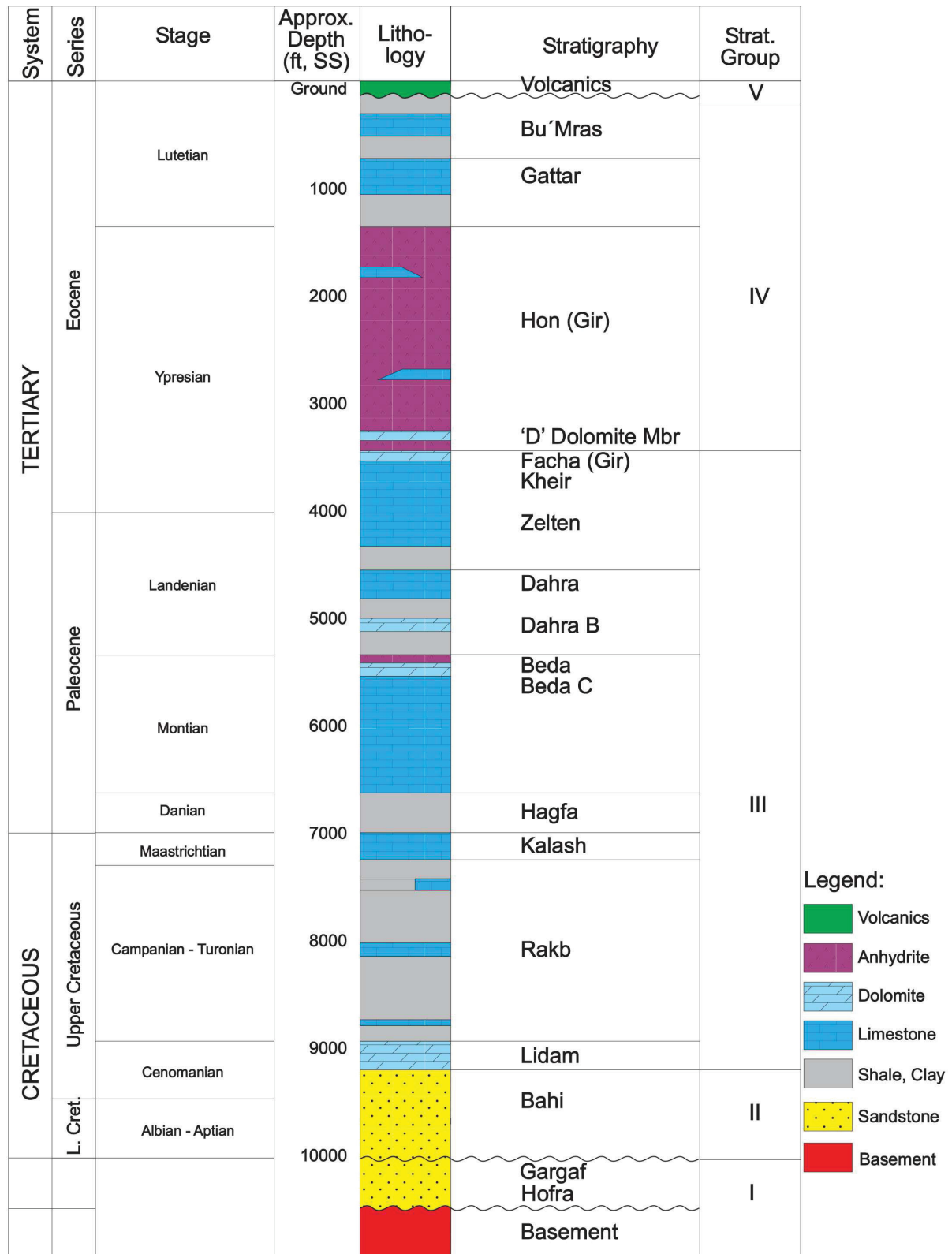
Figure 6.2: Stratigraphic type column of western Sirte Basin (modified after Gokturk and Tarhouni (1999) and Knytl et al. (1996).)

6.2.2 Stratigraphy of Sabah Field

In the Sabah field, a sequence of Bahi Sandstone of unknown thickness overlies the basement. The Bahi is overlain by the Lidam Formation, composed of fine-grained limestone and porous calcarenite. This is succeeded by approximately 2000 ft of marine shale with minor carbonates belonging to the Late Cretaceous Rakb Group and the Kalash Formation. This sequence is unconformably overlain by dark grey marine Hagfa Shale of Palaeocene age, which is conformably overlain by carbonates of the Beda Formation. The dolomitic Beda C reservoir interval is capped by anhydrites that form the seal of the Sabah reservoir. The Beda Formation is succeeded by the Dahra Formation, a dolomitic and argillaceous limestone whose upper part is massive and has good porosity. The argillaceous, fine-grained limestone of the Zelten Formation and the shaly carbonates of the Kheir Formation are the uppermost units of Paleocene age. The Facha Member is the basal unit of the Eocene Gir Formation; it consists of dolomite and limestone deposited in a sabkha environment. The Facha grades upward into the Hon Member of the Gir Formation, an anhydrite with some inter-bedded dolomite and fine-grained limestone. Carbonates of the Gattar Formation, sandstones and carbonates of the Bu'Mras Formation, and basalts of Miocene through Pliocene age complete the sedimentary succession in the Sabah field.

The Sabah main reservoir is in the Beda C interval that was deposited on a widespread carbonate platform during an early Paleocene third–order regression cycle. The regressive nature of the Beda C interval is reflected by the change from a limestone dominated, marine environment at the base of the reservoir, succeeded by a dolomite dominated tidal flat, then a sabkha environment at the top. Numerous parasequences (forth order cycles) originating from high frequency sea level changes are present.

The depositional pattern has influenced reservoir quality in the Sabah field, as rock properties were selectively altered by dolomitisation that occurred during shallow burial when the overlying sediments were laid down in a sabkha environment. Most sedimentary features and textures, especially in the upper part of the reservoir, were destroyed. Fossils were rarely preserved except as moldic porosity that resulted from the dissolution of foraminifera tests.

The reservoir is subdivided into three main zones; a lower dolomite (Zone I), an upper limestone (Zone II), and an intervening low porosity layer (the "Tight Zone"). The base of the reservoir consists of a 20 to 30 ft interval of nonporous limestone, overlain by limestones of gradually improving reservoir quality. Zone I has porosities up to 35% and high permeability, the result of extensive dolomitic alteration. In contrast, the Tight Zone is argillaceous, with porosities ranging between zero and 8%. Zone II consists of limestone that shows little diagenetic alteration. Porosity and permeability are low at the bottom of Zone II but improve upward and become similar to Zone I. The top of the reservoir is an eight to ten feet thick shale, forming the lowest of a series of anhydrite and shale beds that constitute the caprock of the reservoir. Zones I and II are divided vertically into subzones based on geological characteristics and reservoir quality; Figure 6.3 shows the stratigraphic positions of the reservoir subzones.

Figure 6.3: Stratigraphic positions of Sabah reservoir sub-zones based on reservoir quality.

6.2.3 Structure of Sabah Field

The Sabah structure is an anticline about 8 kilometers long in an east-west direction and 5 kilometers wide in a north-south direction. The field is cut into a series of fault blocks by normal faults that trend NW–SE, parallel to the main faults of the western Sirte Basin. These divide the Sabah structure into three main areas, the Eastern, Central and Western Sabah. The "East Sabah fault" separates the Central Sabah from the Eastern Sabah and the "West Sabah fault" separates the Western Sabah from the Central Sabah. The Sabah structure is part of a series of post-Oligocene right-lateral strike-slip faults and anticlines generated in a compressional or wrench-dominated environment (Knytl et al. (1996). The main production of petroleum comes from the central block because of its larger acreage, greater thickness and better porosity, permeability and lower water saturation. The field does not exhibit compartmentalization, indicating that the faults are non-sealing. There are many indications of extensive fracturing, including loss of drilling mud, patterns on dipmeter logs, results from transient permeability tests, and production performance. In addition, fractures are seen in cores and on FMI (Formation MicroImager) logs.

The intensity of fractures in the Sabah field plays a key role in the behavior of the reservoir and the distribution of fluids. The structure map in Figure 6.4 is drawn on the top of the Beda C reservoir and shows well locations and the traces of faults that cut the reservoir interval.
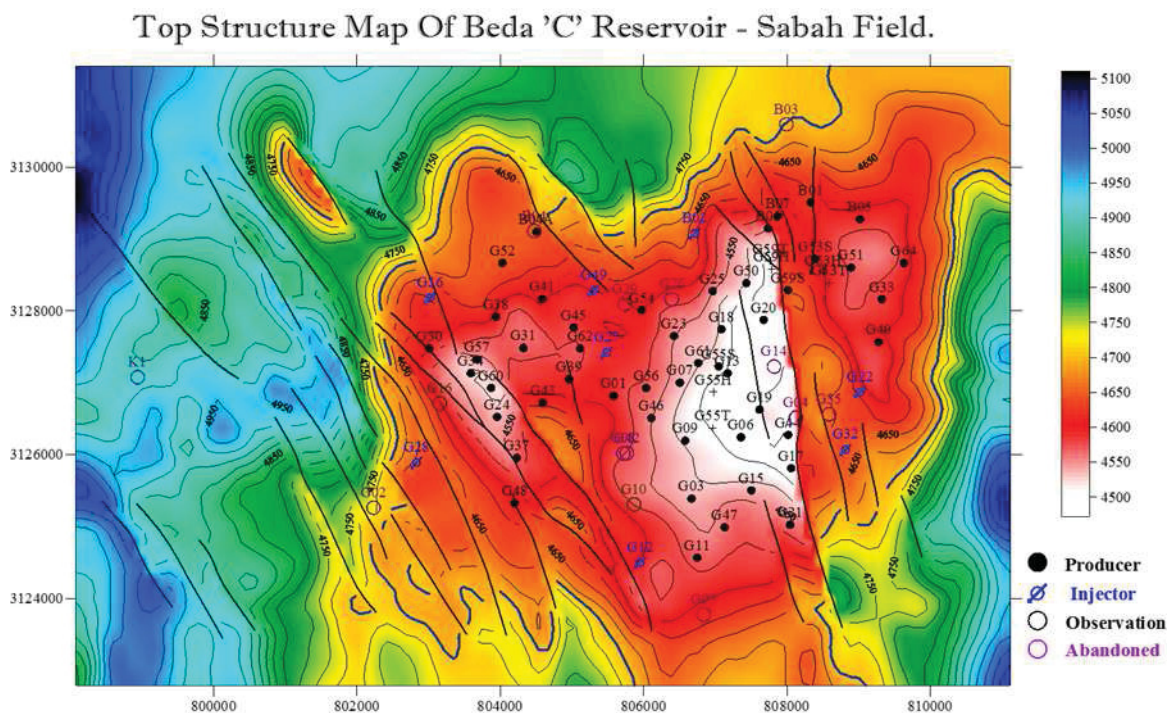
Figure 6.4: Top Structure Map of Beda C Reservoir –Sabah Field

6.3 The Dynamic Reservoir Model

6.3.1 Pressure History of Sabah Field

The reservoir pressure history measured in Sabah wells (Figure 6.4) indicate that the Sabah reservoir is a single body, although faults divide the field into regions with different OWCs and different depths to the top structure, as shown in Figure 6.5.
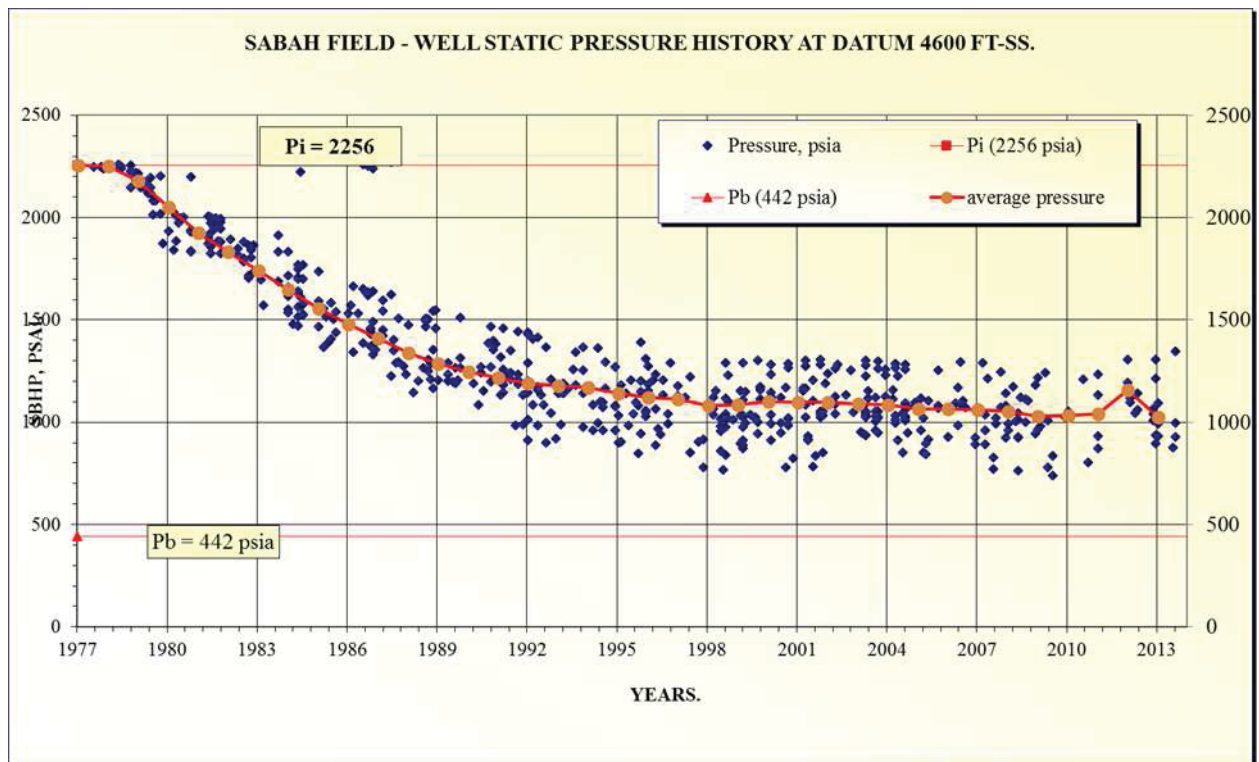
Figure 6.5: Static Pressure History of Sabah Wells at Datum 4600 FT-SS.

6.3.2 Production History of Sabah Field

Several studies have been conducted to develop models of the Sabah reservoir. Figure 6.6 shows the reservoir's structure in 3D view and Figure 6.7 shows an east–west cross section that includes the layers in a flow simulation model. The latest reservoir model covers an area of approximately 28,000 acres and indicates that the original oil in place was 504 MMstb. Seventy development wells have been drilled in the field, producing oil from the Beda C reservoir – most wells are vertical and a few are horizontal. More than 222 MMstb of oil and 806 MMstb of water have been produced as of December, 2013. This corresponds to a field recovery factor of 44%. Peak field oil production was reached early in the life-cycle of the field, at 40 MSTB/D. Oil

production rates then began to decrease and the water cut to increase. The average reservoir pressure had declined during the first 20 years of production by approximately 50%. Reservoir performance is influenced by both a bottom drive and a strong edge aquifer. No plateau rate was established. In 1999, a water injection program was started to help maintain reservoir pressure at about the present level of 1200 psi and to increase sweep efficiency. The current field liquid production rate is around 95 Mstb/day with a water cut of 90%. The production history of the field is shown in Figure 6.8. The performance of individual wells is characterized by a high water cut that develops instantaneously. The well performance shown in Figure 6.9 is representative for all producers in the field.

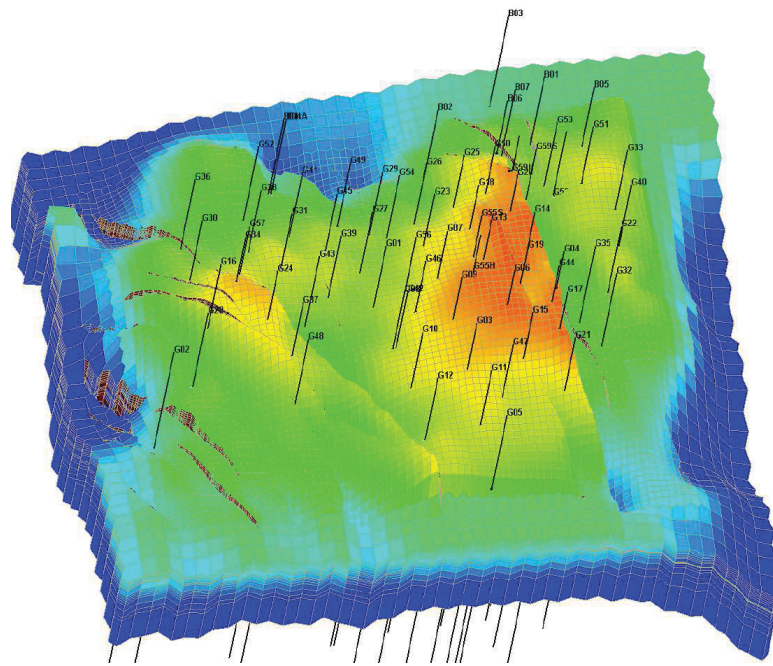Figure 6.6: 3DView showing the top structure and simulation grid of Sabah reservoir model.
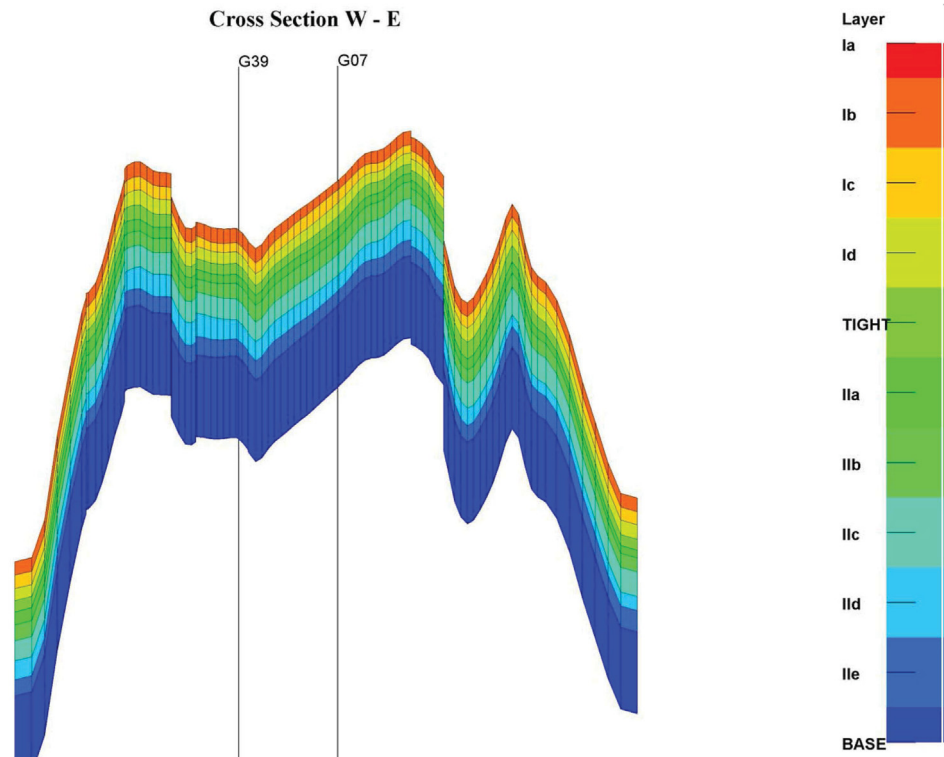
Figure 6.7: East–west cross section of Sabah reservoir model showing the layering of the flow simulation model.
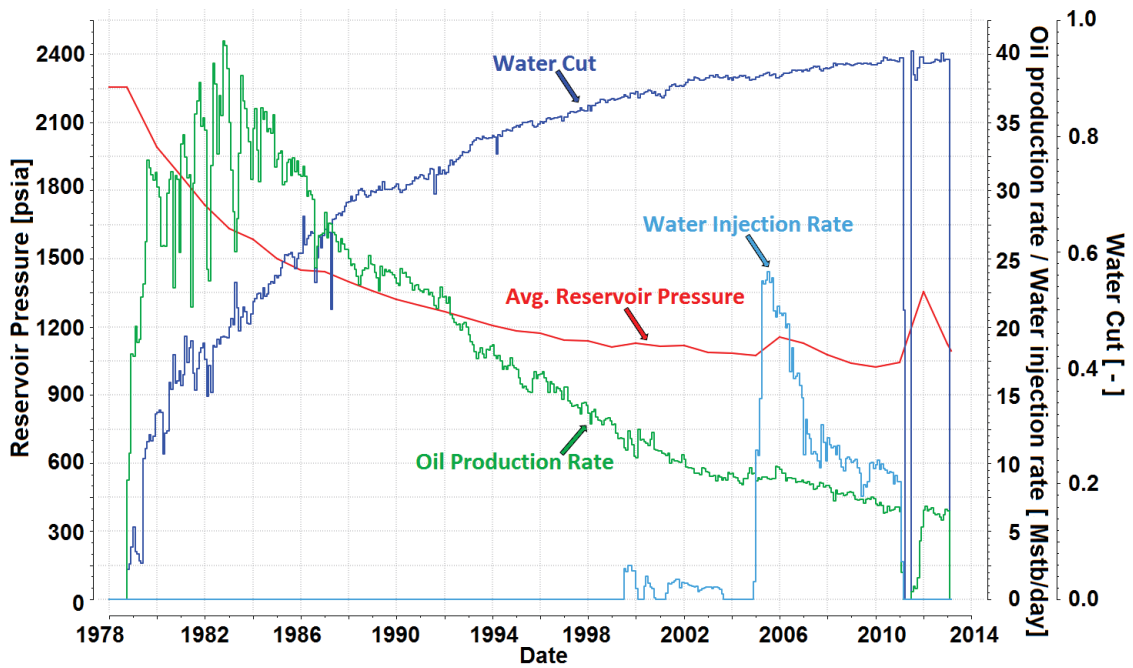
Figure 6.8: Production and injection and pressure history for the entire field.
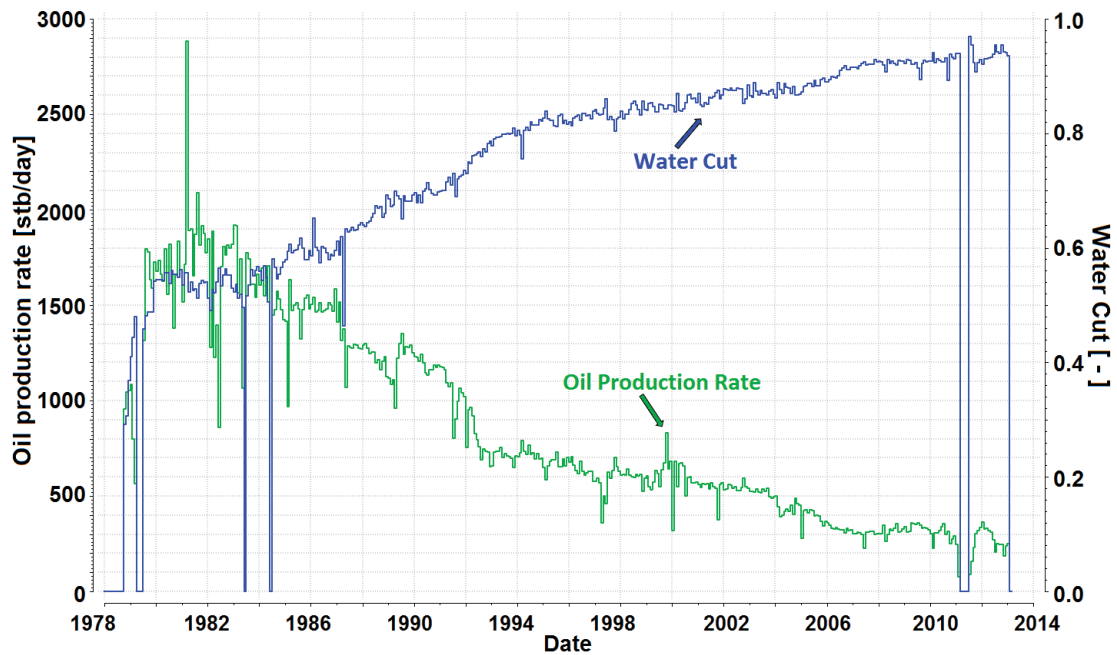
Figure 6.9: Example of a well producing instantaneously at high water cut.

6.3.3 The Simulation Model

For both the simulation model and the material balance calculation the basis is the geocellular model containing normally millions of blocks. Naturally MB calculations can also be conducted directly on an existing reservoir simulation model. For MB calculations the vertical and lateral resolution and the applied gridding technology (pillar grids/corner point geometry for the geological model and Cartesian or unstructured (PEBI) grids for the simulation model) are of no importance. Upscaling a geocellular model to a simulation model preserves the property distributions and the mean values. Naturally this is also valid for the pore volumes, which are one of the main inputs for material balance. Direct usage of a simulation model as basis for MB investigations has the advantage that all the required input data already exist. In the following, the minimum data requirements for a MB model are summarized:

- Grid model initialized in black oil formulation.
- PVT data: Full data set comprised of standard densities, bubblepoint pressure, tabulated data of formation volume factors, solution gas/oil ratio and viscosity.
- SCAL data: rock compressibility factor, relative permeability and capillary pressure functions.
- Production history (oil/gas/water).
- Pressure history, expressed as an average field pressure.
- Depth of the initial phase contacts, namely OWC and GOC, and also their positions during the production history.
- Recovery curve representing the (expected) matrix-fracture interaction.

As a basis for the herein presented field example serves a simulation model with 230,396 active blocks. The grid is an orthogonal one with zigzag fault representation. The model has 16 layers and the lateral resolution is 96x80 blocks. The interface (boundary) towards the edge aquifer facilitates water encroachment for the model and thus pressure support. The location of this outer boundary and all wells is depicted in Figure 6.10. Coloring of the grid blocks shows the initial water saturation distribution of the matrix.
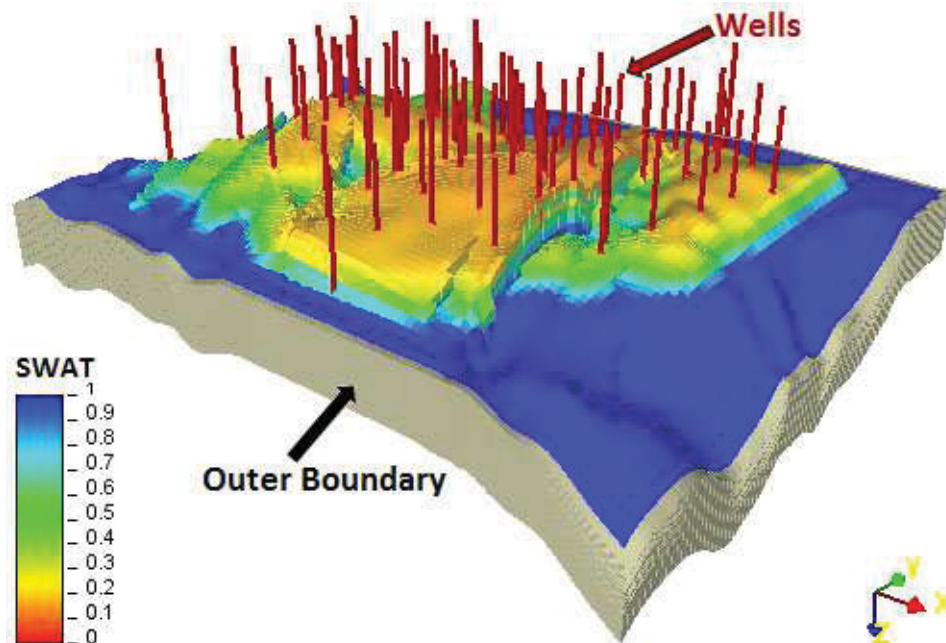
Figure 6.10: 3D view of full field example (initial matrix water saturation, faults, well locations, outer boundary)

The reservoir fluids can be described by one set of PVT data, because no spatial variation or gradients in fluid properties exists. Contrary, SCAL properties (saturation end points and shape of the functions) vary with reservoir zonation. 10 rock regions for the matrix and one for the fracture are introduced. It should be noted that for initializing the reservoir model the variations of the SCAL properties (endpoints and curvature of the capillary pressure functions) was exactly honored. However for the MB calculation itself, no differentiation can be made for the endpoints and the shape of the relative permeability functions. Instead one set of rock functions which is representative for the entire model was used. The value for the connate water saturation equals 30%, for the residual oil saturation respectively 25%. The associated functions are presented in Figure 6.11.
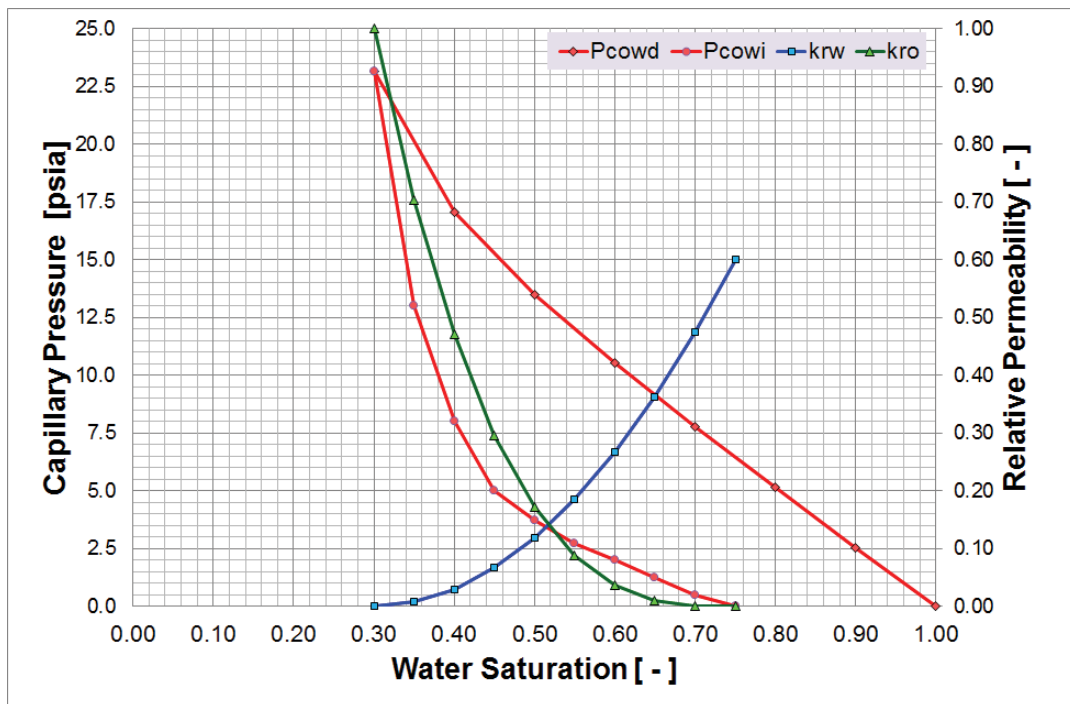
Figure 6.11: SCAL functions representative for the entire model

The initial oil water contact is at a depth of 4700ft SS. During the entire production history the oil remains undersaturated, therefore neither an initial nor a secondary gas cap exists and the reservoir stays in a two phase (oil/water) state all the time. The model top is at 4471ft SS, the model bottom depth equals 5233ft SS. Consequently the maximum oil column thickness measures 229ft. Matrix porosity ranges from 0.5 to 36% with an average of 11%. Constant 0.5% fracture porosity was assumed throughout the entire model. Usage of a recovery curve for regulating the matrix-fracture transfer makes the determination of shape factors superfluous. Therefore also no numbers are given here.

6.4 Motivation for Performing MB on Sabah Field

As already mentioned, the last simulation study of Sabah reservoir was performed in 2007. Based on conclusions drawn at this time, additional wells were drilled. All of them failed their production targets considerably. Consequently, the operating company (ZOC) started to reconsider its actual production strategy. A new simulation study, especially the revision of the geological model and the history matching, would require considerable time. It was decided to perform a material balance calculation based on the existing geological model, with the ambition to answer within shortest possible time the following most critical questions:
- Prevention of further reservoir pressure decline.
- Possibility to reduce or at least not to further increase the water production rates.
- The necessity,/ effectiveness of the water injection program, initiated in 1999.
- Disposal of the produced water to the Sabah reservoir or to other formations.

6.5 Determination of the Phase Contacts of Sabah Field

The procedure used for oil water contact (OWC) determination picks the contact at the depth where water saturation first reaches (or comes close to) 100%. This is sometimes inaccurately called the free water level (FWL). This contact can usually be picked on the resistivity log where resistivity reaches its lowest values in a clean, porous reservoir. However, this method only works if the transition zone is thin and differences in shale content, lithology, porosity, and the existence of residual oil or a tar mat do not mask the pick. In layered reservoir sequences or in wells that show oil-down-to (ODT) due to reservoir conditions such as a tight zone below the oil zone, this method cannot be used to determine a field-wide OWC. In the Sabah field, determining the FWL is not easy because changes in rock quality make identification of the OWC and transition zones from resistivity and water saturation logs difficult.

The oil water contact (OWC) and the original oil water contact (OOWC) have been reviewed using petrophysical information from each of 70 Sabah wells. To assess the OWC, 14 traverses from well to well were made in different directions to investigate the level and movement of the OWC, based on the production history of the field. Figure 6.12 and Figure 6.13 show samples of these (traverses) cross sections.

Identification of OWC depth in the Sabah reservoir it is not straightforward. The OWC is not a horizontal surface because of lateral variation in reservoir rock lithology and reservoir quality. An unambiguous OOWC level can only be identified from well logs where the reservoir rock quality is good and the capillary transition zone is small.

6.5.1 Determination of Original Oil Water Contact

Determining the oil-down-to (ODT) and water-up-to (WUT) depths by interpretation of well logs helps identify the OOWC, and is more effective than attempting to directly identify the OOWC from resistivity logs or capillary pressure measurements. The data from south-north and west-east traverses are plotted on in Figure 6.14 and Figure 6.15. The plots distinguish between data recorded before and after significant production began. From these plots the OOWC was picked at a depth of 4700 ft ss.
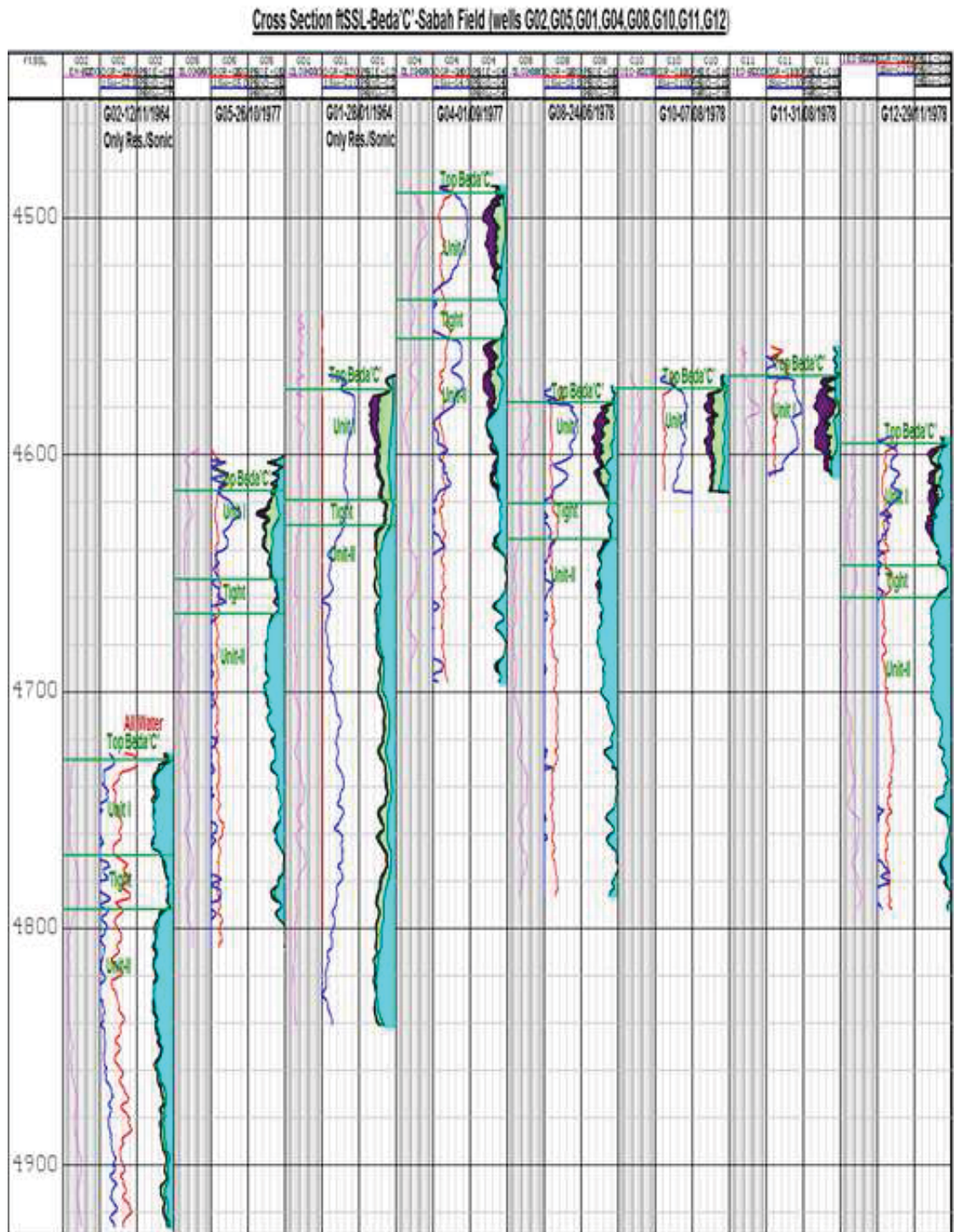
Figure 6.12: Cross section covering Sabah Beda-C wells G02, G05, G01, G04, G08, G10 and G12 showing petrophysical information used for phase contact determination.
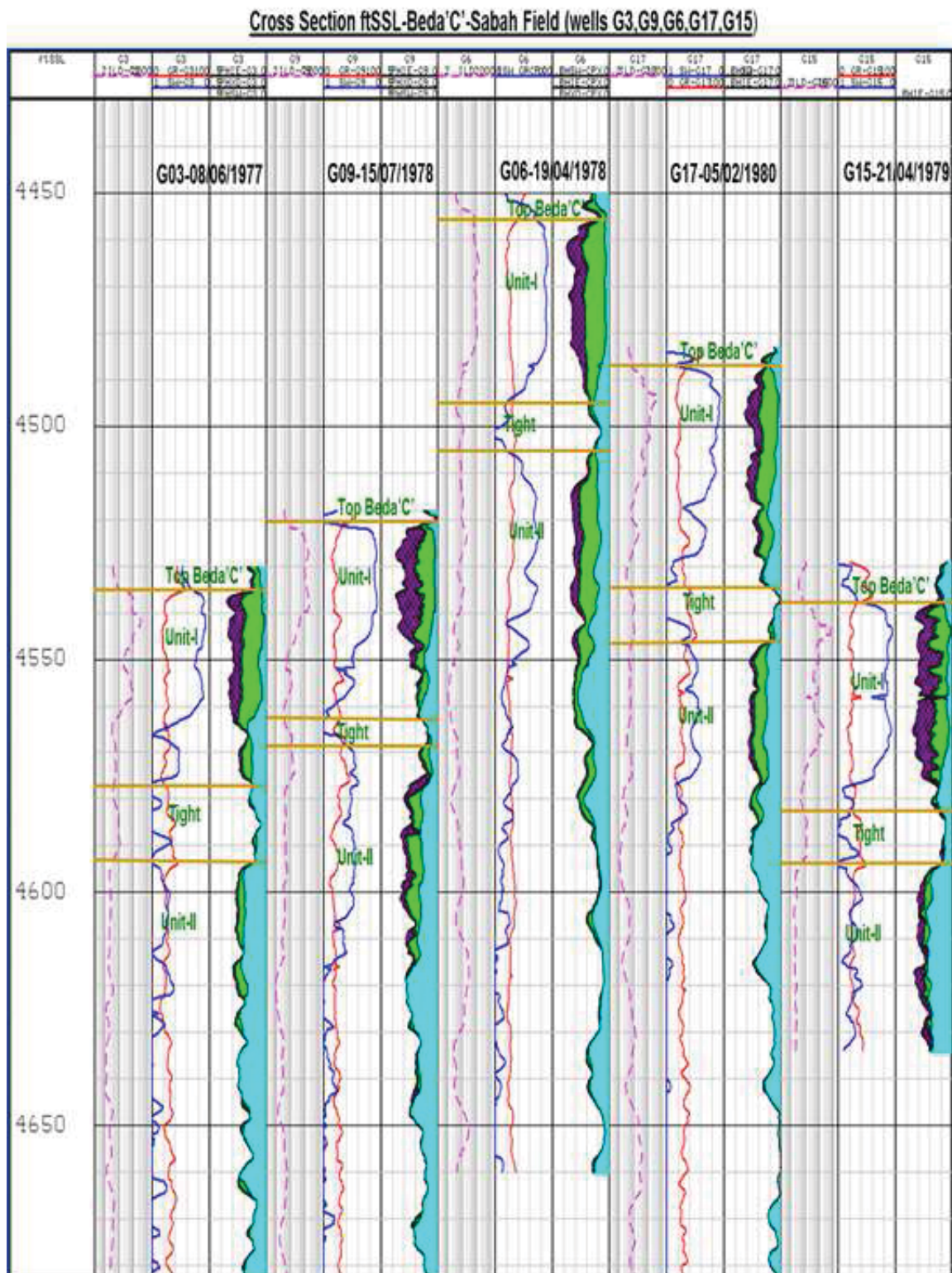
Figure 6.13: Cross section covering Sabah Beda-C wells G03, G,09, G06, G17 and G15 showing petrophysical information used for phase contact determination.
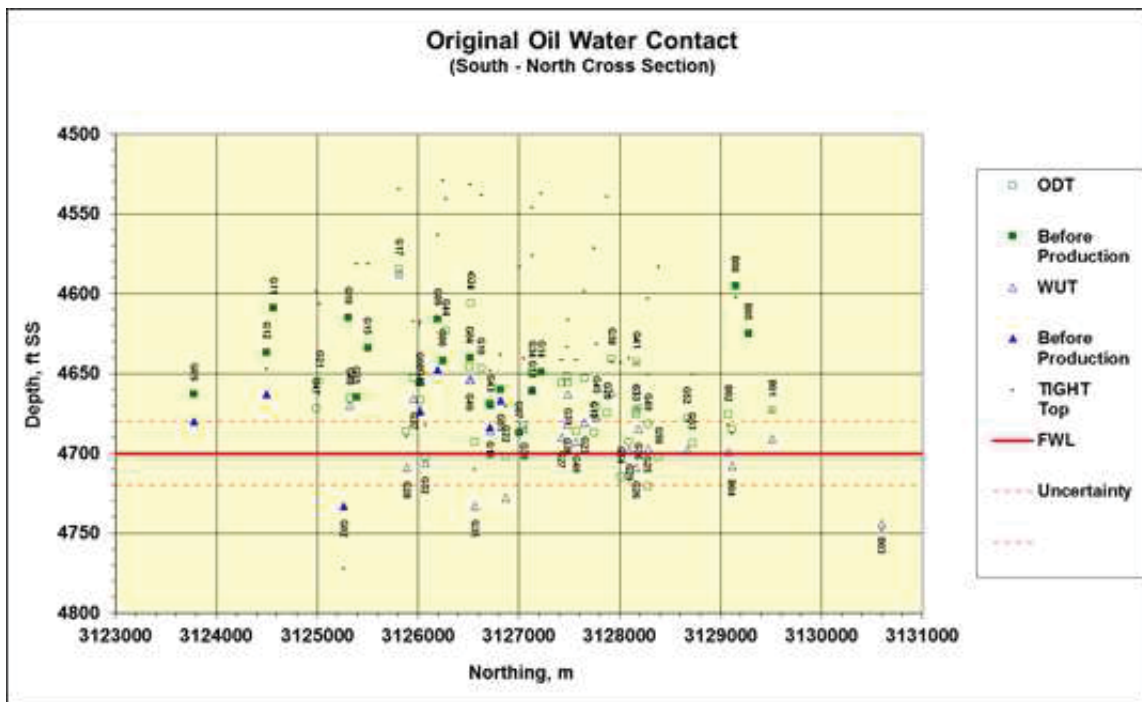
Figure 6.14: Original Oil Water Contact (South – North Traverse) of Sabah Field.
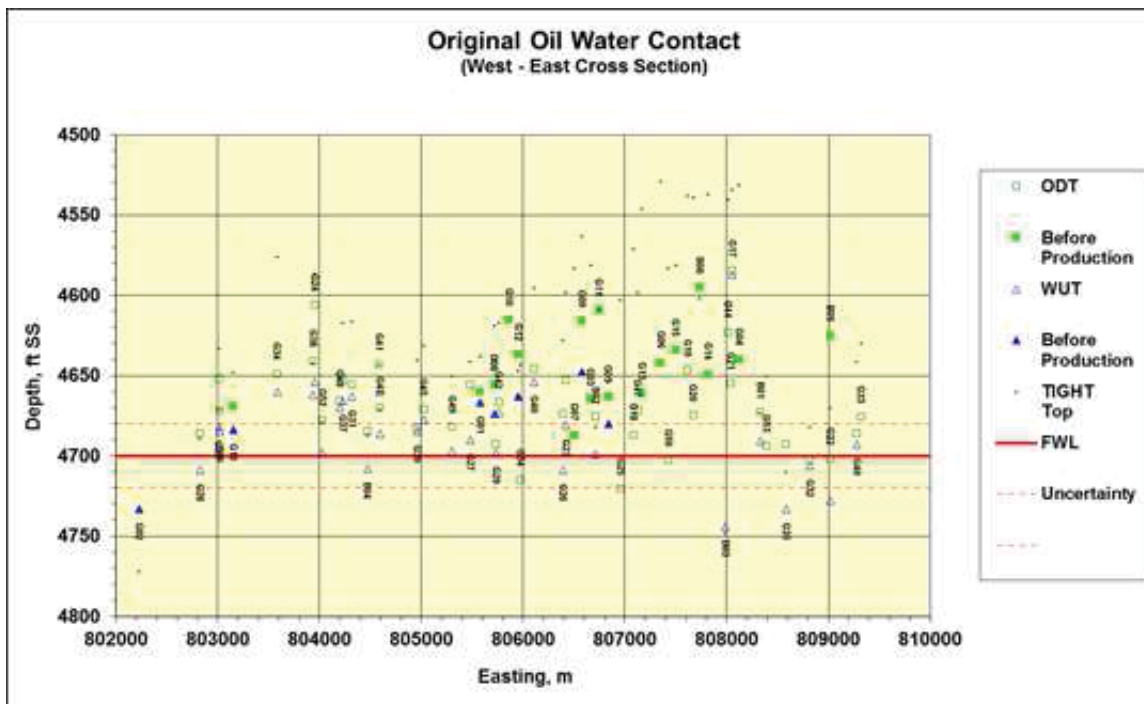
Figure 6.15: Original Oil Water Contact (West – East Traverse) of Sabah Field.

These data indicate that some wells have unexpectedly high oil saturations in the deeper parts of the reservoir below 4700 ft ss. This requires further investigation. Wells drilled with oil based

mud are more likely to exhibit increased oil saturation in deeper reservoir sections. If the calculated oil saturations are dependent on the resistivity of the drilling fluid, we can conclude that the depth of invasion is greater than the depth of investigation of the resistivity tools. This may happen if the reservoir rocks are relatively tight and there was enough time for the mud filtrate to reach equilibrium with the formation fluids. Other influences might be the presence of fractures, which may contribute to the observed effect.

6.5.2 Determination of Dynamic Oil Water Contact

Investigations of the dynamic oil water contact level were based on production performance and petrophysical analyses of newly drilled wells during the life cycle of the Sabah field. Figure 6.16 to Figure 6.19 show the results of petrophysical analysis of selected wells in the field.
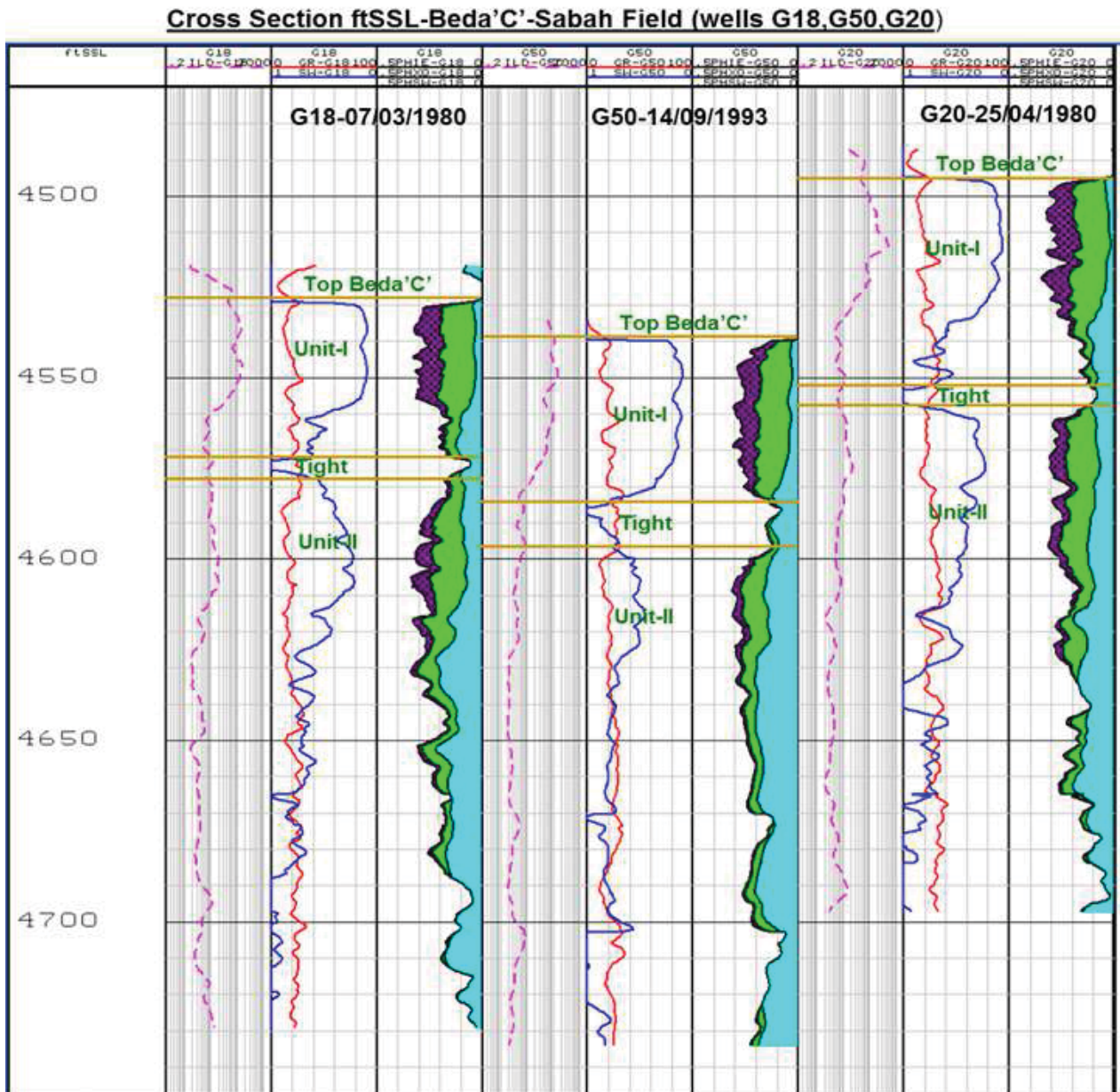
Figure 6.16: Petrophysical Data for Dynamic WOC Determination - Sabah Well to Well Traverses (NE-E).
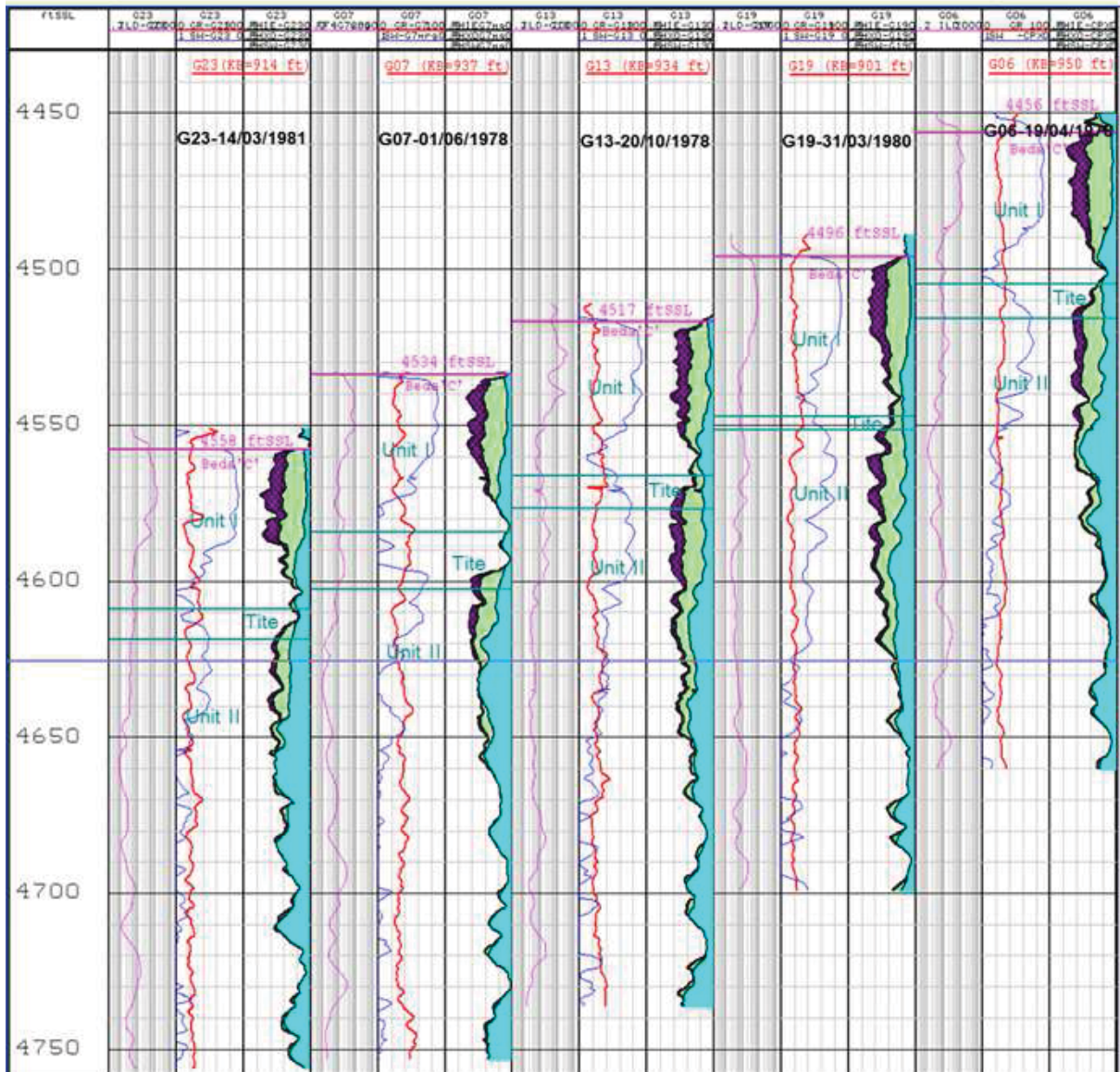
Figure 6.17: Petrophysical Data for Dynamic WOC Determination - Sabah Well to Well Traverses (N-S).
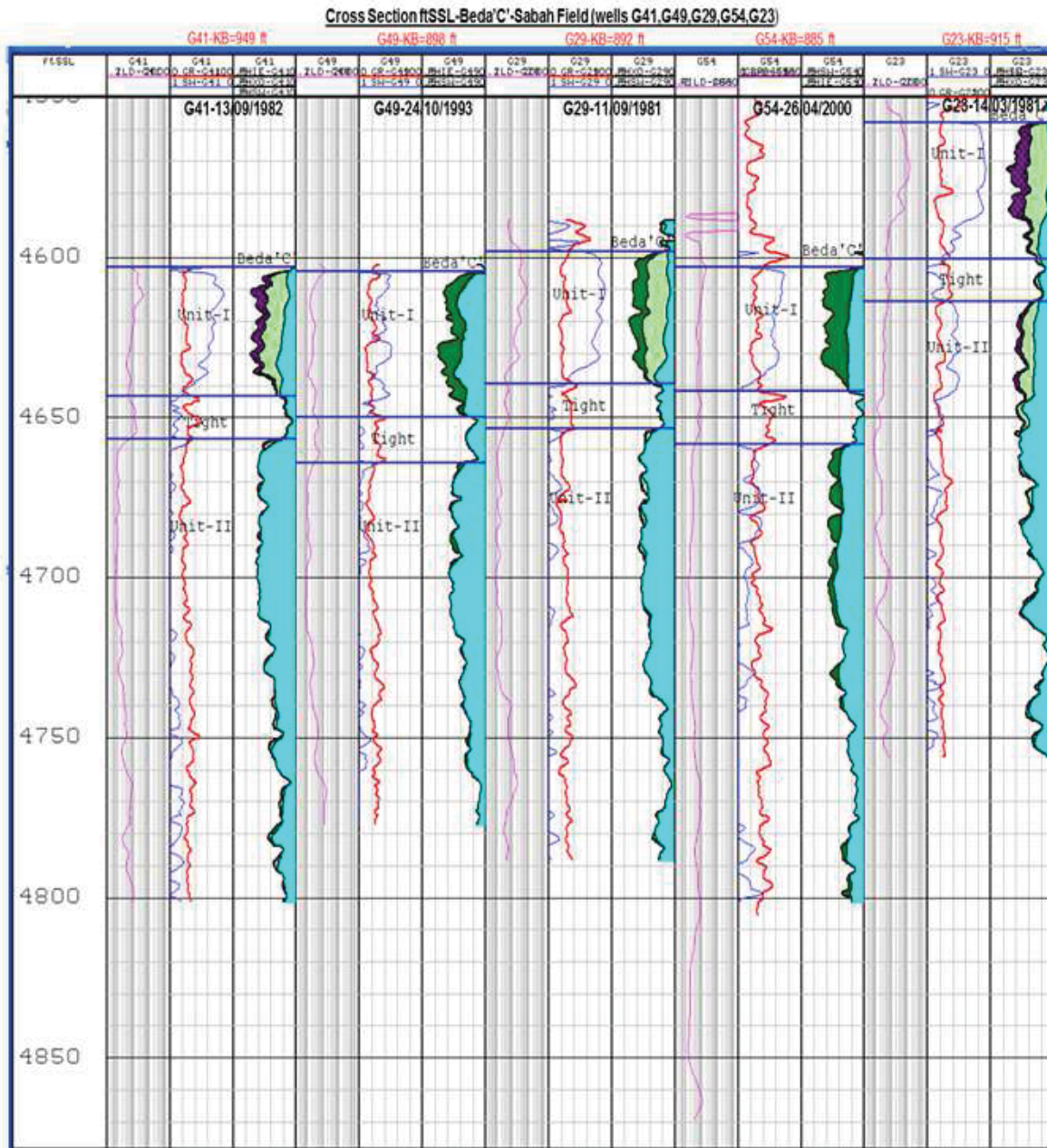
Figure 6.18: Petrophysical Data for Dynamic WOC Determination - Sabah Well to Well Traverses (W-SE).
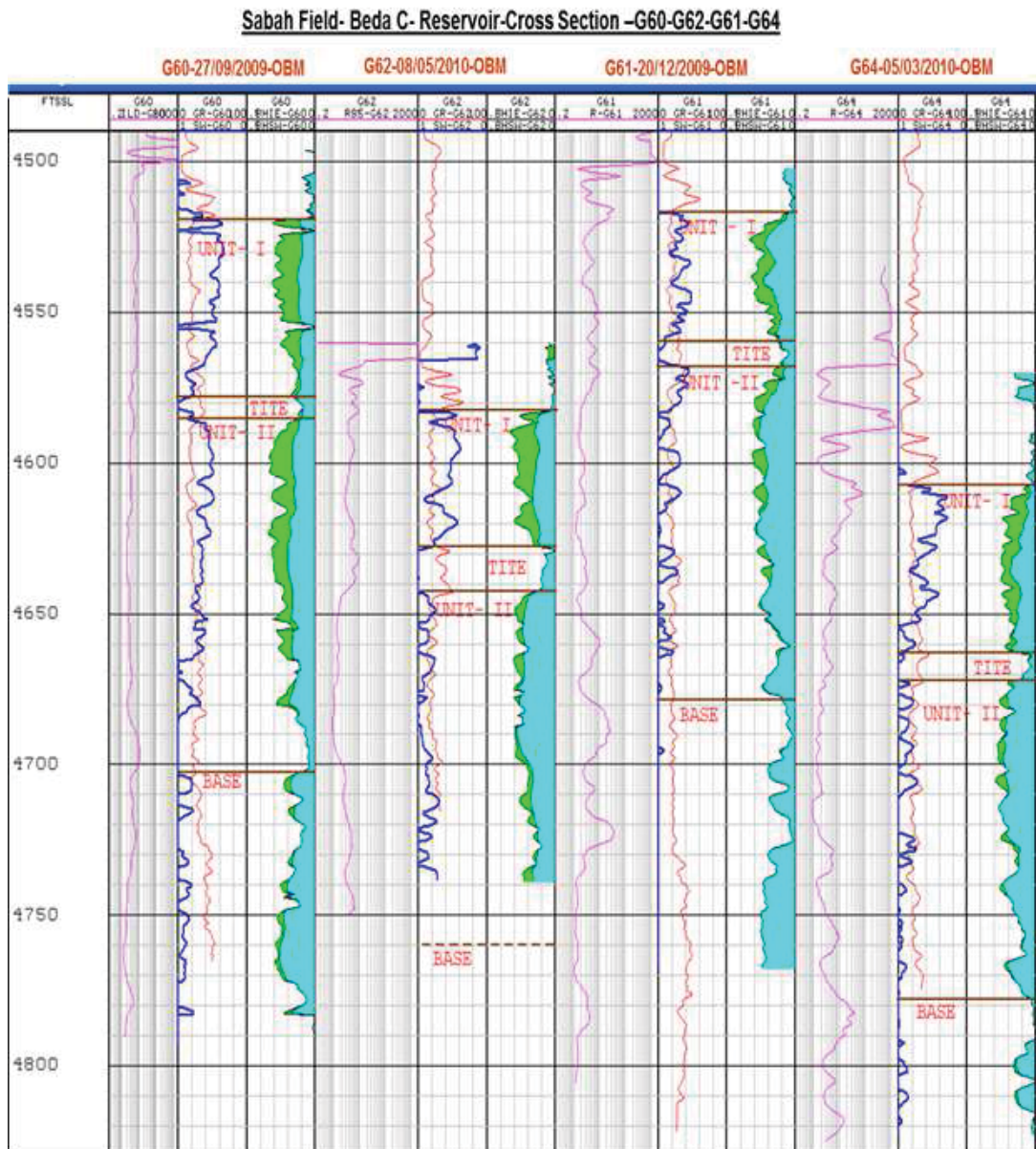
Figure 6.19: Petrophysical Data for Dynamic WOC Determination - Sabah Well to Well Traverses (W-E).

6.6 Determination of Recovery Curve

Previously it was mentioned that different possibilities exist for determining recovery curves applicable for full field investigations such as material balance calculations or numerical flow simulation. Contrary to simulation, where different recovery curves can be applied by introducing so called recovery curve regions, taking into account spatial variations in matrix quality resulting from different rock types, this is not possible for material balance calculations.

Similarly to one average pressure, one set of PVT and SCAL data – where all of them are regarded as representative for the entire field – also just a single recovery curve can be used. To come up with a reliable initial (normalized) recovery curve which can be used as a well suited starting point for phase contact matching a twofold strategy has been followed:

1. Following the workflow proposed by Amiry (2014) a normalized recovery curve based on single matrix block analysis incorporating all available relevant data of the example reservoir was elaborated.

2. Amiry (2014) showed that the recovery curves are scalable regarding shape factor, permeability and porosity and that the actual geometry of the matrix blocks has no influence on the recovery curve. Therefore the spatial variations of those properties can be disregarded when determining the normalized recovery curve. However, this is not true for variations in SCAL data, namely capillary pressure and relative permeability functions. Both, the endpoints and the shapes of the functions, are decisive for the matrix oil recovery, recorded by the recovery curves. To come up with one representative curve, at first single matrix block calculations were conducted for all matrix rock regions, resulting in ten curves. In a next step those curves have been lumped to one single curve. Lumping is the process of unifying different curves by applying a weighted averaging. Details about this process can be found in Amiry (2014). As weighting factor the hydrocarbon pore volume of each rock region compared to the total hydrocarbon pore volume was chosen.

3. Considering the production history of the field a recovery curve was determined.

4. This approach assumes, that at first the entire original oil in place residing within the fracture network will be produced. This means that at early times the matrix blocks do not feed into the fracture network. When this phase is finished, the entire production will be coming from the matrix. This means that the ratio of cumulative production from the matrix system to the original oil in place of the matrix, becomes equivalent to the recovery factor, thus resulting after some smoothing and curve fitting in the desired recovery curve. Naturally this is a simplification, but is regarded as a legal engineering approach.

Ideally, the recovery curves of the two approaches would fit to each other. For the presented field case, this was true for the asymptotic value, this means for the late time of the recovery but not for early times, when the two curves showed considerable differences in shape. Again, a lumping of the curves has been conducted, where the production history derived recovery curve was weighted by three quarters and the one derived from the single matrix block modelling by one quarter. The reason for this weighting is that the production data is regarded to be more reliable than the SCAL measurement which has a high impact on the outcome of the single matrix block calculations.

The resulting recovery curve (the red function displayed in Figure 6.20) is considered to be representative for the entire model and therefore well suited as a starting point for matching the phase contact movement using dual porosity material balance calculations.
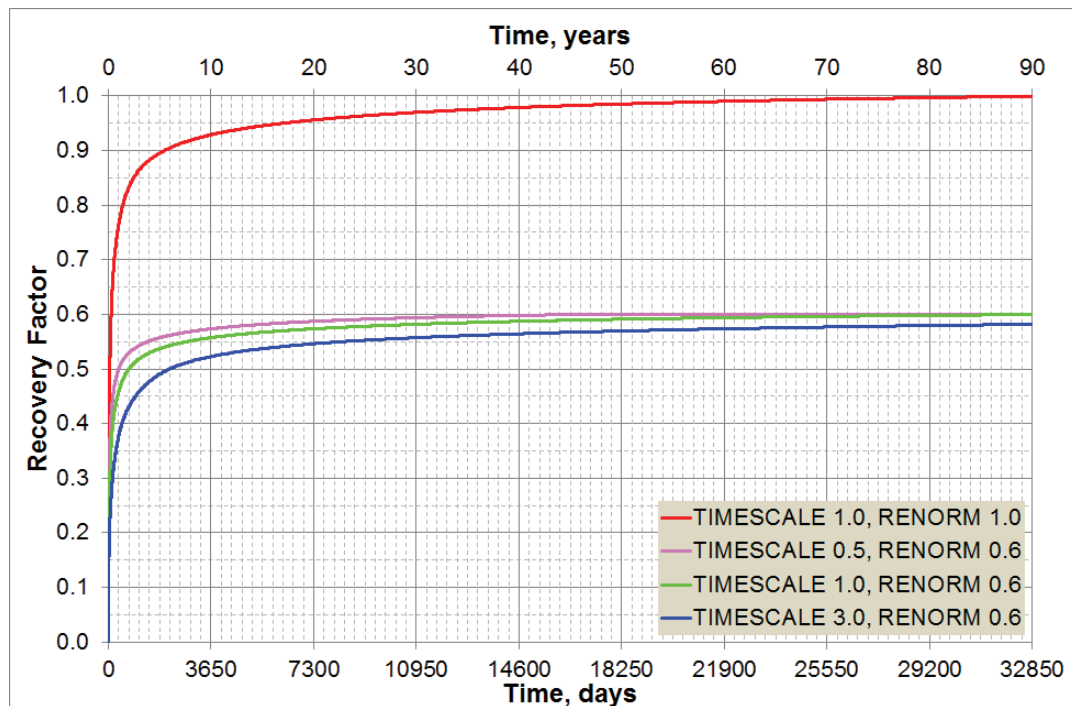
Figure 6.20: Normalized recovery curve used as input and scaled/renormalized recovery curves applied during phase contact matching.

6.7 Material Balance Calculation

For the presented dual porosity material balance calculation the initial distribution of the original oil in place has to be known. For the Sabah reservoir it has been calculated based on the grid model of the most recent simulation model, the initial OWC, the PVT data and the capillary pressure data of the ten rock regions. Having all this data available, the material balance model is initialized in the same way as a simulation model, giving the initial saturation and pressure distribution, on a cell by cell basis. Knowing the cells' pore volume, the original oil in place for each cell, but also for the entire model can be calculated for both domains, the matrix and the fracture domain. Figure 6.21 shows the resulting vertical initial water saturation (S_{wi}) distribution in two cross sections (one in North-South, the other in West-East direction). From these cross-sections the differences in SCAL properties, respectively connate water saturation, per sub-zone of the Sabah field, can clearly be identified. Figure 6.22 shows the vertical distribution of the original oil in place of the matrix covering the entire oil leg between the initial OWC and the top of the reservoir. The curvature of the function is influenced in the vicinity of the OWC by the transition zone and towards the top of the reservoir by the narrowing anticline.
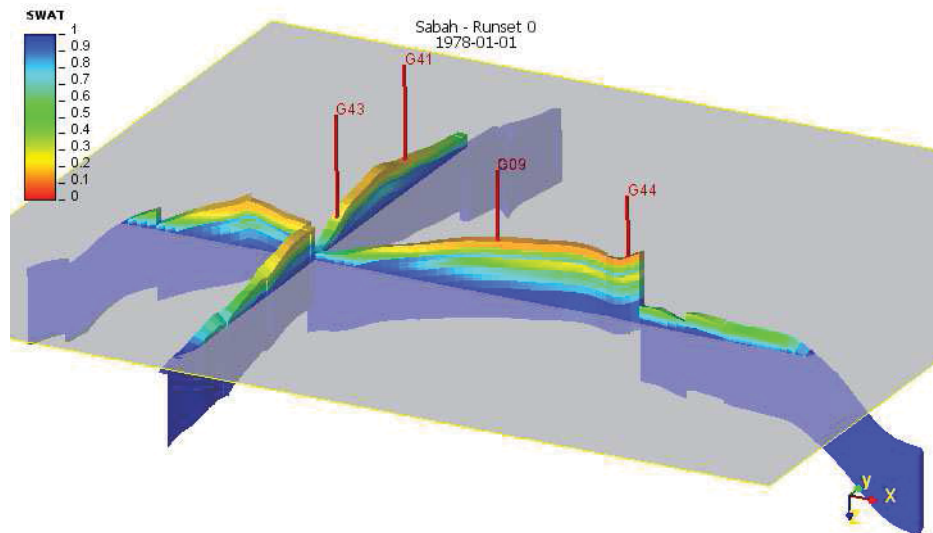
Figure 6.21: Cross-section through wells G09, G41, G43 and G44 showing the initial water saturation distribution in the matrix. The gray plane indicates the location of the initial OWC.
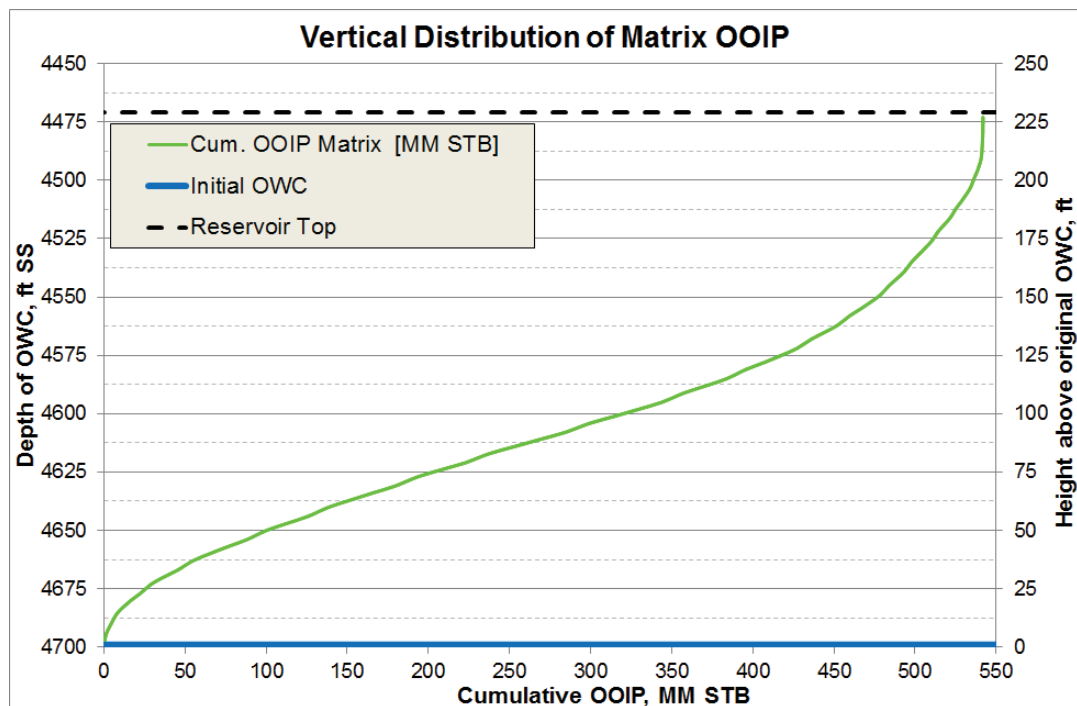
Figure 6.22: Vertical distribution of original oil in place.

For the Sabah field more than 500 static pressure measurements were taken at different well locations in the period from April 1977 until August 2013. Some of the measurements originate from observation wells, some of them from temporarily shut-in production wells. Due to varying shut-in times some of the measurements have been rejected for the pressure analysis. Creation of isobar maps did not unveil pronounced trends or areas with greater pressure

differences, thus the assumption of good communication within the field was proven. Consequently the field's pressure history could be simply calculated as an average from the static bottom hole pressure measurements.

Contrary to determination of the pressure history, coming up with a phase contact history was less straight forward. In theory, the actual position of the phase contacts within the fracture network could be determined by running well logs. Those were recorded for the Sabah field when drilling new wells only. Therefore, the amount of data and also their areal coverage and thus validity is limited. Fortunately, pressure evaluation has shown that no compartments exist, and therefore a more or less even (similar to a plane) rise in OWC can be assumed. Naturally, at the well locations, the general rise of the OWC is superimposed by coning. The assumed OWC movement is indicated in Figure 6.23 by the thick purple line. To account for the uncertainty the purple arrows indicate the confidence intervals. Usually the water table does not rise evenly in a reservoir, consequently, the dynamic OWC is not a horizontal plane. However the current software implementation of the presented dual porosity MB calculation can handle just one value and thus a plane must be assumed. For the future, it can be imagined to extend the implementation similarly to a multi pool material balance calculation, which can handle different region pressures and different outer aquifers, so that different phase contact regions are taken into account.
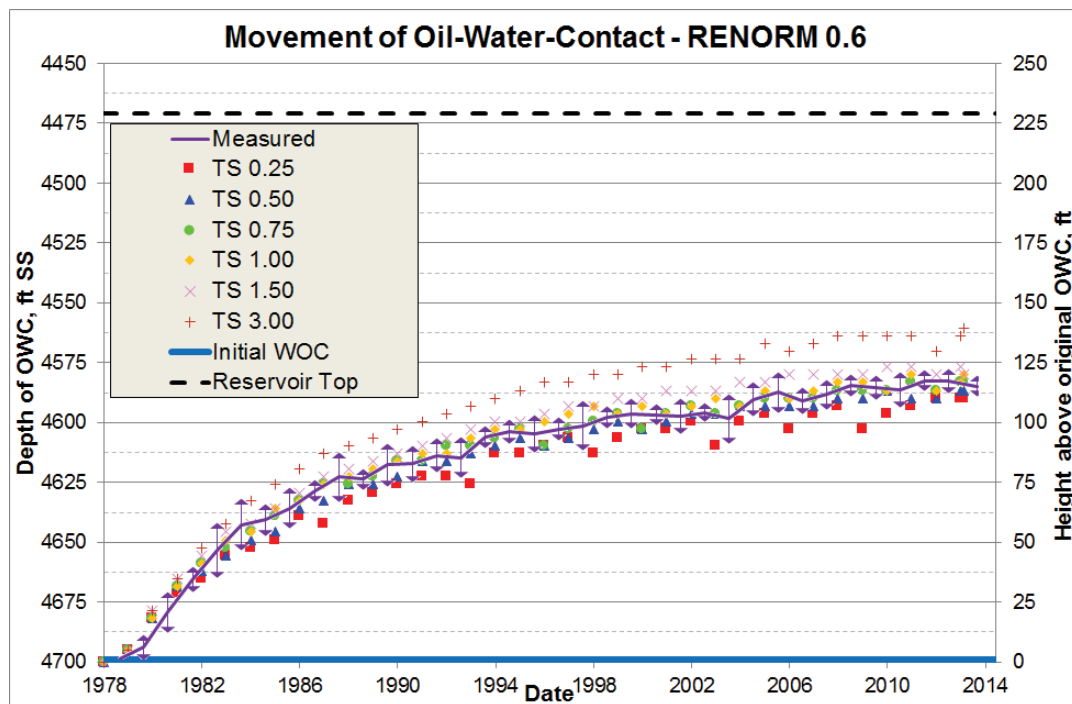
Figure 6.23: Comparison of calculated and observed phase contact data.

Considering the initialized grid model of the reservoir, the tabulated three phase (oil, gas, water) production, pressure and contact movement history, the PVT and SCAL data and the normalized recovery curve are the foundation for performing dual porosity material balance. As the name normalized implies the ordinate values are in the range of zero to one, in other words, the asymptotic value and thus the ultimate recovery of the curve would be unity. This can be clearly

seen from the red curve shown in Figure 6.20. Therefore the normalized input has to be internally renormalized by the used software so that the asymptote converges to a physically realistic value. Besides the ordinate, also the abscissa or, in other words, the time axis can be scaled. This means that without changing the shape of the recovery function and, thus, the characteristics of the matrix-fracture interaction the diligently elaborated input recovery curve can be tuned so that the observed reservoir behavior can be matched. Consequently two factors, the so called renormalization factor $1/\alpha$ and the time scaling factor β, are the only screws to be adjusted for matching the phase contact movement. In addition to the normalized recovery curve Figure 6.20 shows also the rescaled curves for $1/\alpha$=0.6 and β = 0.5, 1.0 and 3.0.

6.7.1 Matching of the Phase Contact Movement

Matching of the phase contact movement is performed iteratively. Starting from initial values for both tuning parameters, and thus giving an initial recovery curve, the entire production history is calculated with the proposed methodology. Afterwards the calculated phase contact positions are compared with the observed ones. If the result is not satisfying, respectively the observed discrepancies are not acceptable one or both of the scaling factors have to be adjusted and the entire procedure is repeated. However, practical experience has shown, that it is better to change always just one single parameter, otherwise it becomes difficult to distinguish the influences of each parameter on the calculated result. Choosing the starting value of the renormalization factor should be based on the available SCAL data. For water-oil displacement this results in:

$$\frac{1}{\alpha} = 1 - \frac{S_{or}}{1 - S_{wi}} \tag{6.1}$$

As already told, for the Sabah Field, ten rock regions, each having different connate water saturations, were identified. The residual oil saturation however is regarded to be constant. Therefore, the starting value of $1/\alpha$=0.643 was determined based on the as representative regarded SCAL functions shown in Figure 6.11.

For the time scaling factor the most straight forward approach would be to start with β = 1. Compared to numerical reservoir simulation, the CPU time required for a single MB run is negligible. Depending on the length of the available production history a run finishes within a couple of minutes. This allows testing of many different parameter combinations to come up with the most suitable recovery curve for describing the matrix-fracture interaction.

6.7.2 Discussion of the Results

In total 36 different combinations of the renormalization factor $1/\alpha$ and the time scaling factor β have been investigated for the presented example. The tested $1/\alpha$ values were in the range of 0.2 to 0.65 and those for β were in the range of 0.005 to 3. Figure 6.23 compares the measured

and the calculated OWC for combinations of $1/\alpha = 0.6$ and β values ranging from 0.25 to 3. The measured data is shown as a solid purple line, with confidence intervals at the data points. The calculated oil water contacts are shown with markers only.

Investigating Figure 6.23 in detail, it can be seen that none of the tested pairs of $1/\alpha$ and β values perfectly reproduce the measured - respectively most likely - OWC development, especially not over the entire 35 years of production history. It is clear that in order to reliably predict the reservoir performance, a tight match towards the end of history is more relevant than at early times. Considering the spread in measured data, expressed by the confidence intervals, the OWC development calculated for $1/\alpha = 0.6$ and $\beta = 0.75$ shown with green circles in Figure 6.23 gives the best fit. Therefore, this parameter combination was chosen as a basis for the prediction scenario described later on.

6.7.3 Determination of Best Fitting Analytical Aquifer Model

Considering Equation 4.14 the water influx requirements for matching the production and pressure history are known as a function of time. Based on this data an analytical aquifer model is determined which allows to calculate the water influx into the reservoir for prediction scenarios. For determining the best fitting analytical aquifer model the following error function should be minimized:

$$erf = \sum_{j=1}^{N} \omega_j [W_e(t_j) - W_e^a(t_j)]^2 \tag{6.2}$$

where $W_e(t_j)$ is the water influx determined during the material balance calculation, $W_e^a(t_j)$ is the water influx from one of the available analytical models (Fetkovich (1971), Vogt and Wang (1987), Carter and Tracy (1960)) and ω_j is a weighting factor based on the elapsed production time. It expresses that water influx taking place at a later time has more importance than early ones. This allows reducing transient effects occurring most likely at early times. An iterative procedure that is also well suited for software implementation is described by Mittermeir et al. (2004).

For the herein used full field example the best fitting aquifer model is of Fetkovich type. The governing parameters, maximum encroachable water and aquifer productivity index equal W_{ei} = 4,739.81MMrbl and J_w = 108.55 rbl/(psia.day), respectively. Before applying the Fetkovich analytical aquifer model and its parameter combination to the prediction runs it has to be verified. To do so, the history period has to be re-calculated with MB, but instead of calculating the required water influx from an outer aquifer for matching the average reservoir pressure (input), the average reservoir pressure (output) will be determined by the analytical model. On the left of Figure 6.24 the field performance (average reservoir pressure, oil production rate and water cut) for the history is shown. It should be noted that for this period two pressure curves are displayed. The red one corresponds to the pressure history. Therefore, the intervals between the data points (date where the average reservoir pressure was determined based on the static

bottom hole pressure measurements) are interpolated linearly. On the contrary, the pressure in the prediction mode is calculated with the beforehand identified best fitting analytical aquifer model. Of course, some differences between the two pressures can be observed, however, they are acceptable from an engineering point of view.
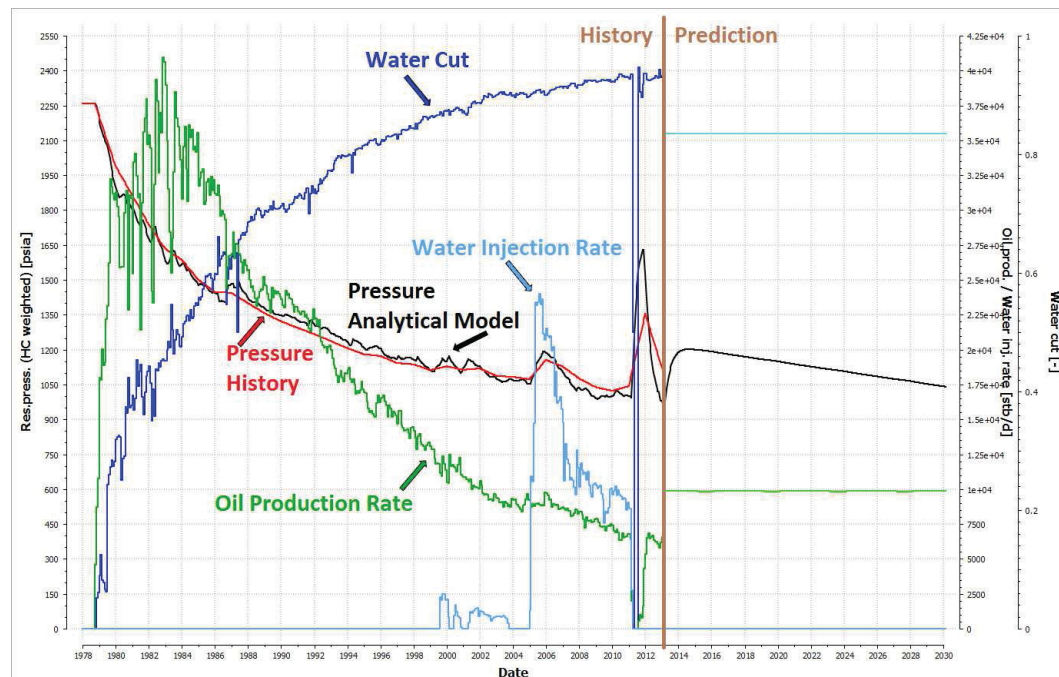
Figure 6.24: Forecasted reservoir performance with constant target oil rate and fixed water cut.

6.7.4 Prediction of Future Field Performance

Having determined the matched recovery curve and the best fitting analytical aquifer model, the prerequisites for calculating predication scenarios with material balance for dual porosity reservoirs are given. The engineer only has to decide on a future scenario by providing a target production. This allows a fast screening of possible production strategies on field level. As a matter of fact, individual well performances cannot be predicted in this way. This area is reserved for reservoir simulation. However, material balance provides a valuable tool for developing an understanding of the reservoir and the dominating recovery mechanisms. One of the advantages of the proposed workflow is that reservoir simulation and material balance are conducted on the identical model. Therefore switching between both modeling tools is always possible.

As mentioned previously, ZOC aims to maintain average reservoir pressure and also desires to cut back the high field water cut. The influence of water injection on field performance (this means pressure development and water cut) is controversial. On the one hand, it might lead to stabilization of average field pressure decline, on the other hand the possibility exists, that the

water is just cycled inside the fracture network and thus resulting only in operational costs for water treatment and pumps, but does not generate revenues by recovering additional oil. In case the Sabah Field would be a classical - this means non-fractured reservoir - water injection might be a good solution. However, since Sabah is a neutral to oil-wet naturally fractured reservoir, it is more likely that the matrix-fracture oil transfer is not influenced by the injected water.

To verify this assumption the following scenario was setup. Water injection, which is currently suspended anyhow, will not be put into operation again. The material balance model will be operated for another 17 years, this means until 2030. To reduce the amount of water produced that has to be treated and disposed, the water cut should be reduced from currently above 90% to 85%. At the same time, the field oil production should be increased from currently approximately 9,500 STB/D to future 10,000 STB/D. For reasons of simplicity, constant rates have been assumed for the prediction scenario. At first glance it sounds impossible to increase the field oil rate and decrease the field water cut.

However, the right side of Figure 6.24 presenting the field performance (average reservoir pressure, oil production rate and water cut) for the prediction period shows that this seemingly contradiction of increased net production and reduced water cut is feasible, due to the nature of this naturally fractured reservoir. Oil recovery from the matrix is governed by the capillary imbibition and gravity drainage, but not by drawdown. The above outlined scenario means that the liquid production rate would drop from currently 95 MSTB/D to 60 MSTB/D. Additionally, it can be clearly seen from Figure 6.24 that at first the average reservoir pressure will increase sharply by about 200 psia and will moderately drop until the end of the prediction period to the actual level. This pressure response can be explained by the decrease of gross production and the strong outer aquifer.

Figure 6.25 shows the oil water contact movement for the history period and also the forecasted rise. Finally, Figure 6.26 compares the matrix oil recovery factors per tranche as a function of depth for the end of history and end of prediction. Also from this plot the rise of the water table can be identified.

For the demonstrated case dual porosity MB calculation shows that an increased of field oil rate and reduced water cut is theoretically feasible. The question how to apply this finding to the field, respectively how to modify the production operations, has to be answered by reservoir simulation. Only a numerical reservoir model allows to assess individual well performance and their prediction. Note, that there is a difference between a tank model, the numerical reservoir model and the real reservoir. However material balance always was a valuable tool for reservoir engineers for quick assessment of reservoir performance and production planning. From now onwards it is also possible to use it for naturally fractured reservoirs.
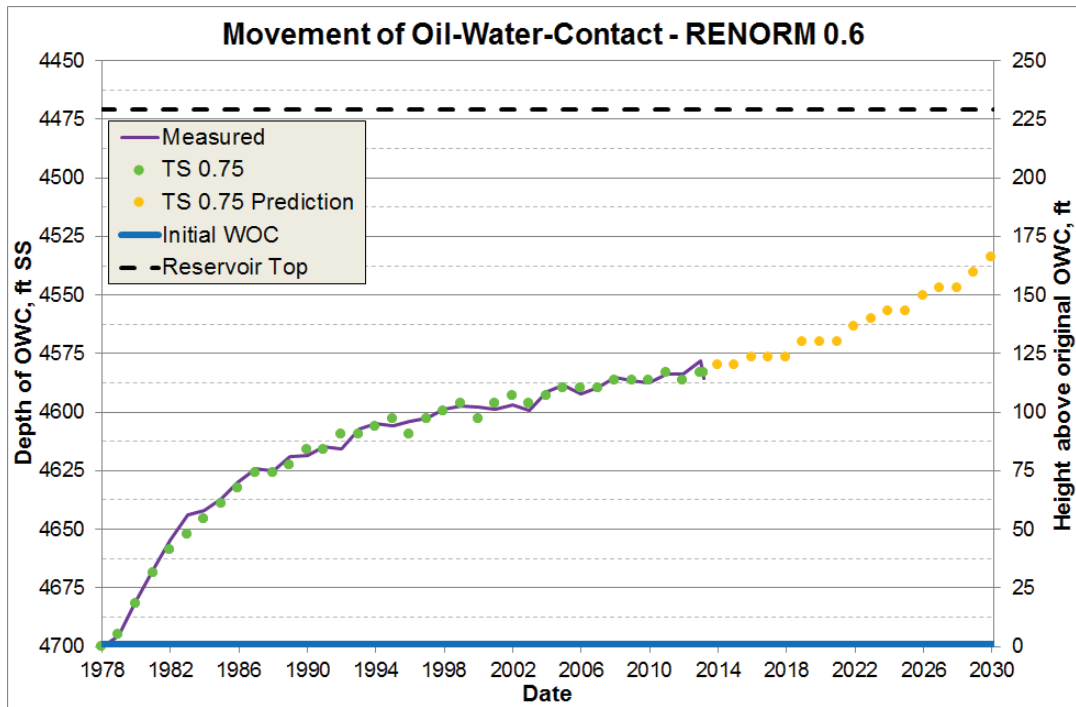
Figure 6.25: Forecasted movement of oil water contact.
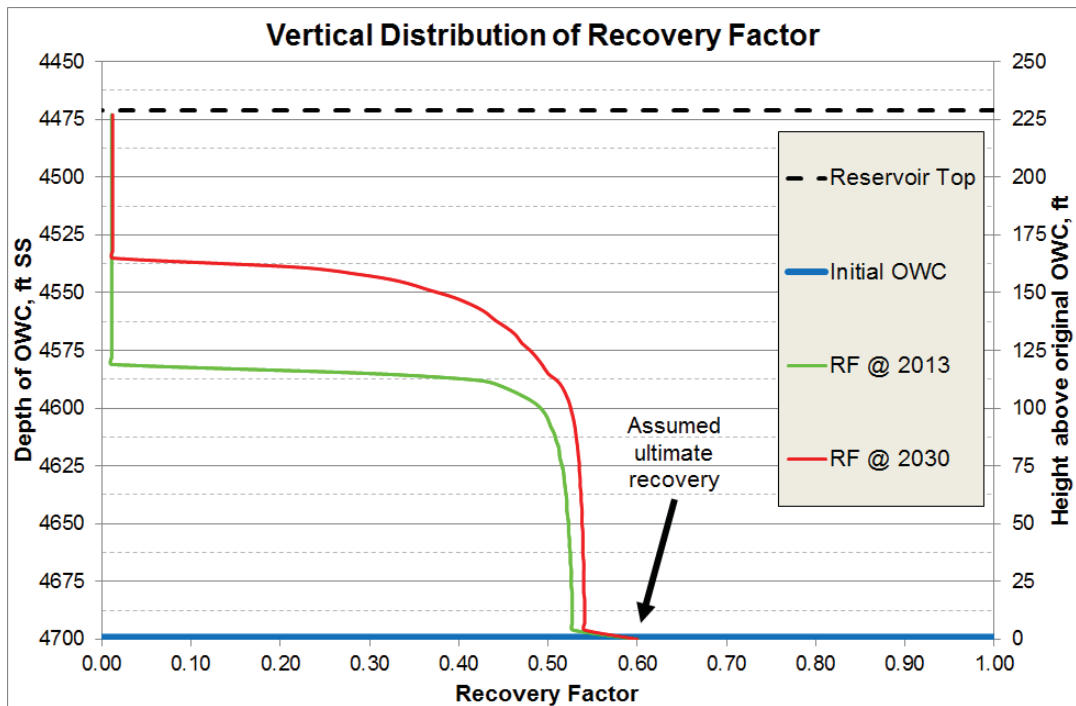
Figure 6.26: Vertical distribution of matrix recovery factors at end of history and end of prediction period.

Chapter 7

Conclusions

1. The method invented by Mittermeir (2015) successfully combines the classical material balance and displacement efficiency calculations. With this approach a realistic dual porosity material balance calculation - this means considering the physics of matrix oil recovery - became possible.

2. The validity of this statement is stated for the first time by the successful application of the scheme on the dual porosity Sabah field.

3. By matching phase contact movements a recovery curve describing the matrix-fracture interaction could be determined. Such a curve can be used for subsequent numerical reservoir simulation, too.

4. However, the applied method – similar to conventional single porosity material balance – cannot replace numerical reservoir simulation. Nevertheless, the strengths but also the limitations of MB calculations, makes it a valuable tool for the practicing reservoir engineer. MB calculation are an excellent and fast screening tool for quick assessing reservoir performance and production planning.

5. As for conventional MB calculations, the parameters of an analytical aquifer model can be determined. Also, sensitivities in determining the original oil in place can be run.

6. Dual porosity MB calculations in addition to numerical reservoir simulation can reduce the uncertainties related to modelling naturally fractured dual porosity reservoirs.

Chapter 8

References

Abushaikha and Gosselin (2008) Matrix-Fracture Transfer Function in Dual-Medium Flow Simulation: Review, Comparison, and Validation, Paper SPE 113890 presented at the Europec/EAGE Annual Conference and Exhibition, Rome, Italy, June 9-12.

Al-Kobaisi *et al.* (2009) A Critical Review for Proper Use of Water/ Oil/ Gas Transfer Functions in Dual-Prosity Naturally Fractured Reservoirs: Part II, SPE 124213

Amiry, M.T. (2014) Modeling Flow Behavior in Naturally-Fractured Reservoirs. PhD Thesis, Montanuniversität Leoben, Leoben, Austria (February 2014).

Babadagli T. (2001) Recovery of Heavy Matrix Oil by Capillary Imbibition in Naturally Fractured Reservoirs, Paper SPE 69843 presented at the 2001 SPE International Thermal Operations and Heavy Oil Symposium, Porlamar, Margarita Island, Venezuela, March 12-14.

Babson,E.C. (1944) Prediction of Reservoir Behavior from Laboratory Data, 944120-G SPE Journal Paper.

Bashiri and Kasiri (2011) Revisit Material Balance Equation for Naturally Fractured Reservoirs, Paper SPE 150803 presented at Nigeria Annual International Conference and Exhibition, Abuja, Nigeria, July 30 - Aug. 03.

Balogun,A.S., Kazemi, H., Ozkan, E., Al-Kobaisi, M., and Ramirez, B. (2007) Verification and Proper Use of Water-Oil Transfer Function for Dual Porosity and Dual Permeability Reservoirs, Paper SPE 104580 presented at the SPE Middle East Oil and Gas Show and Conference, Bahrain 11-14 March

Balogun *et al.* (2009) Verification and Proper use of Water-Oil Transfer Function for Dual-Porosity and Dual-Permeability Reservoirs, SPE 104580, SPE J. Paper.

Barenblatt G.E., Zheltov I.P., Kochina I.N. (1960) Basic Concepts in the Theory of Seepage of Homogeneous Liquids in Fissured Rocks, J. Appl. Math. Methods (USSR) **24**, 1286-1303.

Blaskovich F.T., Cain G.M., Sonier F., Waldren D., Webb S. (1983) A Multicomponent Isothermal System for Efficient Reservoir Simulation, Paper SPE 11480 presented at the Middle

East Oil Technical Conference, Manama, Bahrain, March 14-17.

Bourbiaux B., Kalaydjian F. (1990) Experimental Study of Cocurrent and Countercurrent Flows in Natural Porous Media, SPE Reservoir Evaluation & Engineering, **5**, 3, 361-368.

Bourbiaux B., Cacas M.C., Sarda S., Sabathier J.C. (1997) A Fast and Efficient Methodology to Convert Fractured Reservoir Images into a Dual-Porosity Model, Paper SPE 38907 presented at the SPE Annual Technical Conference and Exhibition, San Antonio, Tx, Oct. 5-8.

Bourbiaux B., Cacas M.C., Sarda S., Sabathier J.C. (1998) A Rapid and Efficient Methodology to Convert Fractured Reservoir Images into a Dual-Porosity Model, Oil Gas Sci. Technol. - Rev. IFP **53**, 6, 785-799.

Bourbiaux B., Granet S., Landereau P., Noetinger B., Sarda S., Sabathier J.C. (1999) Scaling Up Matrix-Fracture Transfers in Dual-Porosity Models: Theory and Application, Paper SPE 56557 presented at the SPE Annual Technical Conference and Exhibition, Houston, Texas, Oct. 3-6.

Bourbiaux B., Basquet R., Cacas M.C., Daniel J.M., Sarda S. (2002) An Integrated Workflow to Account for Multi-Scale Fractures in Reservoir Simulation Models: Implementation and Benefits, Paper SPE 78489 presented at the 10th Abu Dhabi International Petroleum Exhibition and Conference, Abu Dhabi, United Arab Emirates, Oct. 13-16.

Bourbiaux B., Basquet R., Daniel J.M., Hu L.Y., Jenni S., Lange A., Rasolofosaon P. (2005) Fractured Reservoirs Modelling: A Review of the Challenges and Some Recent Solutions, First Break **23**, September.

Bourbiaux B. (2010) Fractured Reservoir Simulation: a Challenging and Rewarding Issue, Oil Gas Sci. Technol. - Rev. IFP **65**, 2, 227-238.

Cacas M.C., Daniel J.M., Letouzey J. (2001) Nested Geological Modelling of Naturally Fractured Reservoirs, Petrol. Geosci. **7**, S43-S52

Carter, R.D. and Tracy, G.W. (1960) An Improved Method for Calculating Water Influx. In Petroleum Transactions, AIME, Vol.219, 415-417.

Chen W.H., Wasserman M.L., Fitzmorris R.E. (1987) A Thermal Simulator for Naturally Fractured Reservoirs, Paper SPE 16008 presented at the 9th Reservoir Simulation Symposium, San Antonio, TX, Feb. 1-4.

Chen, J., Miller, M.A. and Sepehrnoori, K. (1995) Theoretical Investigation of Countercurrent Imbibition in Fractured Reservoir Matrix Blocks, Paper SPE 29141 presented at the SPE Symposium of Reservoir Simulation, San Antonio, TX, USA, Feb 12-15.

Chen C.Y., Horne R.N., Fourar M. (2004) Experimental Study of Liquid-Gas flow structure effects on relative permeabilities in a fracture, Water Resour. Res. 40, W08301.

Coats, K.H. (1988) Implicit Compositional Simulation of Single-Porosity and Dual-Porosity Reservoirs, Presented at the First International Forum on Reservoir Simulation, Alpbach, Sept.

12-16, and SPE 18427.

Czerniak, S.O. (2015) Applicability and Limitations of the Warren-Root Transfer Function in Calculation of the Fracture-Matrix Fluid Exchange, MS Thesis at the Montanuniversität Leoben, Austria, 2015.

Famy, C., Bourbiaux, B. and Quintard, M. (2005) Accurate Modeling of Matrix-Fracture Transfer in Dual Porosity Models: Optimal Subgridding of Matrix Blocks, Paper SPE 93115 presented at the 2005 SPE Reservoir Simulation Symposium, Houston, TX, USA, Jan. 31-Feb. 2.

Fenwick D.H., Roggero F. (2003) Updating Stochastic Reservoir Models with New Production Data, Paper SPE 84467 presented at the SPE Annual Technical Conference and Exhibition, Denver, Colorado, U.S.A., Oct. 5-8.

Feraille M., Manceau E., Zabalza-Mezghani I., Roggero F., Hu L.Y., Reis L. (2003) Integration of Dynamic Data in a Mature Oil Field Reservoir Model to Reduce the Uncertainty on Production Forecasting, AAPG, Salt Lake City.

Feraille M., Roggero F. (2004) Uncertainty Quantification for Mature Field Combining the Bayesian Inversion Formalism and Experimental Design Approach, 9th European Conference on the Mathematics of Oil Recovery, Cannes, France, Aug. 30-Sept. 2.

Fetkovich, M.J. (1971) A Simplified Approach to Water Influx Calculations-Finite Aquifer Systems. Journal of Petroleum Technology 23 (7): 814-828. SPE-2603-PA. http://dx.doi.org/10.2118/2603-PA

Firoozabadi A., Ottesen B., Mikklesen M. (1992) Measurements of Supersaturation and Critical Gas Saturation, SPE Formation Evaluation, **7**, 4, 337-344.

Firoozabadi A. (2000) Recovery Mechanisms in Fractured Reservoirs and Field Performance, J. Can. Petrol. Technol. **39**, 11, 13-17.

Fung L.S.K. and Collins, D.S. (1991) An Evaluation of the Improved Dual Porosity Model for the Simulation of Gravity Effects in Naturally Fractured reservoirs, 91-03-06 PETSOC Journal Paper - 1991.

Fung, L.S.K. (1991) Simulation of Block-to-Block Processes in Naturally Fractured Reservoirs, 20019-PA SPE Journal Paper - 1991.

Geiger S., Matthäi S., Niessner J., Helmig R. (2009a) Black-Oil Simulations for Three-Component – Three-Phase Flow in Fractured Porous Media, SPE J. 14, 2, 338-354..

Geiger S., Huangfu Q., Reid F., Matthäi S., Coumou D., Belayneh M., Fricke C., Schmid K. (2009b) Massively Parallel Sector Scale Discrete Fracture and Matrix Simulations, Paper SPE 118924 presented at the SPE Reservoir Simulation Symposium, The Woodlands, Texas, USA, Feb. 2-4.

Ghaedi, M., Masihi M., Heinemann,Z.E. and Ghazanfari M.H. (2015) In-situ Wettatbility Determination of Fractured Reservoir Based on the Recovery Curve Method, submitted to Transp. Porous Med., under revision.

Gharsalla M.M., Heinemann Z.E., Mittermeir G.M. 2014. Application of Material Balance Calculation to the Fractured Dual Porosity Sabah Field. *BKL Köolaj és Földgáz*, Budapest, Hungary, **147** (7): 1-17.

Gillespie P.A., Howard, C.B..Walsh J.J. and Watterson, J. (1993) Measurement & Characterisation of Spatial Distribution of Fractures, Tectonophysics **226**, 113-141, 1993.

Gilman J., Kazemi H. (1983) Improvements in Simulation of Naturally Fractured Reservoirs, SPE J. **23**, 4, 695-707.

Gilman J., Kazemi H. (1988) Improved Calculations for Viscous and Gravity Displacement in Matrix Blocks in Dual-Porosity Simulators, J. Petrol. Technol. **40**, 1, 60-70.

Gilman, J.R. (2003) Practical Aspects of Simulation of Fractured Reservoirs, paper presented at the Seventh International Forum on Reservoir Simulation, Baden-Baden, Germany.

Gokturk, E. and Tarhouni, N. 1999. 3D Seismic Interpretation of Sabah Field. November 1999.

Gurpinar, O. and Kossack, C.A. (2000) Realistic Numerical Models for Fractured Reservoirs, Paper SPE 59041 presented at the SPE International Petroleum Conference and Exhibition, Mexico, Feb. 1-3.

Heinemann, Z.E. (2004) Using Recovery Curves in Modeling Natural Fractured Hydrocarbon Reservoirs", Proposal for a PhD Research Project at the Montanuniversität Leoben, Austria, March 2004.

Heinemann, Z.E. and Mittermeir, G.M., (2012) Derivation of the Kazemi-Gilman-Elsharkawy Generalized Dual Porosity Shape Factor, Transp. Porous Med., 91(1), 123-132.

Heinemann, G.F.,Harrer A. W., Mittermeir G.M., and Heinemann Z.E. (2007) An imperative workflow for modeling of naturally fractured reservoirs on different scales, paper SPE 107180 presented at SPE Europec/EAGE Annual Conference and Exhibition, London, United Kingdom, 11-14 June 2007.

Heinemann, Z. E., Mittermeir, G.M. and Gharsalla, M.M. (2014). Successful Application of Material Balance Calculation to a Fractured Dual Porosity Field. Paper SPE 172325-MS presented at the Annual Caspian Technical Conference and Exhibition held in Astana, Kazakhstan, 12-14 November. http://dx.doi.org/10.2118/172325-MSP

Hill A.C., Thomas G.W. (1985) A New Approach for Simulating Complex Fractured Reservoirs, Paper SPE 13537 presented at the Middle East Oil Technical Conference and Exhibition, Bahrain, March 11-14.

Hu L.Y. (2000) Gradual deformation and iterative calibration of Gaussian-related stochastic models, Math. Geol. **32**, 1.

Johns, R.T. and Jalali-Yazdi (1991) Comparison of pressure-Transient Response in Intensely and Sparsely Fractured Reservoirs, 18800-PA SPE Journal Paper - 1991

Katz,D.L. (1936) A Method of Estimating Oil and Gas Reserves, 936018-G SPE Journal Paper - 1936, Trans. AIME vol 118, pp. 18ff.

Kazemi H., Merrill L.S., Porterfield K.L., Zeman P.R. (1976) Numerical Simulation of Water-Oil Flow in Naturally Fractured Reservoirs, SPE. J. **16**, 6, 317-326.

Kazemi *et al.* (1979) Numerical Simulation of Water Imbition in Fractured Cores, SPE. J.

Kazemi, H., Gilman,J.R. and El-Sharkawy, A.M. (1992) Analytical and Numerical Solution of Oil Recovery from Fractured Reservoirs Using Empirical Transfer Functions, SPE Reservoir Engineering, pp.219-227.

Kleppe and Morse (1974) Oil Production from Fractured Reservoirs by Water Displacement, Paper SPE 5084 presented at 49th Annual Fall Meeting of the SPE-AIME, Houston, Texas, Oct. 6-9.

Knytl, J., Brydle, G., Greenwood, D., Earth Sciences Society of Libya. National Oil Corporation Libya. (1996) Tectonic History and Structural Development of the Kaf-Themar Trend of the Western Sift Basin. Sedimentary basins of Libya: The geology of Sirte Basin Symposium; 1st, Sedimentary basins of Libya: The geology of Sirte Basin; 167-200.

Kossack, C.A. (2006) Simulation of Gas/Oil Displacements in Vuggy and Fractured Reservoirs, Paper SPE 101674 presented at the SPE Annual Technical Conference and Exhibition, San Antonio, TX, USA, Sept. 24-27.

Lange E.A. (1998) Correlation and Prediction of Residual Oil Saturation for Gas-Injection Enhanced Oil-Recovery Processes, SPE Reservoir Evaluation & Engineering. **1**, 2, 127-133.

Lemonnier and Bourbiaux (2010) Simulation of Naturally Fractured Reservoirs. State of the Art, Part1, Physical Mechanisms and Simulator Formulation, Oil & Gas Science and Technology-Rev. IFp, Vol.65, No. 2, pp. 239-262, DOI:10.2516/ogst/2009066.

Li *et al.* (2013) An Improved Approach to Simulate Low-Permeability Fractured Reservoirs with Dynamic Hybrid Dual-Porosity Model, Paper SPE 166665 presented at Asia Pacific Oil & Gas Conference and Exhibition, Jakarta, Indonesia, Oct. 22-24.

Lim, K.T, Aziz K. (1995) Matrix-fracture transfer schape factors for dual-porosity simulators. J.of Petroleum siwnse and Engineering 13 p.169-178.

Litvak B. (1985) Simulation and Characterization of Naturally Fractured Reservoirs, Proceedings of the Reservoir Characterization Technical Conferences, Dallas, April 29-May 1, Academic Press, New York.

Mansur, M.A. 1987. Sabah Field. Geological Report, September 1987

Mezghani M., Fornel A., Langlais V., Lucet N. (2004) History Matching and Quantitative Use of 4D Seismic Data for an Improved Reservoir Characterization, Paper SPE 90420 presented at the SPE Annual Technical Conference and Exhibition, Houston, TX, Sept. 26-29.

Mittermeir, G.M., Pichelbauer J., and Heinemann Z.E. (2004) Automated Determination of Aquifer Properties from Field Production Data. Paper presented at the 9th European Conference on Mathematics of Oil Recovery (ECMOR IX), Cannes, France, 30 August -2 September.

Mittermeir, G.M. (2015) Material-Balance Method for Dual-Porosity reservoirs With Recovery Curved to Model the Matrix/Fracture Transfer, SPE Reservoir Evaluation & Engineering, 2015.

Moinfar *et al.* (2011) Comparison of Discrete and Dual-Permeability Models for Multiphase Flow in Naturally Fractured Reservoirs, Paper SPE 142295 presented at the SPE Reservoir Simulation Symposium, Woodlands, Texas, USA, Feb. 21-23.

Monifar, A., Varavei, A., Sepehmoori,K. and Johns T.R. (2013) Development of a Coupled Dual Continuum and Discrete Fracture Model for Simulation of Unconventional Reservoirs. SPE Reservoir Simulation Symposium held in The Woodland, Texas USA, 18-20 February 2013.

Mora and Wattenbarger (2009) Analysis and Verification of Dual Porosity and CBM Shape Factors, Journal of Canadian Petroleum Technology, Vol. 48 No. 2.

Mora and Wattenbarger (2009) Comparison of Computation Methods for CBM Performance, ournal of Canadian Petroleum Technology, Vol. 48 No. 4.

Muskat, M. and Taylor, M.O. (1946) Effect of Reservoir Fluid and Rock characteristics on Production Histories of Gas drive Reservoirs. Trans.AIME 1946.

Penuela, G., Idrobe, E.A., Ordonez,A., Medina, C.E. and Meza, N. (2001) A New Material Balance Equation for Naturally Fractured Reservoirs Using a Dual System Approach, paper SPE 68831 presented at the 2001 Western Regional Meeting, Bakersfield, CA, March 26-30.

Pirker B., Mittermeir G., and Heinemann, Z.E. (2007) Numerically Type Curves for Assessing Matrix Recovery Factors, Paper SPE 107074 presented at SPE Europed/EAGE Annual Conference and Exhibition, London, United Kingdom, June 11-14.

Pirker, B., Heinemann, Z.E. (2008) Method to Preliminary Estimation of the Reserves and Production Forecast for Dual Porosity Fractured Reservoirs, paper SPE 113378, prepared for presentation at the 2008 SPE EUROPEC/EAGE Annual Conference and Exhibition held in Rome, Italy, 9 - 12 June 2008.

Pirker B., Harrer, A.W., Heinemann, Z.E. (2008) Reserve Estimation for Naturally Fractured Reservoirs Using Numerically Derived Recovery Curves. prepared for presentation at the 11th European Conference on the Mathematics of Oil Recovery (ECMOR XI) held in Bergen, Norway, 8 - 11 September 2008.

Pirker, B. (2008) A New Approach for Modeling Dual Porosity Reservoirs Using Recovery Curves, PhD Dissertation, Montanuniversität Leoben, Nov.2008.

Pirson,S.J.: "Oil Reservoir Engineering", McGraw-Hill Book Company, New York, 1958.

Pirson, S.J. (1945) The Engineering Approach to Oil Reservoir Controls, Oil Weekly, Dec.31. pp22ff.

Pirson, S.J. (1958) Oil Reservoir Engineering, McGraw-Hill Book Company Inc. NY 1958.

Por G.J., Boerrigter P., Maas J.G., de Vries A. (1989) A Fractured Reservoir Simulator Capable of Modeling Block-Block Interaction, Paper SPE 19807 presented at the SPE Annual Technical Conference and Exhibition, San Antonio, TX, Oct. 8-11.

Pruess K., Narasimhan T.N. (1985) A Practical Method for Modeling Fluid and Heat Flow in Fractured Porous Media, SPE J. **25**, 1, 14-26.

Quandalle P., Sabathier J.C. (1989) Typical Features of a Multipurpose Reservoir Simulator, SPE Reserv. Eng. J. **4**, 4, 475-480.

Ramirez *et al.* (2009) A Critical Review for Proper Use of Water/Oil/Gas Transfer Functions in Dual-Porosity Naturally Fractured Reservoirs: Part I, SPE Reservoir Evaluation & Engineering.

Reiss L.H., Bossie Codreanu D., Lefebvre du Prey E.J. (1973) Flow in Fissured Reservoirs, Paper SPE 4343 presented at the Second Annual European Meeting of AIME, London, England, April 2-3.

Rossen R.H. (1977) Simulation of Naturally Fractured Reservoirs with Semi Implicit Source Terms, SPE J. **17**, 3, 201-210.

Rossen R.H., Shen E.I.C. (1989) Simulation of Gas/Oil Drainage and Water/Oil imbibition in Naturally Fractured Reservoirs, SPE Reserv. Eng. J. **4**, 4, 464-470.

Sabathier J.C., Bourbiaux B., Cacas M.C., Sarda S. (1998) A New Approach of Fractured Reservoirs, Paper SPE 39825 presented at the SPE International Petroleum Conference & Exhibition, Villahermosa, Mexico, March 3-5.

Saidi A.M. (1983) Simulation of Naturally Fractured Reservoirs, Paper SPE 12270 presented at the Reservoir Simulation Symposium, San Francisco, CA, November 15-18.

Schilthuis, R.J. (1936) Active Oil and Reservoir Energy, 936033-G SPE Journal paper - 1936.

Sandoval *et al.* (2009) The New, Generalized Material Balance Equation for Naturally Fracured Reservoirs, Paper SPE 122395 presented at SPE Latin American and Caribben Petroleum Engineering Conference, Cartagena, Colombia, May 31 - June 3.

Shanks, D. (2013) Oil Rim Tool Measures Reservoir Fluids Continuously in Real Time, Below Pump, 0313-0034-JPT SPE Journal Paper - 2013.

Sonier F., Souillard P., Blaskovich F.T. (1986) Numerical Simulation of Naturally Fractured Reservoirs, Paper SPE 15627 presented at the 61st SPE Annual Technical Conference and Exhibition, New Orleans, LA, Oct. 5-8.

Su *et al.* (2013) Dynamic Matrix-Fracture Transfer Behavior in Dual-Porosity Models, Paper SPE 164855 presented at EAGE Annual Conference and Exhibition incorporating SPE Europe, London, United Kingdom, June 10-13.

Tarner, J. (1944) How different Size Gas Caps and Pressure Maintenance Programs Affect Amount of Recoverable Oil, Oil Weekly, (June 12, 1944) 144, No2, 32-34.

Thomas, L.K., Dixon, T.N., and Pierson, R.G. (1983) Fractured Reservoir Simulation", SPE Journal, 638-648 (Feb. 1983) Trans. AIME, 243.

Ueda, Y., Murata, S., Watanabe, Y. and Funatsu, K. (1989) Investigation of the Shape Factor Used in the Dual-Porosity Reservoir Simulator, Paper SPE 19469 presented at the SPE Asia-Pacific Conference held in Sydney, Australia, Sept. 13-15.

Uren, L.Ch. (1950) Petroleum Production Engineering, McGraw-Hill Volume 3.

van der Meer, F.D. and Cloetingh, S.A.P.L. (1993) Intraplate stresses and the subsidence history of the Sirte basin, Libya. In: Tectonophysics :The International Journal of Integrated Solid Earth Sciences, 226 (1993)1-4 pp. 37-58.

Van Everdingen, A.F. and Hurst W. (1949) The Application of the Laplace Transformation to Flow Problems in Reservoirs. Journal of Petroleum Technology **1** (12): 305-324. SPE-949305-G. http://dx.doi.org/10.2118/949305-G

Vogt, J.P. and Wang, B. (1987) Accurate Formulas for Calculating the Water Influx Superposition Integral, Paper SPE 17066 presented at the SPE Eastern Regional Meeting geld in Pittsburgh, Pennsylvania, 21-23 Oct. http://dx.doi.org/10.2118/17066-MS

Warren, J.E., and Root P.J. (1963) The Behavior of Naturally Fractured Reservoirs, SPEJ, September, 245-255, 1963, Trans.AIME, 228.

Wuthicharn, K. and Zimmerman, R.W. (2011) Shape Factors for Irregularly Shaped Matrix Blocks, paper SPE 148060 presented at the SPE Reservoir Characterisation and Simulation Conference and Exhibition, held in Abu Dhabi, UAE, 9-11 Oct. 2011.

Yamamoto *et al.* (1971) Compositional Reservoir Simulator for Fissured Systems, The Single-Block Model, SPE 2666, SPEJ.

Chapter 9

Nomenclature

Symbols

A	-	surface area, L^2, ft^2
B	-	formation volume factor, L^3/L^3, RB/STB
c	-	compressibility, Lt^2/m, 1/psia
$\vec{d}_{kn}$	-	distance vector
E	-	efficiency/recovery factor
E_R	-	recovery efficiency
erf	-	error function
G	-	initial free gas volume, L^3, scf
G_I	-	cumulative injected gas, L^3, scf
G_p	-	cumulative gas production, L^3, scf
J_w	-	aquifer productivity index, L^4t/m, bbl/(day-psi)
k	-	permeability, L^2, D
k_a	-	apparent matrix permeability, L^2, D
k_r	-	relative permeability
K_{ogc}	-	tranche containing the actual oil/gas contact
K_{owc}	-	tranche containing the actual oil/water contact
$\bar{\bar{k}}$	-	normalized permeability tensor
L	-	characteristic dimension, L, ft
m	-	gas cap factor
N	-	original oil in place, L^3, STB
N_P	-	cumulative oil production, L^3, STB

n	-	number of surfaces A_{kn}
$\vec{n}_{kn}$	-	normal unit vector
P	-	pressure, m/Lt^2, psia
Q	-	cumulative production, L^3, STB
Q_{mf}	-	cumulative matrix-fracture oil transfer, L^3, STB
q	-	production rate or flow rate, L^3/t, STB/day
q_{omf}	-	fracture-matrix transfer oil rate, L^3/t, STB/day
q_{gmf}	-	fracture-matrix transfer gas rate, L^3/t, STB/day
q_{wmf}	-	fracture-matrix transfer water rate, L^3/t, STB/day
R	-	gas/oil ratio, L^3/L^3, scf/STB
R_s	-	solution gas/oil ratio, L^3/L^3, scf/STB
R_P	-	production gas/oil ratio, L^3/L^3, scf/STB
$\overline{R_p}$	-	average production gas/oil ratio, L^3/L^3, scf/STB
S	-	saturation
t	-	time, t, days
t_v	-	virtual time, t, days
t_D	-	dimensionless time
V	-	volume, L^3, ft^3,RB
W	-	original water amount, L^3, STB
W	-	water influx, L^3, STB
w	-	cumulative water production, L^3, STB
W_e	-	water encroachment, L^3, STB
W_{ej}	-	cumulative water encroachment, L^3, STB
W_I	-	cumulative injected in place, L^3, STB
W_P	-	cumulative water production, L^3, STB
ΔN_P	-	incremental oil production, L^3, STB

Greek Symbols

α	-	reciprocal of ultimate recovery
β	-	time-scaling factor
ϕ	-	porosity
Φ	-	phase potential, m/L³, psia
Φ_{of}	-	the fracture oil potential m/L³, psia
Φ_{om}	-	the matrix oil potential m/L³, psia
λ	-	mobility, L³t/m, D/cp
μ	-	viscosity, m/Lt, cp
∇	-	divergence operator
Δ	-	difference operator
σ	-	shape factor, 1/L², 1/ft²
ω	-	weighting factor

Subscripts

a	-	apparent
b	-	bubblepoint
c	-	connate
c	-	capillary
D	-	Dimensionless
f	-	fracture
g	-	gas phase
i	-	initial conditions
j	-	timepoint index
$j+1$	-	new timepoint index
k	-	tranche index
m	-	matrix
max	-	maximum
mf	-	matrix-fracture
M	-	tranche for top of reservoir
o	-	oil phase
p	-	production

p	-	pore
s	-	solution gas in stock-tank oil,
t_j	-	production time
υ	-	virtual
w	-	water phase
w	-	water phase
x	-	in x direction
y	-	in y direction
z	-	in z direction
ϕ	-	pore

Superscripts

a	-	analytical
g	-	gas
n	-	normalized
w	-	water

Abbreviations

$bbls$	-	barrels
DFM	-	Discrete Fractured Models
DFN	-	Discrete Fracture Network
DCM	-	Dual Continuum Modeling
DST	-	Drill Stem Test
FWL	-	Free Water Level
$H5$	-	Heinemann-Five
GOC	-	Gas Oil Contact
GOR	-	Gas Oil Ratio
GWC	-	Gas Water Contact
IOC	-	International Operating Companies
MB	-	Material Balance

MDT - Modular Dynamics Tester

MINC - Multiple Interacting Continua

MLRM- Multilevel Reservoir Modeling

NFR - Naturally Fractured Reservoir

NOC - National Oil Company

ODT - Oil Down To

OGC - Oil Gas Contact

OOIP - Original Oil In Place

OWC - Oil Water Contact

OOWC- Original Oil Water Contact

PV - Pore Volume

PVT - Pressure-Volume-Temperature

RCI - Reservoir Cauterization Tool

RFT - Repeat Formation Tester

RCM - Recovery Curve Method

SCAL - Special Core Analysis

SMB - Single Matrix Block

TDRM- Top-Down Reservoir Modeling

TZ - Transition Zone

WC - Water Cut

WUT - Water Up To

w - water